Marquette University
e-Publications@Marquette

Dissertations (2009 -) | Dissertations, Theses, and Professional Projects

Spectral Characterization of Cytochromes P450 Active Site and Catalytic Intermediates

Daniel Kaluka
Marquette University

Recommended Citation
Kaluka, Daniel, "Spectral Characterization of Cytochromes P450 Active Site and Catalytic Intermediates" (2012). *Dissertations (2009 -)*. Paper 231.
http://epublications.marquette.edu/dissertations_mu/231

SPECTRAL CHARACTERIZATION OF CYTOCHROMES P450 ACTIVE SITE AND CATALYTIC INTERMEDIATES

By

Daniel Kaluka, B.Sc., M.S.

A Dissertation submitted to Faculty of the Graduate School,
Marquette University,
in Partial Fulfillment of the Requirements for
the Degree of Doctor of Philosophy

Milwaukee, Wisconsin

December 2012

ABSTRACT
SPECTRAL CHARACTERIZATION OF CYTOCHROMES P450 ACTIVE SITES AND CATALYTIC INTERMEDIATES

Daniel Kaluka, B.Sc., M.S.

Marquette University, 2012

Cytochromes P450 (P450s) have been the subject of intense research for over six decades. Though it is widely accepted that a highly reactive Fe(IV)=O π-cation radical, or the so called compound I, facilitates the oxidation of relatively inert hydrocarbons, spectroscopic characterization of this putative intermediate has eluded detection under turnover conditions, presumably due to its very short lifetime. In this work, chemically inert substrates of P450s have been utilized in a new approach to capture and stabilize this transient intermediate and characterize it with resonance Raman (RR) spectroscopy, which is a well established tool for studying heme proteins. Specifically, perfluorodecanoic acid has been utilized as an inert surrogate substrate of a thermophilic cytochrome P450 designated CYP119 and RR and cryoradiolysis methods were employed to characterize the enzymatic intermediates under turnover conditions.

In a separate project, a recent and more efficient approach for the isotopic labeling of the prosthetic group in heme proteins has been exploited to produce a ^{13}C labeled analogue of the soluble bacterial cytochrome P450cam (P450cam). Briefly, the HU227 strain of *E. coli* that lacks the δ-aminolevulinic acid (δ-ALA) synthase gene was employed in the heterologous expression of P450cam harboring a prosthetic group labeled with ^{13}C at the C_m and C_α positions by growing cells in the presence of [5-^{13}C] δ-ALA, which was synthesized in four steps from [2-^{13}C] glycine. This system has been utilized as proof of principle for the strategy of defining active site structure in mammalian cytochromes P450 using NMR methods to furnish necessary experimental restrictions in docking routines, which are commonly employed in determining the relative affinities of drug candidates. Noting that few crystal structures of substrate bound complexes of drug metabolizing P450s exist, a truncated CYP2D6 gene has been designed following a recently published procedure and efforts were made to heterologously express a selectively ^{13}C enriched analogue of this important drug metabolizing enzyme.

ACKNOWLEDGEMENTS

Daniel Kaluka, B.Sc., M.S.

My heartfelt thanks go to Professor James R. Kincaid for his continued mentorship throughout my time in his research group. I will forever be grateful for his guidance and his major contribution to my career development. I would also like to express my appreciation to my Committee members, Professors Daniel S. Sem, Michael. D. Ryan and Adam Fiedler for useful discussions throughout my studies and writing of this dissertation. I am so grateful to Professor Michael, D. Ryan for kindly offering his UV-vis instrument and glove box for use in my research. I would also like to thank, again, Professor Daniel S. Sem and Dr. Cai Sheng for their valuable discussions and technical assistance in NMR spectroscopy. My sincere gratitude is also extended to my group members, Drs. K. Czarnecki and P. Mak for introducing me to resonance Raman spectroscopy and continued technical advice and support.

Finally, I would like to express my heartfelt thanks to my wife, Priscah, daughter, Rufaro and son, Immanuel for their continued support throughout my academic career. I also would like to thank my parents for believing in me and their love.

TABLE OF CONTENTS

LIST OF TABLES

LIST OF FIGURES

LIST OF SCHEMES

CHAPTER 1 GENERAL INTRODUCTION

1.1 Cytochromes P450

Klingenberg (1958) is credited for the identification of the first cytochrome P450 in rat liver michrosomes.[1] A little later, in the early 1960s, Omura and Sato observed a characteristic Soret absorption maximum around 450 nm in the UV spectrum (Figure 1.1.1) of a carbon monoxide saturated liver microsomes sample incubated with sodium diothionite[2] These observations led to wide-ranging exploration of a class of heme proteins known as cytochromes P450 (P450s).

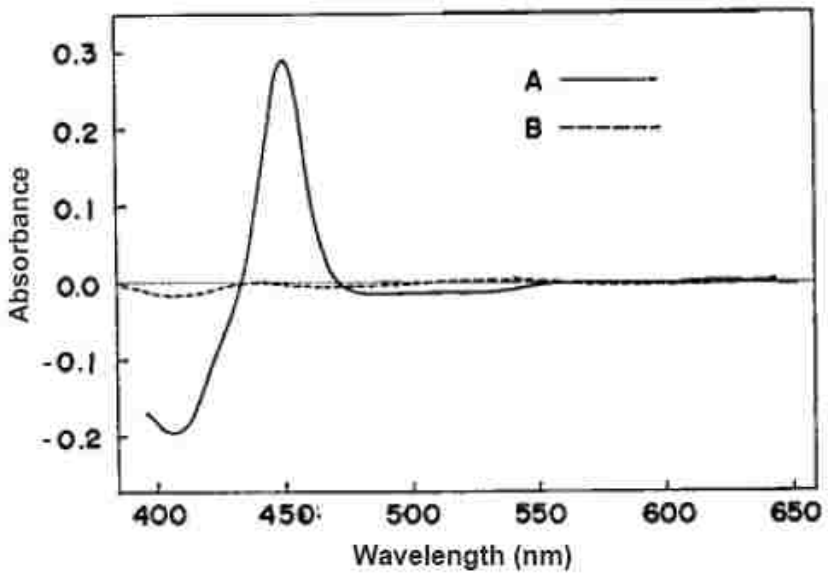

Figure 1.1.1 The Fe (II)-CO difference spectra of liver michrosomes. **A**, $Na_2S_2O_4$ reduced microsomes; **B**, aerobic microsomes.[2]

These single polypeptide chain heme proteins of between 400-500 amino acid residues are found in all five biological kingdoms.[3,4] The name heme proteins is derived from the characteristic iron-porphyrin prosthetic group or the so-called heme, in the

active site of these proteins. Natural occurring heme types include heme a, b, c and d (Figure 1.1.2)[5,6] Heme b bearing proteins have been the subject of intensive structure function studies. The prosthetic group's attachment to the surrounding protein matrix accounts for the apparent versatility and ubiquitous nature of these metalloproteins.[7] The heme group in P450s is covalently linked to the protein via an Fe–S bond (provided by a cysteinic sulfur acting as the fifth ligand) bond at the proximal side of the prosthetic group, whereas most other heme proteins such as, hemoglobin and myoglobin exhibit a histidyl imidazole linkage.[8,9]Additional covalent attachments with the heme peripheral groups have been documented for lactoperoxidases and myeloperoxidases.[10,11]

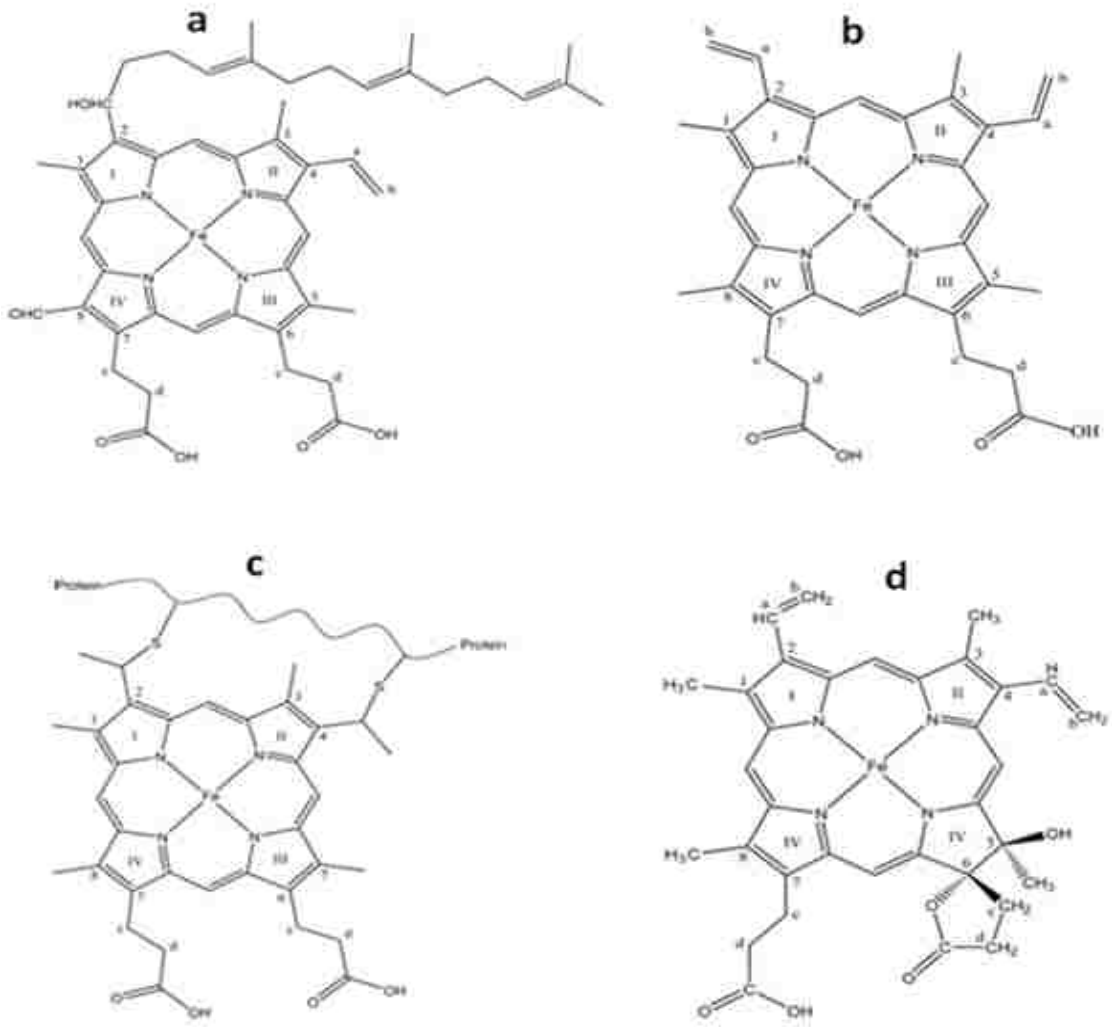

Figure 1.1.2 The structures (and numbering) of the natural occurring heme groups (**a-d**)[5,6]

The heightened research focus on this class of heme proteins stems primarily from their role as biological catalysts. P450s have been reported to bind and cleave molecular oxygen generating a potent intermediate capable of hydroxylating even relatively inert hydrocarbon substrates.[12,13]This interesting chemistry has been observed in a variety of important biological processes that include biosynthesis of lipids, steroids, antibiotics and the degradation of xenobiotics (Figure 1.1.3).[7] It is obviously of immense practical interest to gain a better understanding of this apparently ubiquitous chemistry exhibited by these important biological catalysts.

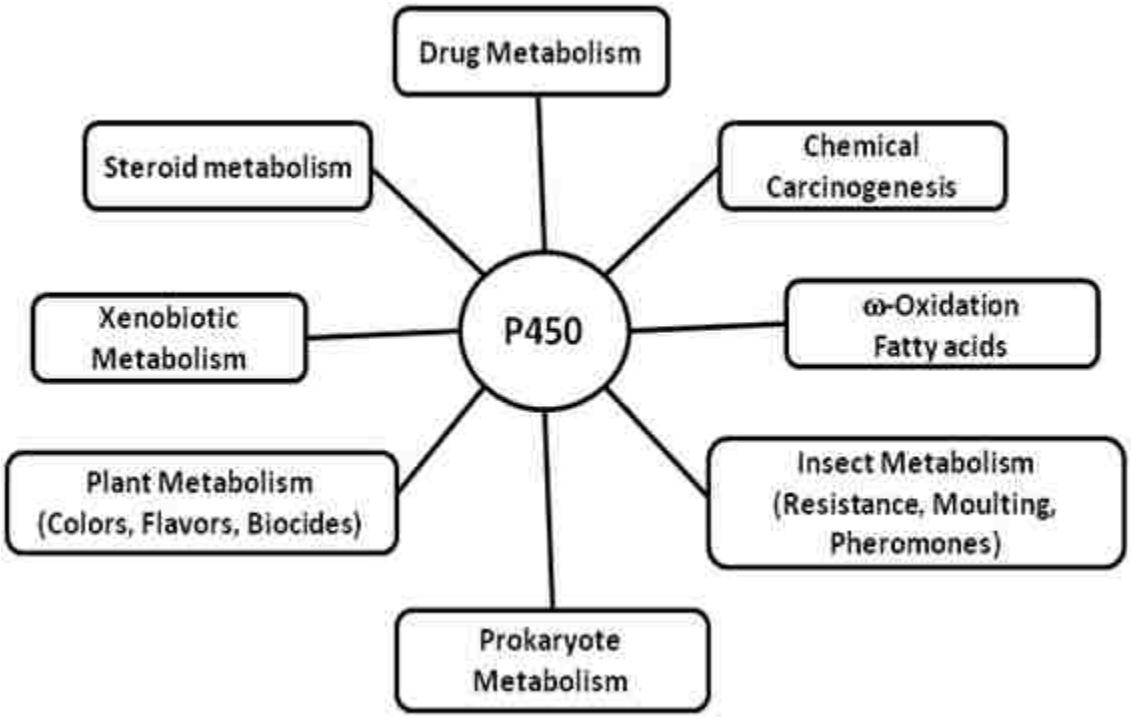

Figure 1.1.3 The many roles of P450cam in metabolism[7]

1.1.1 The P450s catalytic cycle

The advancement in genomic studies has seen the unraveling of greater than 3000 genes encoding P450s in plant, fungi, bacterial and mammalian sources.[3,4] Among these, a soluble heme protein known as cytochrome P450cam (P450cam) from the bacteria *Pseudomonas putida* has been well studied. [14–16] Researchers attempting to better understand the chemistry of P450s have taken advantage of this probably best characterized prototype of the P450 superfamily. Crystal structure studies have detected the presence of a hydrogen bonded water cluster in the substrate-free enzyme's distal

pocket.[15,17–19] In the resting state, one of the water molecules is bound to the iron-porphyrin complex giving a hexa-coordinated low spin ferric form of the enzyme (Figure 1.1.4).[20] It has now been well documented that binding of camphor (or its analogues) or redox partners by P450cam induce structural changes with important functional significance.[21,22] In the catalytic cycle shown in Figure 1.1.4, binding of substrate to a relatively planar hexa-coordinated iron-porphyrin complex induces a spin state change to a 5-coordinate high spin (5CHS) form of the enzyme (**2**). In P450cam, it has been shown that binding of substrate and its redox partner, putidaredoxin, modulates the heme equilibrium redox potential (from -303 mV to -173 mV) signifying susceptibility to reduction of the 5CHS P450cam (Figure 1.1.5).[21,23–25] Delivery of one electron equivalent, by putidaredoxin, is followed by binding of oxygen, giving rise to a dioxygen adduct of P450cam (**4**). Spectroscopic characterization of this intermediate in P450cam is well documented.[26–29] Addition of a second electron by the redox partner produces the heme-bound peroxo intermediate (**5a**). This intermediate (**5a**) and its protonated form, the ferric hydroperoxo species (**5b**) have recently been characterized by electronic absorption, EPR and resonance Raman spectroscopic methods.[20,28,30] Proton assisted scission of the dioxygen bond of the hydroperoxo species results in the formation of the transient reactive intermediate of P450s (**6**), the equivalent of the so-called compound I of peroxidases. This elusive intermediate has eluded spectroscopic characterization under turnover conditions.

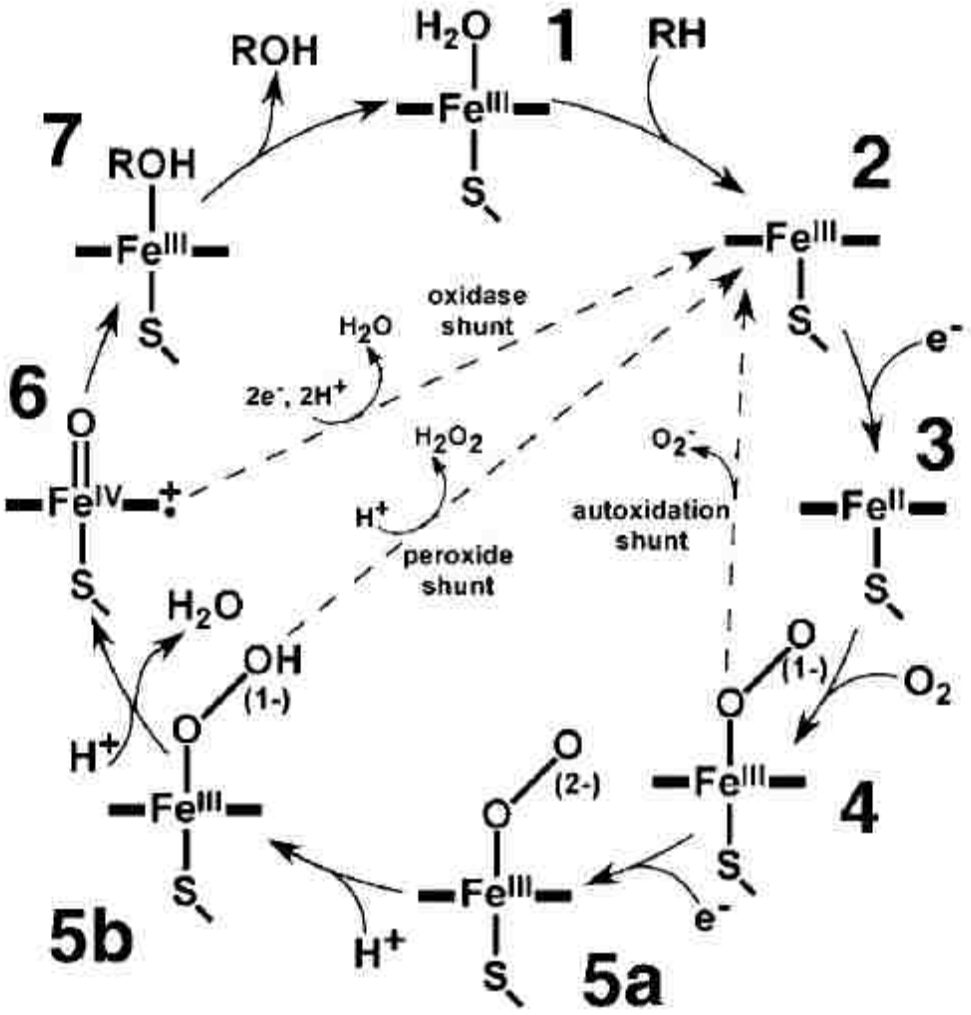

Figure 1.1.4 The catalytic cycle of P450cam[20]

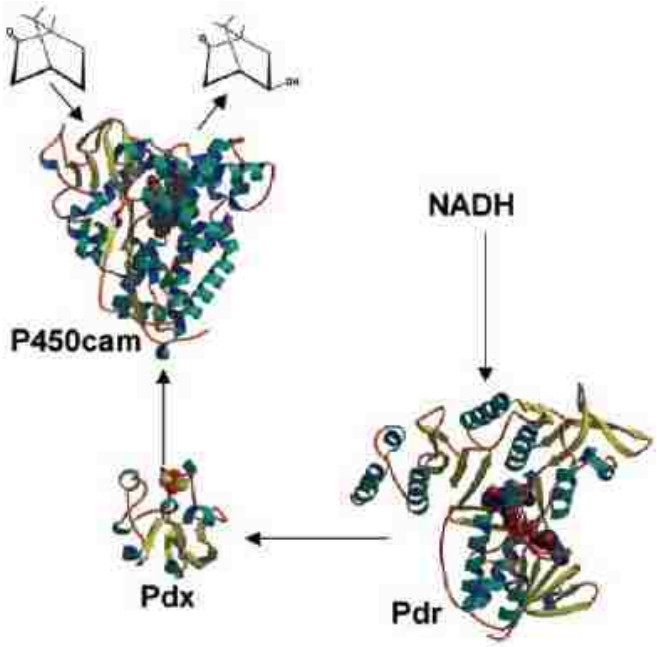

Figure 1.1.5 The structures of all the three components of P450cam[23]

1.1.2 Heme iron interactions with diatomic ligands

Important structural data have been obtained by taking advantage of the fact that these heme proteins are capable of binding exogenous diatomic ligands such as NO, CO and CN^- in addition to the endogenous O_2 discussed above for P450cam. The binding of these ligands to the iron-porphyrin complex through σ- and π-interactions gives rise to linear or bent geometries (Figure 1.1.6).[31–33] The dispositions of these ligands in the active site, which can be spectroscopically interrogated, have been used as probes reporting on active site architecture that can influence important functional properties of heme proteins. Two σ type interactions are possible: one in which the metal d_{z^2} orbital overlaps with the ligand lone pair and another involving the metal d_{z^2} and the ligand π* orbitals. The strength of the metal-ligand bond depends on the extent of orbital overlap, thus weak bonding exists between metal and a ligand exhibiting a high energy π* orbital.

For example, the strength of σ-bonding interaction increases from CO, NO to O_2 as the π*-orbital energy decreases. In π-interactions, back donation of electrons from the filled metal d_{xy} and d_{yz} orbitals to the vacant ligand π* orbital results in the strengthening of the M-X bond and weakening of the X-Y bond. Although the nature of these interactions defines the theoretical geometry of the M-X-Y linkage, distortions are to be expected in the protein matrix due to the interactions between the ligand and amino acid residues in close proximity.[6]

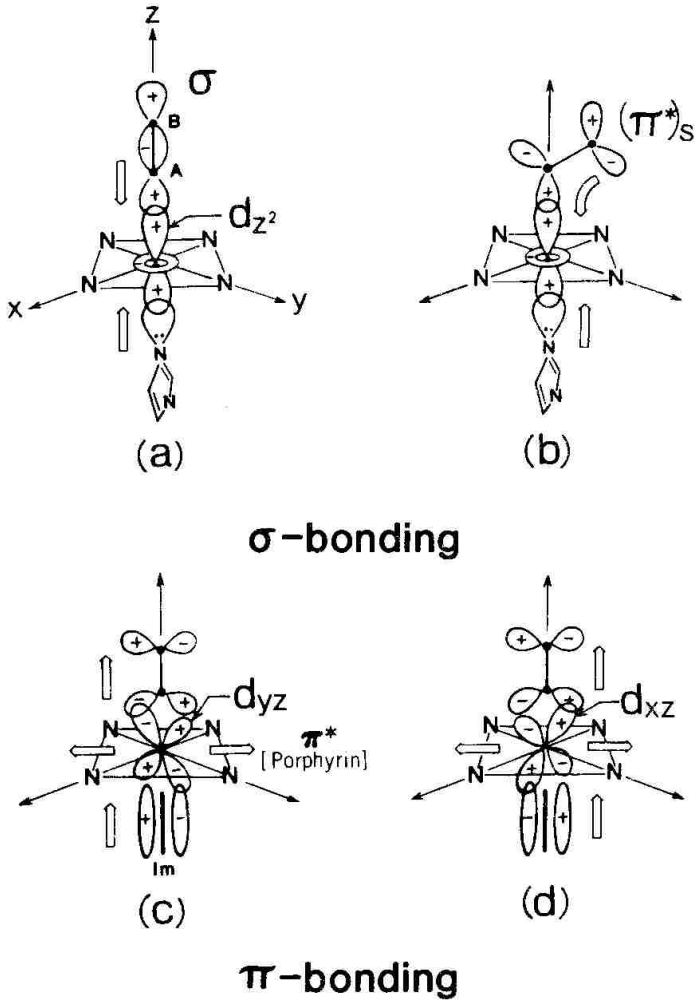

Figure 1.1.6 Schematic representation of σ- and π-bonding in heme proteins.[8]

1.1.3 Optical properties of cytochromes P450

The optical properties exhibited by cytochromes P450 enzymes allows for the use of a variety of spectroscopic tools in the quest for an understanding of the inherent chemistry observed in these proteins. The heme group in P450s gives rise to strong π-π* electronic transitions in the visible region due to the extended nature of the porphyrin aromatic system. The spectral features of a typical metalloporphyrin, ferrocytochrome c, are shown in the figure below (Figure 1.1.7).[6] The characteristic bands include an intense band at around 400 nm, the so-called B or Soret band and a pair of weak bands near 520 nm and 550 nm, referred to as Q_0(or α) and Q_1(or β) bands, respectively. The unsubstituted tetrapyrrole macrocycle has D_{4h} symmetry exhibiting two degenerate lowest unoccupied π* orbitals (LUMO) of e_g symmetry and two highest filled π orbitals (HOMO) of a_{1g} and a_{2u} symmetries. The energies of the two HOMOs are nearly the same allowing strong configuration interaction of the possible transitions, $A_{1u} \rightarrow E_g$ and $A_{2u} \rightarrow E_g$; addition of the transition dipoles gives rise to the strong Soret band whereas they nearly cancel out for the Q_0 transition. The apparent increase in intensity observed for the Q_1 transition is a result of vibronic mixing with the B transition.[6,34]

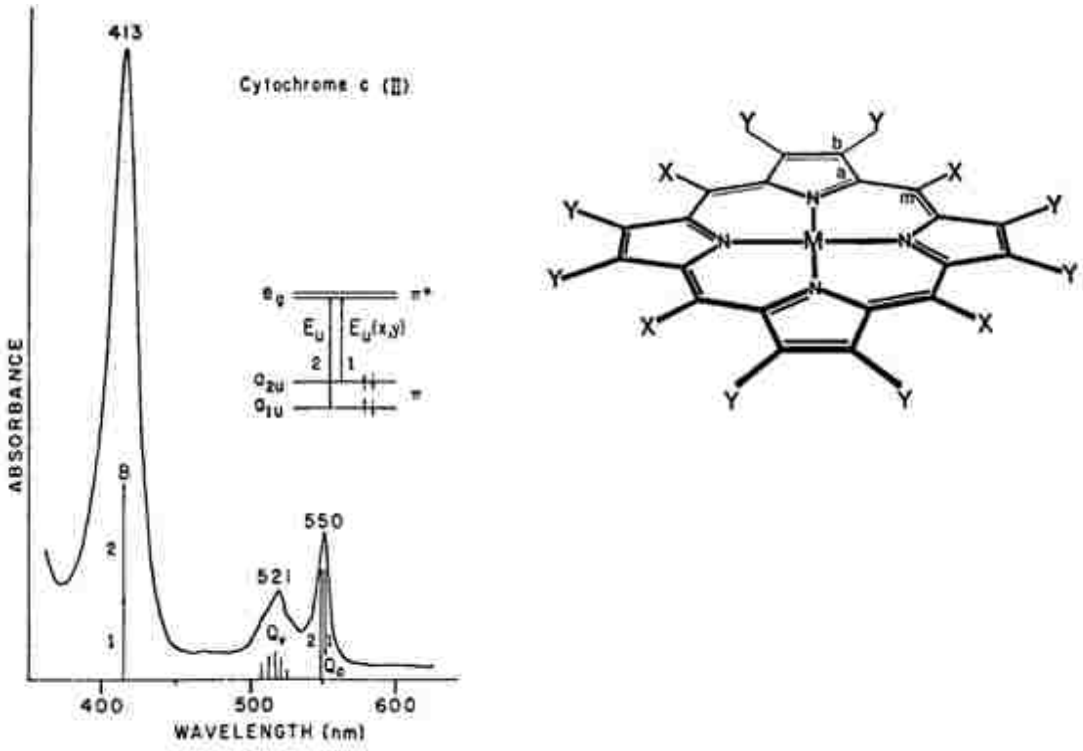

Figure 1.1.7 Absorption spectrum of Cytochrome c and the structure of a metalloporphyrin with D_{4h} symmetry[6]

The 6 coordinate low spin (6CLS) substrate-free P450cam exhibits a Soret absorption maximum at 418 nm, which shifts down to 391 nm upon binding of substrate. The downshift is associated with spin state change from the 6CLS to 5CHS (Figure 1.1.8).[35] Cytochrome P420cam, the inactive form of P450cam, has a Soret band at 420 nm, which is presumably the reduced carbonmonoxy form (reduced P420-CO form) exhibiting histidyl ligation. The proximal thiolate fifth ligand is thought to be replaced by a histidyl residue resulting in a lack of enzymatic activity giving evidence of the critical role played by the axial ligand in heterolytic cleavage of the dioxygen species trans to it.[36] However, later studies have suggested that the P420 form may be reasonably described as possessing a protonated thiol axial ligand.[37]

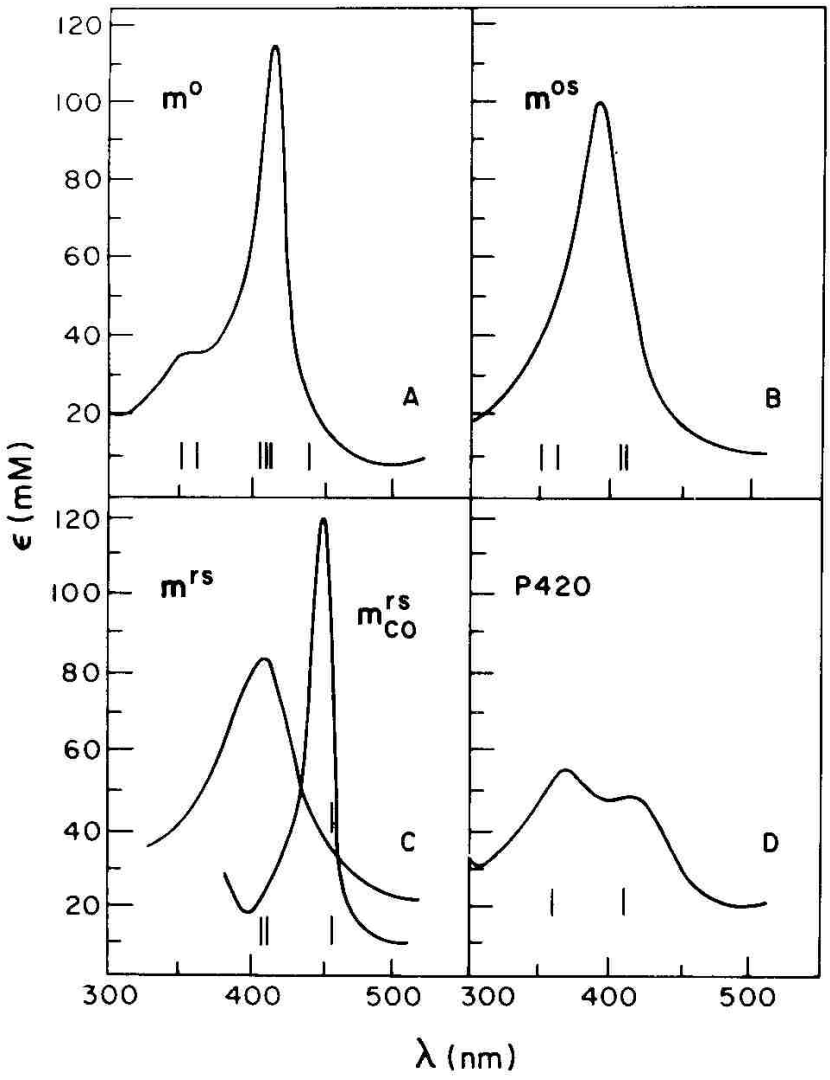

Figure 1.1.8 Absorption spectra of different forms of P450cam in the Soret region; Fe(III) substrate free (m^o), Fe(III) substrate bound (m^{os}), Fe(II) substrate bound (m^{rs}), Fe(II)-CO substrate bound (m^{rs}_{co}).[35]

1.2 Raman Spectroscopy

The Raman Effect phenomenon results when light from a laser source impinges upon a molecule and interacts with the electron cloud of the bonds making up the molecule. Interaction with the incident radiation may result in vibrational excitation of the molecule from its electronic ground state, ν_0 and/or a less populated vibrational excited state, ν_1 to a virtual energy state. Stokes Raman scattering, or the so-called spontaneous Raman Effect, is generated following vibrational relaxation whereby the energy of the scattered light is less than the incident radiation. Vibrational relaxation from a virtual excited to the electronic ground state (ν_0) results in Rayleigh or elastic scattering; that is, the energy of the incident photon is the same as that of the emitted photon. Excitation of the molecule already in a vibrational excited state (ν_1) followed by relaxation to a lower vibrational level (ν_0) produces anti-Stokes Raman scattering, as shown in the figure below (Figure 1.2.1). As expected and in accordance with the Maxwell-Boltzmann distribution law, Stokes Raman scattering exhibits stronger intensities than anti-Stokes since the vibrational excited levels (ν_1) are far much less populated than the ground state (ν_0); i.e., the intensities of the anti-Stokes Raman lines decreases rapidly as the vibrational frequencies increase. Consequently, conventional Raman spectroscopy considers the Stokes lines in which the scattered light intensities are reported as a function of the frequency difference from the monochromatic source or more commonly as Raman shifts. Key to the exhibition of the Raman Effect is the polarizability of the molecule with respect to the vibrational coordinate. The degree of polarizability is reflected in the Raman scattering intensity, whereas Raman shifts report on the molecular vibrational levels.

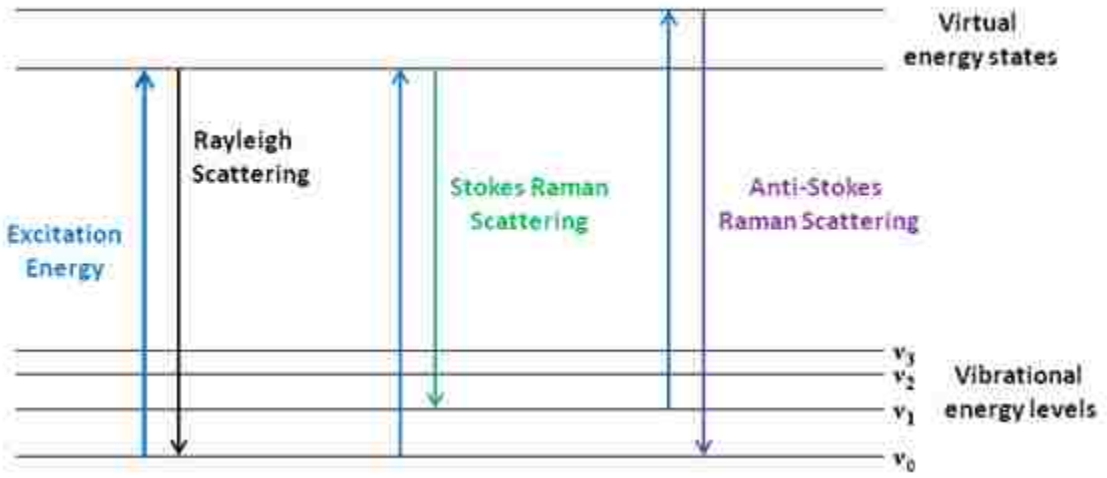

Figure 1.2.1 Schematic representation of the Raman Effect

1.2.1 Resonance Raman Spectroscopy

Resonance Raman spectroscopy involves measuring enhanced Stokes lines as the excitation frequency approaches the energy of the electronic transition of the target chromophore. The technique is ideally suited for studying complex biological molecules like heme proteins inasmuch as it permits active site interrogation owing to its ability to selectively enhance vibrational modes of the chromophoric heme prosthetic group.[38] This powerful spectroscopic tool has long been established as an exquisite probe of active site structure for a wide range of heme proteins and enzymes.[6,38,39] The technique offers a major advantage over IR spectroscopy in that there is no interference from water making it a method of choice for studying vibrational properties of proteins, samples of which are typically in aqueous buffers. The vibrational modes of the prosthetic heme group buried in the active site of these large biological polymers are selectively enhanced by exploiting laser (excitation) lines which are in or near resonance with the Soret or Q bands electronic transitions.

Isotopic labeling (^{15}N, ^{13}C and ^{2}H) of high symmetry model compounds, such as metal complexes of tetraphenylporphyrin (H_2TPP), octaethylporphyrin (H_2OEP), etioporphyrins (H_2(EtioI)) and (H_2(EtioIII), has been used to unambiguously assign heme core vibrational modes.[40,41] If each peripheral substituent of the iron protopophyrin IX complex is considered as a point mass, the heme has D_{4h} symmetry giving a total of 37 atoms and 105 vibrational modes. The modes consist of 71 in-plane (ip) modes (2N-3) and 34 out-of-plane (oop) modes (N-3) and are classified as follows:

$$\Gamma_{ip} = 9A_{1g} + 8A_{2g} + 9B_{1g} + 9B_{2g} + 18E_u$$

$$\Gamma_{oop} = 3A_{1u} + 6A_{2u} + 5B_{1u} + 4B_{2u} + 8E_g$$

Of the 71 in-plane vibrational modes 35 (g symmetry) are Raman active whereas 18 (E_u) are infrared active. These modes have been assigned for Ni^{2+} complexes of OEP, porphine and TPP using isotopic substitution and normal coordinate analysis and are given in the table below (Table 1.2.1).[6,42–45]

Most applications have focused on the so-called marker bands in the high frequency region, which effectively document oxidation and spin states of the central iron, in addition to providing a reliable indicator of heme core size.[6,40] The oxidation marker band (ν_4), occurring at ~1360 cm^{-1} in Fe(II) and ~1375 cm^{-1} in Fe(III) species, is ascribable to the pyrrole ring symmetric stretch, which is very sensitive to the oxidation state of the central iron. The so-called spin state marker bands (ν_2, ν_3 and ν_{10}) report on the core size and spin state of the iron center (Table 1.2.1). In recent years it has become increasingly apparent that low frequency modes (100-600 cm^{-1}) in the RR spectra of heme proteins are quite sensitive to active site structure changes that can induce out-of-

plane distortions of the macrocycle or alter the orientation of the heme peripheral substituents[46–55] (see Figure 1.1.1 for protoheme labeling scheme).

Table 1.2.1 Assignment and frequencies of in-plane vibrational modes of some nickel porphyrins complexes[6]

Symmetry	ν_i	Description	NiOEP	NiP	NiTPP
A_{1g}	ν_1	$\nu(C_m\text{-}X)$	[3041]	[3042]	1235
	ν_2	$\nu(C_\beta C_\beta)$	1602	1575	1572
	ν_3	$\nu(C_\alpha\text{-}C_m)_{sym}$	1520	1459	1470
	ν_4	ν(Pyr half ring)$_{sym}$	1383	1376	1374
	ν_5	$\nu(C_\beta\text{-}Y)_{sym}$	1138	[3097]	[3097]
	ν_6	ν(Pyr breathing)	804	995	1004
	ν_7	δ(Pyr def)$_{sym}$	674	731	889
	ν_8	ν(Ni-N)	360/343	369	402
	ν_9	$\delta(C_\beta\text{-}Y)_{sym}$	263/274	1066	1079
B_{1g}	ν_{10}	$\nu(C_\alpha\text{-}C_m)_{asym}$	1655	1650	1594
	ν_{11}	$\nu(C_\beta C_\beta)$	1577	1505	1504
	ν_{12}	ν(Pyr half ring)$_{sym}$	1331	1319	1302
	ν_{13}	$\delta(C_m\text{-}X)$	1220	1185	238
	ν_{14}	$\nu(C_\beta\text{-}Y)_{sym}$	1131	[3097]	[3097]
	ν_{15}	ν(Pyr breathing)	751	1003	1009
	ν_{16}	δ(Pyr def)$_{sym}$	746	730	846
	ν_{17}	$\delta(C_b\text{-}Y)_{sym}$	305	1060	784
	ν_{18}	ν(Ni-N)	168	237	277
A_{2g}	ν_{19}	$\nu(C_\alpha\text{-}C_m)_{asym}$	1603	1611	1550
	ν_{20}	ν(Pyr quarter ring)	1394	1354	1341
	ν_{21}	$\delta(C_m\text{-}X)$	1307	1139	[257]
	ν_{22}	ν(Pyr half ring)$_{asym}$	1121	1005	1016
	ν_{23}	$\nu(C_\beta\text{-}Y)_{asym}$	1058	[3087]	[3087]
	ν_{24}	δ(Pyr def)$_{asym}$	597	806	828
	ν_{25}	δ(Pyr rot.)	551	429	560
	ν_{26}	$\delta(C_\beta\text{-}Y)_{asym}$	[243]	1317	1230
B_{2g}	ν_{27}	$\nu(C_m\text{-}X)$	[3041]	[3041]	1269
	ν_{28}	$\nu(C_\alpha\text{-}C_m)_{sym}$	1483	1504	[1481]
	ν_{29}	ν(Pyr quarter ring	1407	1368	1377
	ν_{30}	ν(Pyr half ring)$_{asym}$	1160	1003	1004
	ν_{31}	$\nu(C_\beta\text{-}Y)_{asym}$	1015	[3088]	[3087]
	ν_{32}	δ(Pyr def)$_{asym}$	938	819	869
	ν_{33}	δ(Pyr rot.)	493	435	450
	ν_{34}	$\delta(C_\beta\text{-}Y)_{asym}$	197	1193	1191
	ν_{35}	δ(Pyr tranl.)	144	197	109
E_u	ν_{36}	$\nu(C_m\text{-}X)$	[3040]	[3042]	[1254]
	ν_{37}	$\nu(C_\alpha\text{-}C_m)_{asym}$	[1637]	1624	[1586]
	ν_{38}	$\nu(C_\beta C_\beta)$	1604	1547	[1552]
	ν_{39}	$\nu(C_\alpha\text{-}C_m)_{sym}$	1501	1462	[1473]
	ν_{40}	ν(Pyr quarter ring)	1396	1385	[1403]
	ν_{41}	ν(Pyr half ring)$_{sym}$	[1346]	1319	[1331]
	ν_{42}	$\delta(C_m\text{-}X)$	1231	1150	[233]
	ν_{43}	$\nu(C_\beta\text{-}Y)_{sym}$	1153	[3097]	[3097]
	ν_{44}	ν(Pyr half ring)$_{asym}$	1133	1033	[1003]
	ν_{45}	$\nu(C_\beta\text{-}Y)_{asym}$	996	[3087]	[3100]
	ν_{46}	δ(Pyr)$_{asym}$	927	806	[864]
	ν_{47}	ν(Pyr breathing)	766	995	[1023]
	ν_{48}	δ(Pyr)$_{sym}$	605	745	[895]
	ν_{49}	δ(Pyr rot.)	544	366	[512]
	ν_{50}	ν(Ni-N)	[358]	420	[436]
	ν_{51}	$\delta(C_b\text{-}Y)_{asym}$	328	1064	[1093]
	ν_{52}	$\delta(C_\beta\text{-}Y)_{sym}$	263	1250	[1213]
	ν_{53}	δ(Pyr transl)	212	282	[306]

1.2.2 RR spectroscopy of cytochromes P450

RR spectroscopy has unraveled a wealth of information on the structure and function of cytochrome P450cam, which has since been considered as a prototype for the cytochrome P450 gene family.[35,56–58] The heme vibrational modes of the substrate-free and substrate bound forms of both the ferric and ferrous states of P450cam have been assigned (Table 1.2.2).[36] In the high frequency region the oxidation state marker band (ν_4) occurring at 1374 cm^{-1} for the 6CLS substrate free P450cam (m^o) and 1370 cm^{-1} for the 5CHS camphor bound P450cam (m^{os}) are characteristically shifted to lower frequency as compared to other heme proteins (Figure 1.2.2, **A**). This was attributed to the presence of a strong electronic donating axial fifth ligand of the iron center, which has since been documented to be the mercaptide of cysteine.[39,59] RR studies of isotopically labeled P450cam confirmed the presence of the Fe-S bond, exhibiting a ν(Fe−S) that occurs at 351 cm^{-1} that is observed only for the (5CHS) substrate bound form (Figure 1.2.3).[56] The 6CLS substrate free P450cam spin state marker bands occurring at 1503 and 1638 cm^{-1} down shift to 1488 and 1624 cm^{-1}, respectively, upon binding of substrate, indicating spin state conversion to the 5CHS camphor bound P450cam (Figure 1.2.2, **B**).[60]

Table 1.2.2 P450cam heme modes assignment[36]

Sample	ν_8	ν_{35}	δCbCαCβ	ν_7	ν_{15}	ν_4	ν_3	ν_2	ν_{10}
m^o	347	379	424	678	753	1373	1503	1584	1635
m^{os}	347	379	424	678	755	1372	1488	1570	1623
m^r	345	378	418	674	747	1345	1468	1563	1601
m^{rs}	345	378	415	674	747	1345	1466	1564	1601
$m^r{}_{co}$	352	379	423			1371	1497	1588	
$m^{rs}{}_{co}$						1372	1498	1583	1626

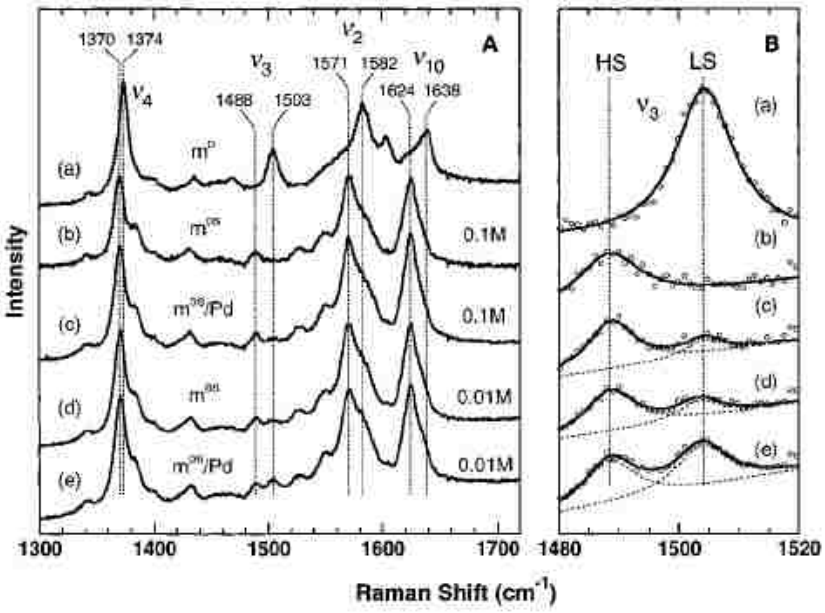

Figure 1.2.2 Resonance Raman spectra of ferric P450cam and its complex with oxidized putidaredoxin in the (**A**) high frequency region and (**B**) ν_3 spin state marker regions[60]

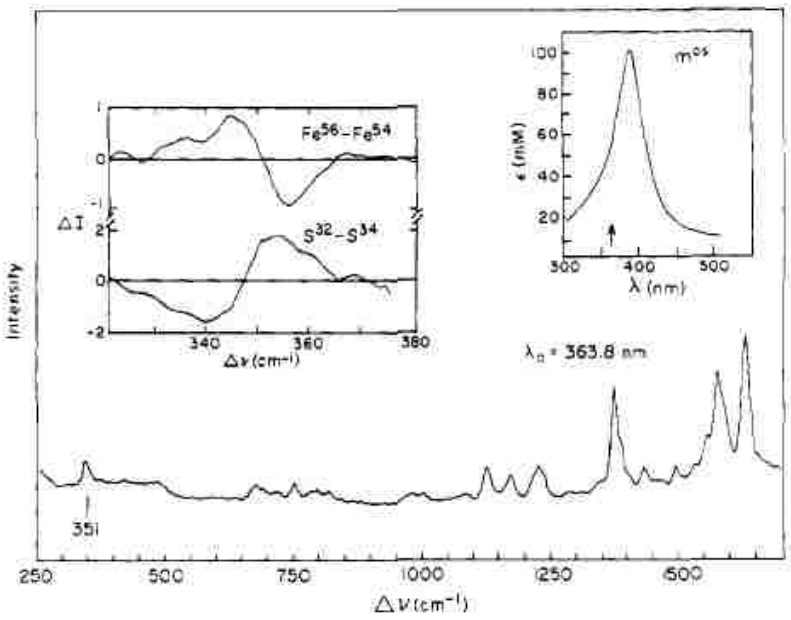

Figure 1.2.3 Resonance Raman spectrum of ferric camphor-bound P450cam is shown in the lower curve. The insert on the right is the absorption spectrum indicating the excitation line and on the left are the difference spectra in the region of the 351 cm^{-1} Raman mode[56]

The RR spectrum of the reduced 5CHS substrate bound form of P450cam (m^{rs}) exhibits anomalously low frequency ν_4 (1346 cm^{-1}) and ν_3 (1466 cm^{-1}) modes compared to other ferrous heme proteins due to the strong π donation by the axially coordinated cysteine thiolate.[39] In the P450cam catalytic cycle (Figure 1.1.4), reduction of the substrate bound P450cam is followed by oxygen binding resulting in the formation of a relatively unstable dioxygen adduct of P450cam (**4**). RR evidence of the formation of the dioxygen adduct were provided by Champion and coworkers,[61] who observed the strongly enhanced ν(O−O) mode near 1140 cm^{-1}, and by Hu *et al*,[62] who observed the ν(Fe−O_2) at ~540 cm^{-1}. Interestingly, Hu and coworkers also showed that two ν(O−O) are seen at 1139 cm^{-1} and 1147 cm^{-1} for the dioxygen adduct of the P450cam/adamantanone complex. The detection of the two ν(O−O) modes was attributed to the existence of two distinct substrate configurations at the binding site, this proposal

being consistent with X-ray crystallography results reported for the adamantanone-bound P450cam (Figure 1.2.4).[63]

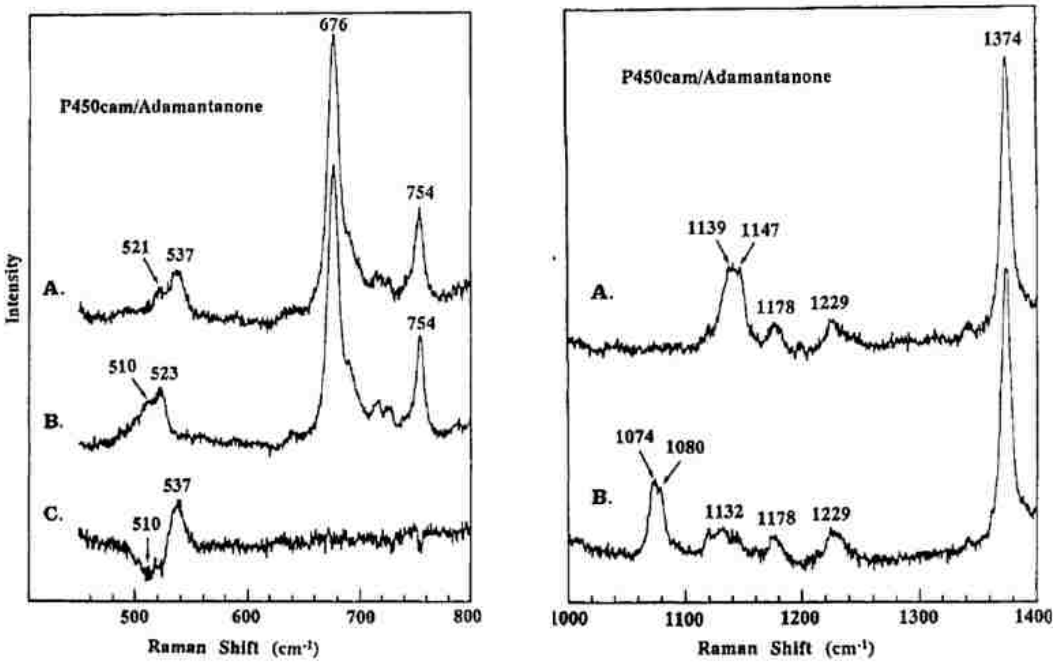

Figure 1.2.4 The low (left traces) and high (right traces) frequency spectra of the dioxygen adduct of adamntanone bound P450cam; trace A, $^{16}O_2$; trace B, $^{18}O_2$; trace C, difference spectrum A-B[62]

More recently, cryogenic RR detection of the $\nu(^{16}O-^{16}O)$ mode occurring at 1140 cm^{-1} and the corresponding $\nu(^{18}O-^{18}O)$ at 1074 cm^{-1} of the oxyferrous complex of the D251N mutant of P450cam has been reported (Figure 1.2.5).[20] In the natural catalytic cycle, the overall rate limiting step in the hydroxylation of camphor is the reduction of the dioxygen adduct. This step is facilitated by the redox partner, putidaredoxin, which delivers a second electron to the dioxygen-bound ferrous state of P450cam yielding the ferric peroxo intermediate. These species do not accumulate to large enough population due to their rapid decay under turnover conditions, complicating spectral investigation

efforts. A cryoradiolytic reduction method, which utilizes γ-rays to generate free electrons from frozen aqueous buffer containing glycerol, was developed by Symons[64] and further refined by Hoffman and Davydov, and coworkers[30,65–68] and has been employed in the reduction of cryotrapped oxyferrous complex of P450cam. An EPR and ENDOR study of cryoradiolytically reduced dioxygen adducts of wild type and D251N mutant P450cam reported generation of the hydroperoxo and peroxo intermediates respectively.[30,65] The peroxo intermediate in the wild type protein, eluded detection following irradiation owing to the active site structure, which facilitates delivery of the first proton of catalysis even at 77 K yielding the hydroperoxo intermediate instead.[30,65] On the other hand, in the D251N mutant P450cam, proton delivery to the active site is hindered. This gave a distinct EPR signature characteristic of the peroxo intermediate, which, upon annealing, converted to a spectrum consistent with the hydroperoxo intermediate.[30,65] In another study, utilization of this mutant permitted RR detection of two isotopically sensitive modes occurring at 553 cm^{-1} and 792 cm^{-1} exhibiting shifts of 27 and 38 cm^{-1} respectively.[20] These have been reasonably assigned to the ν(Fe−O) and ν(O−O) of the peroxo intermediate of the cyroreduced oxyD251N samples since no H/D shifts were observed at 77 K (Figure 1.2.6). Proton delivery to the active site in this mutant was cleverly achieved by annealing the peroxo species to ~ 180 K; resulting in the hydroperoxo intermediate characterized by RR spectroscopy.[20] As expected H/D shifts in the RR spectra of annealed samples of irradiated oxyD251N were observed for the modes occurring at 564 cm^{-1} and 774 cm^{-1} consistent with the ν(Fe−O) and ν(O−O) stretching frequencies of the hydroperoxo intermediate of the D251 mutant P450cam (Figure 1.2.7).[20] However, the highly reactive ferryl species, the equivalent of the so-

called compound I of peroxidases, presumably formed by cleavage of the O−O bond, has eluded spectroscopic characterization under turnover conditions.

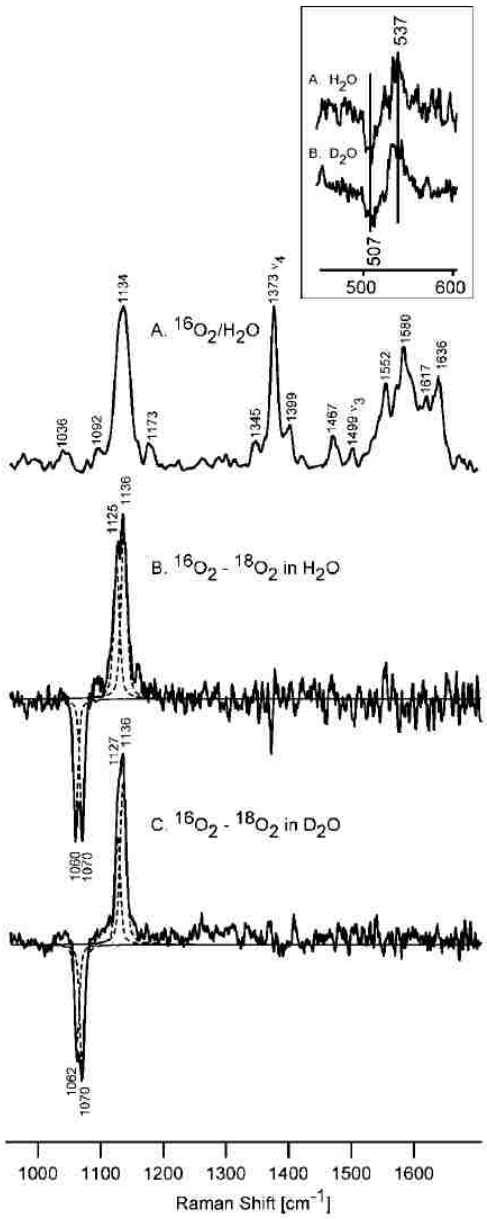

Figure 1.2.5 The high frequency RR spectra of the dioxygen complex of the D251N mutant of P450cam. Inset shows the difference spectra in the low frequency ν(Fe−O) region[20]

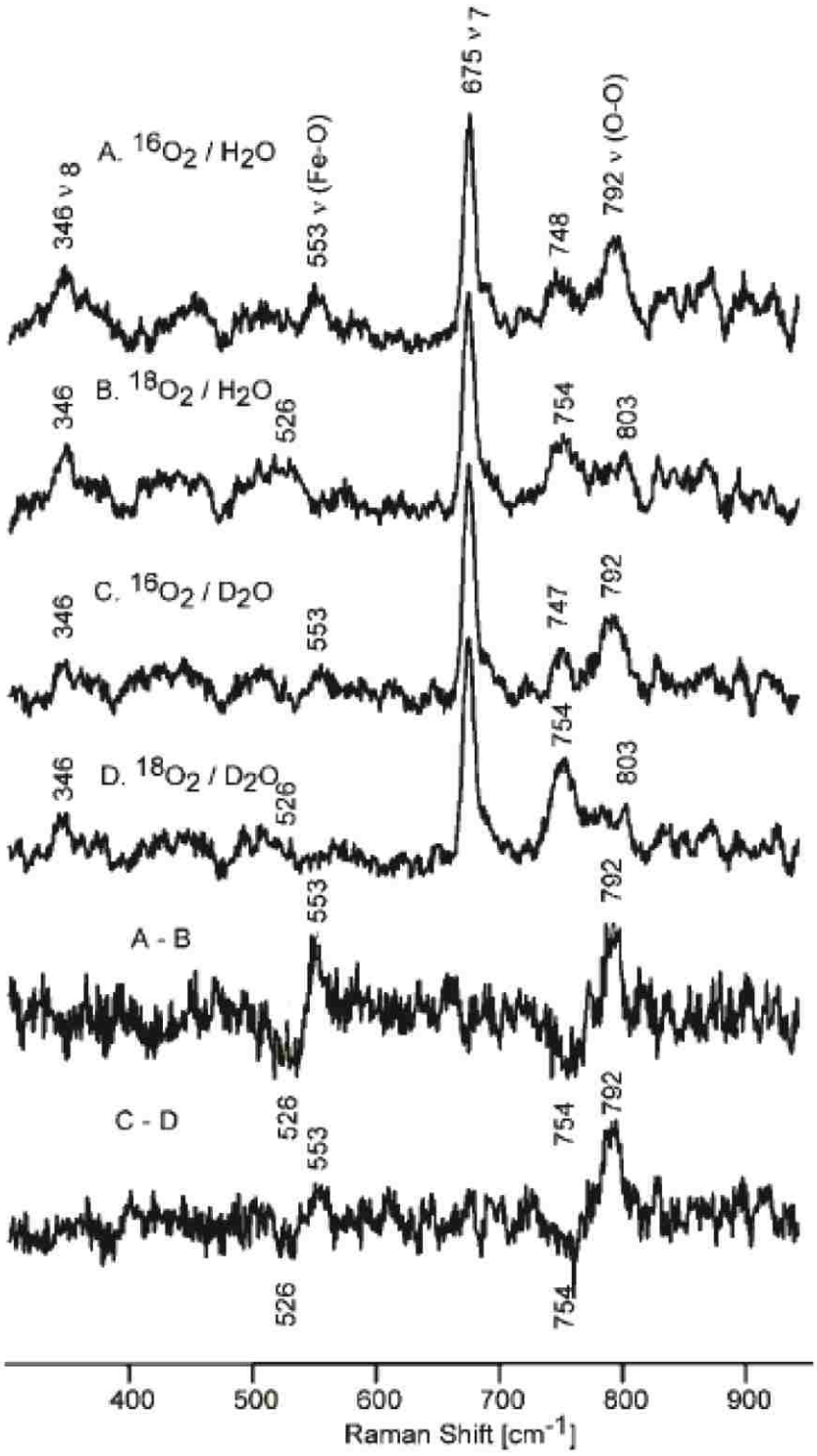

Figure 1.2.6 RR spectra of irradiated dioxygen adducts of P450 D251N in H_2O buffer, spectra A ($^{16}O_2$) and B ($^{18}O_2$), and in D_2O buffer, spectra C($^{16}O_2$) and D ($^{18}O_2$). The two bottom traces shows the difference spectra of $^{16}O2$-$^{18}O_2$ in H_2O and D_2O buffers[20]

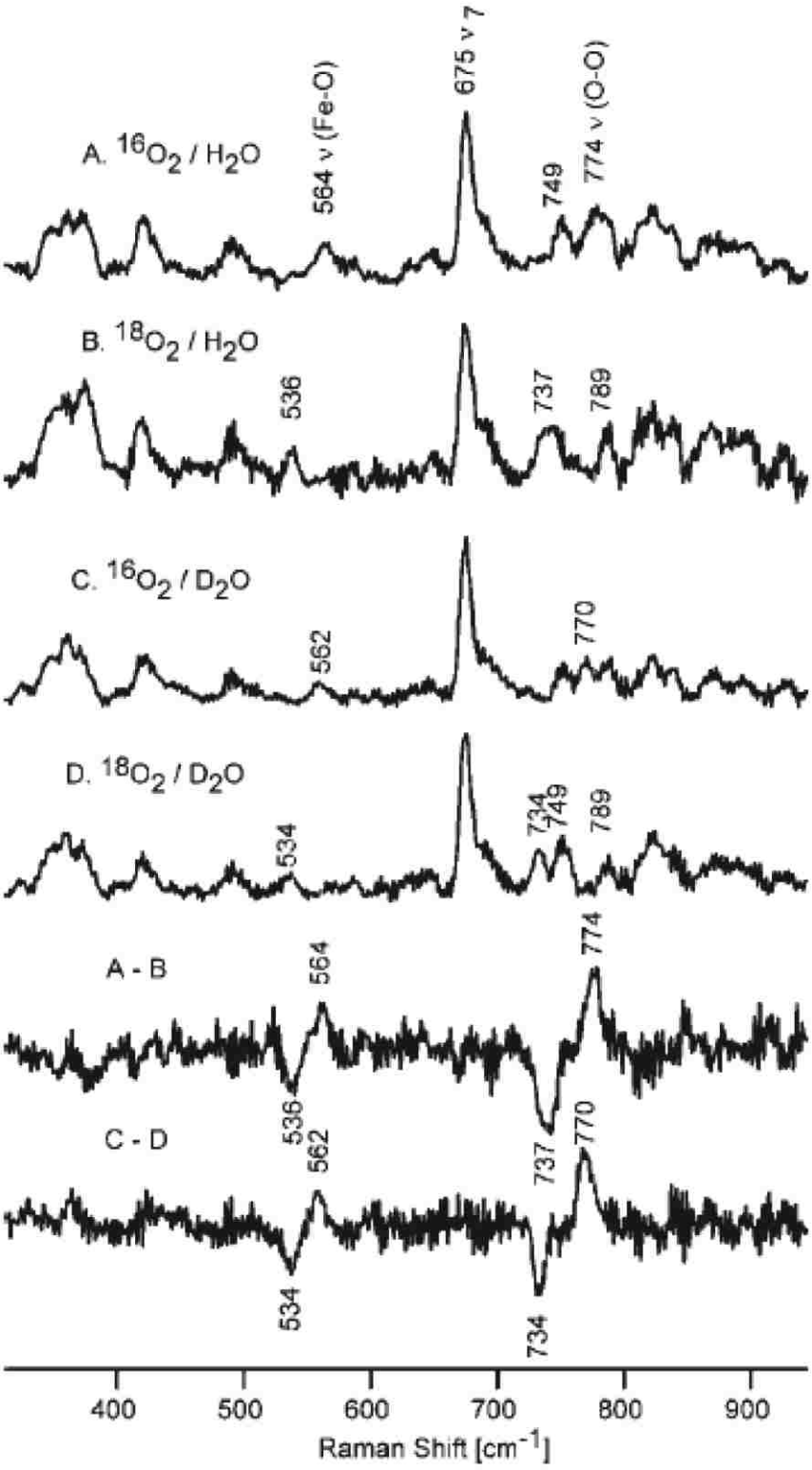

Figure 1.2.7 RR spectra of irradiated and annealed (at 185 K) samples of oxyD251N in H_2O buffer, spectra A ($^{16}O_2$) and B ($^{18}O_2$), and in D_2O buffer, spectra C ($^{16}O_2$) and D ($^{18}O_2$). The two bottom traces show the difference spectra of $^{16}O_2$-$^{18}O_2$ in H_2O and D_2O buffers[20]

1.3 NMR spectroscopy of heme proteins

Nuclear magnetic resonance (NMR) spectroscopy of heme proteins dates back to 1962 when the first ^{1}H NMR of a paramagnetic cytochrome *c* was obtained.[69,70] Researchers have since then utilized NMR methods unveiling a wealth of useful structural and functional properties of heme proteins in solution, which is an obviously important addition to structural determination, a realm previously dominated by x-ray crystallography. Paramagnetic heme proteins induce enhanced relaxation of surrounding NMR detectable signals due to electron-nuclear hyperfine interaction as a function of nuclei distances from the heme iron.[71] As a consequence the prosthetic group chemical shifts experience isotropic shifts and are well resolved outside the diamagnetic protein envelope. These paramagnetic shifts are composed of scalar (contact) and dipolar (through space) contributions of the unpaired electron onto surrounding nuclei.[71] The observation of well resolved heme proton signals has allowed for the development of NMR methods employed in the investigation of structure and dynamics in paramagnetic proteins. One obvious drawback of these extremely short relaxation times of paramagnetic signals is their inherent large line widths as compared to corresponding isostructural diamagnetic molecules. This finding complicates efforts to utilize multi-dimensional NMR experiments in structural studies due to loss of magnetization. Methods have, however, been developed to enhance the paramagnetic signals in heme proteins and allowed for the assignment of heme methyl resonances. Specifically, the so-called paramagnetic signals enhancement (PASE) method was applied in 1D and 2D experiments of high and low spin ferric complexes of the bacterial P450cam leading to the assignment of heme ^{1}H methyl resonances (Table 1.3.1).[72]

Table 1.3.1 ^{1}H NMR assignments of the heme methyl resonances for ferric high and low spin P450cam[72]

	Fe^{III} (+ cam) high-spin 313 K	Fe^{III} (– cam) low-spin 298 K	Fe^{III}–nBuNC low-spin 313 K	Fe^{III}–nBuNC low-spin 298 K	Fe^{III}–EtNC low-spin 298 K
5-CH_3	37.6	19.3	24.9	25.9	25.4
1-CH_3	33.5	14.2	16.8	17.1	17.2
8-CH_3	58.1	–	4.9	5.4	5.5
3-CH_3	52.6	–	–1.5	–1.7	–1.7

Binding of exogenous high field ligands such as the cyanide ion shifts the heme iron spin state from high to low spin, which exhibits slightly reduced line widths and affords some increased stability of the protein as in the case of P450cam allowing for high temperature experiments.[72] The assignment of heme proton resonances of the cyano complex of P450cam has been reported previously (Figure 1.3.1).[73]

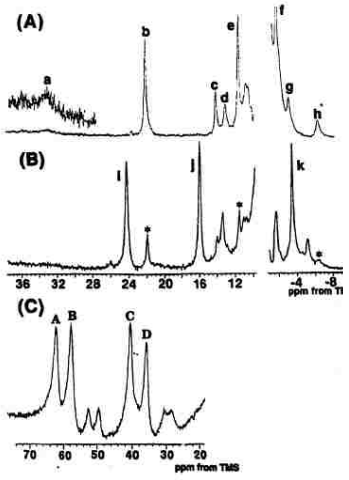

P450cam signal	*Chemical shift (ppm)*			*Assignment*
	Wild-type	*T252A*	*T252V*	
a	33.1	34.5	29.6	
b	22.1	22.1	22.1	8-CH_3 [a,b]
c	14.1	14.4	–[c]	
d	13.0	12.7	–[c]	Propionate α-CH[a]
e	11.5	11.1	12.8	3-CH_3[a,b]
f	–1.6	–1.6	–2.4	CH_3 for (Val or Leu)[a]
g	–3.0	–3.2	–[c]	
h	–6.3	–6.2	–6.7	
i	24.3	24.1	24.2	Heme methyl[a]
j	16.0	16.8	16.9	Heme methyl[a]
k	–3.4	–3.2	–3.6	
A	62.1	61.8	62.7	5- or 1-CH_3[b]
B	57.8	57.8	58.5	5- or 1-CH_3[b]
C	40.1	39.8	40.1	8-CH_3[b]
D	35.8	37.6	38.7	3-CH_3[b]

Figure 1.3.1 ^{1}H NMR of camphor-free (B), camphor bound (B) cyanoP450cam and ferric high spin camphor bound P450cam. Insert table shows assignment of heme proton resonances.[73]

As mentioned previously, ligands in the distal pocket of the heme proteins have been used as spectroscopic probes. Recently, Sem and coworkers have demonstrated the use of ^{13}C-methyl isocyanide bound to the heme iron of both bacterial and mammalian P450s as a potential NMR probe for the elucidation of structural and electronic changes in P450 active sites.[74]

^{13}C NMR (an established powerful ally of ^{1}H NMR) application in the study of heme proteins has previously lagged behind mainly due to the low sensitivity and natural abundance of the ^{13}C nuclei, but has recently gained a lot of interest due to the impressive development of high field NMR instruments and methods for judiciously enriching specific carbon atoms of the heme prosthetic group. An understanding of the heme biosynthetic pathway coupled with the developments in recombinant DNA technology has allowed for the production of isotopically enriched prosthetic groups (Figure 1.3.2). ^{13}C labeled heme groups have been produced by supplementing bacterial cultures with labeled δ-aminolevulinic acid (ALA), which is the first committed precursor in the heme biosynthetic pathway (Figure 1.3.3).[75–77]

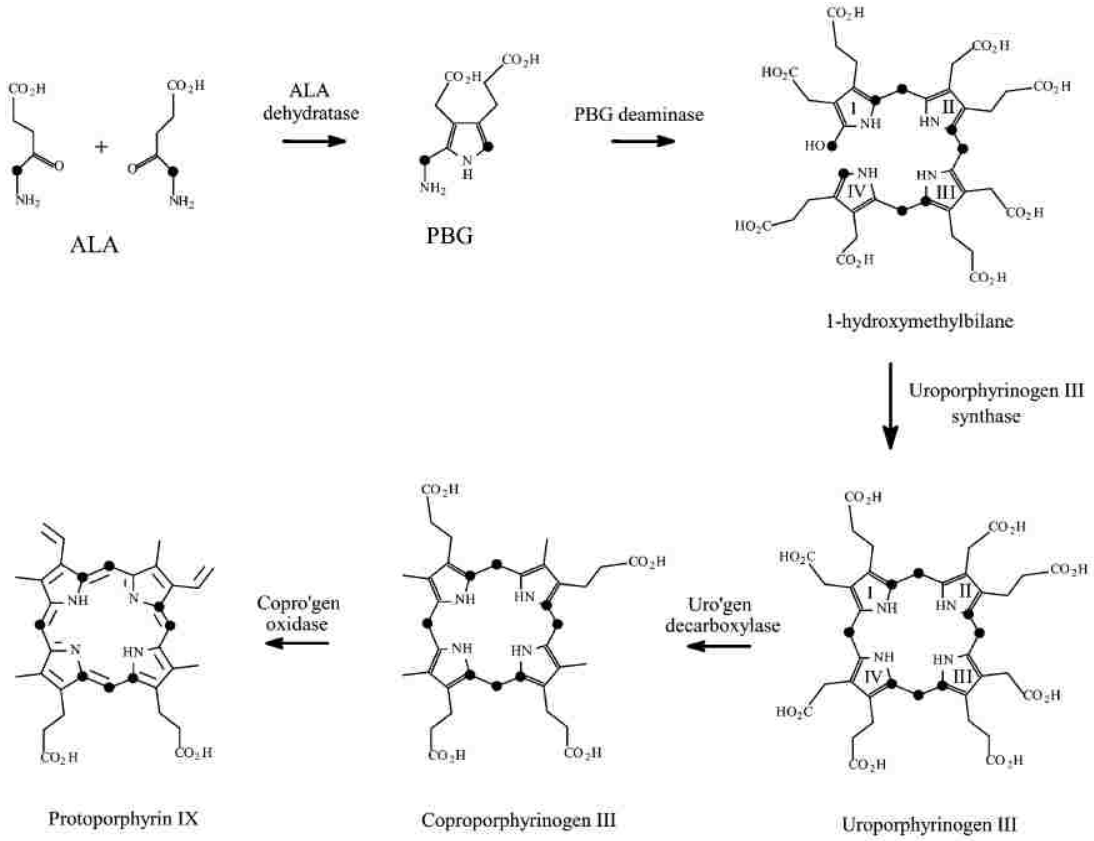

Figure 1.3.2 Biosynthesis of ^{13}C enriched (black dots) protoporphyrin IX[75]

Recently, an *E.coli* strain, the so-called HU227, lacking the δ-aminolevulinic acid (δ-ALA) synthase gene has been exploited for the heterologous expression of P450s harboring prosthetic groups, which are close to 100% ^{13}C labeled at the C_m and C_α positions (Figure 1.3.3, **B**), by growing the cells in the presence of [5-^{13}C] δ-aminolevulinic acid (ALA).[78]

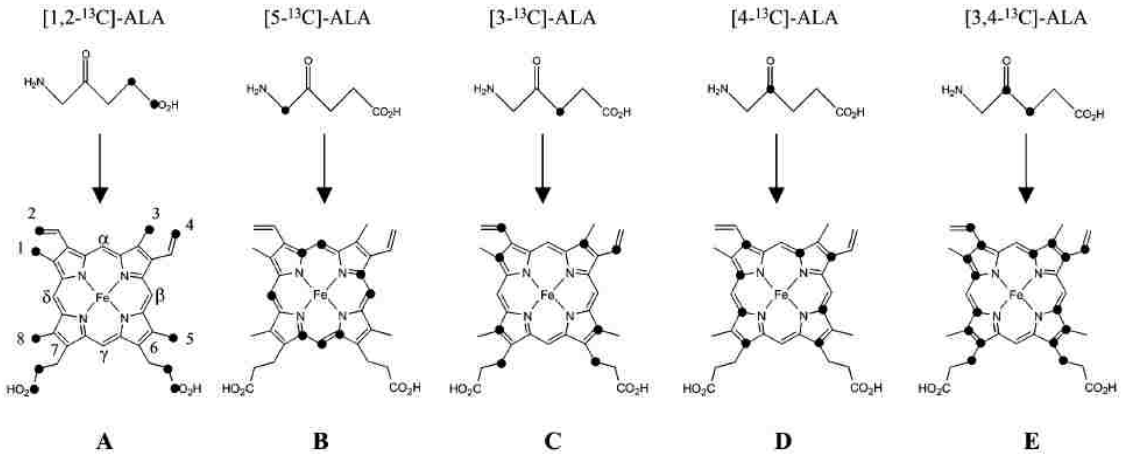

Figure 1.3.3 Enrichment of the heme group at various positions using isotopically labeled δ-ALA[75]

These developments have allowed the utilization of ^{13}C NMR as a useful tool in the elucidation of important structural information in paramagnetic heme proteins.^{13}C chemical shifts in enriched samples of ferric high spin myoglobin have been demonstrated to report on the coordination state of the heme protein.[79] Selective ^{13}C enrichment of the bacterial cytochrome c_{552} heme cofactor was achieved by expressing the cells in minimal media supplemented with [5-^{13}C] δ-ALA.[80] The observation of meso signals, which otherwise may prove to be a challenge owing to their being buried in the protein diamagnetic region, was made possible by ^{13}C enrichment allowing for the application of a proton-detected single-bond correlation experiment commonly known as ^{1}H-^{13}C heteronuclear multiple-quantum correlation (HMQC). This correlation of coupled heteronuclear spins across a single bond provides connectivities between proton and carbon nuclei of a given compound. The 2D spectrum shown in Figure 1.3.4[80], exhibits crosspeaks correlated to attached nuclei at the four meso positions.

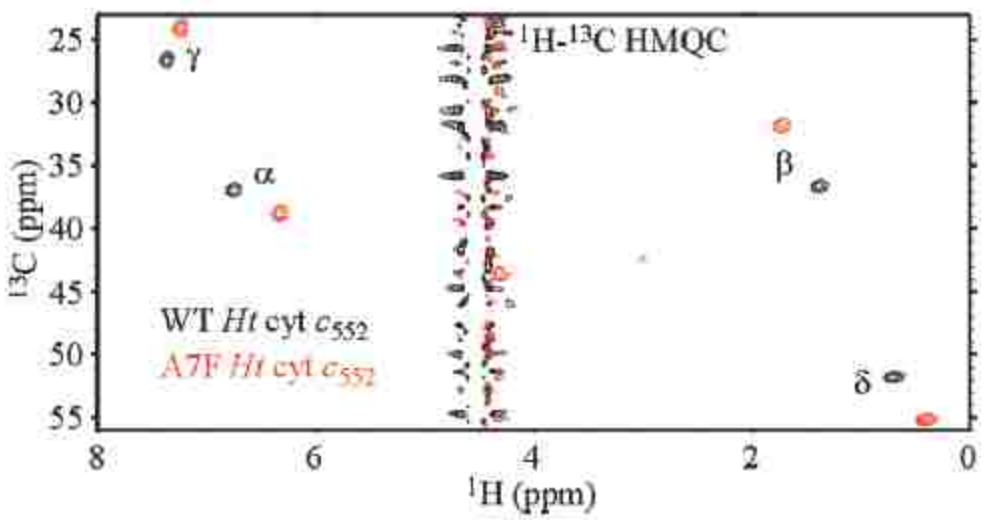

Figure 1.3.4 ^{1}H-^{13}C HMQC spectra of oxidized wild type (WT) and mutant AF7 [5-^{13}C] δ-ALA *Hydrogenobacter thermophilus* (*Ht*) cytochrome c_{552}[80]

The assignment of meso ^{1}H and ^{13}C resonances was achieved by ^{1}H-^{13}C HMQC and ^{1}H-^{1}H nuclear Overhauser effect (NOE) experiments. NOE experiments involve the magnetic interaction of nuclei spins through space or the so-called dipolar coupling in contrast to scalar coupling in the HMQC technique. Thus the technique can be used in 3D structural investigations establishing spatial proximity between protons. These techniques were exploited to demonstrate the potential of the heme meso ^{1}H and ^{13}C resonances as NMR probes for heme ruffling OOP deformations.[80] The ability to selectively enrich the heme core carbon opens up the possibility of utilizing NOE experiments in mapping the active site architecture. This finding is potentially ground breaking in as much as it allows for active site interrogation of proteins in solution, including drug metabolizing P450s, for which few crystal structures with substrates exists.

Computational docking is routinely employed in the prediction of binding affinities of potential substrates and inhibitors of drug metabolizing P450s. Essentially a lowest energy P450-substrate/inhibitor complex is obtained after optmization, which

involves calculatation of energies of interaction between protein and ligand. Unfortunately, efficient and accurate prediction of protein-ligand interactions by these computational methods is compromised by the inherent flexibility of drug metabolism P450s binding sites, such as in CYP2D6, which metabolizes 20-30% of all drugs. NOE experiments on P450s bearing heme groups or active site residues with judiciously placed isotopic labels could be exploited in defining solution phase active site structure. Specifically, NOE measurements of interatomic distances between reference points on the heme group and active side residues will provide a map of the substrate-free active site. Employing several substrates in the pocket and obtaining NOE derived distances between reference points (^{13}C- enriched heme core carbons and /or ^{13}C-labeled amino acid residues in the active site) and substrate protons will provide information on the flexibility/rigidity of P450s active site. Inasmuch as mapping of these flexible active sites is computationally demanding, employing expereimentally derived interatomic distances in docking routines would speed the process and potentially lead to more accurate pridictions of substrate or inhibitor interactions with the drug metabolizing P450.

1.4 Specific issues to be addressed in this work

1.4.1 Utilization of chemically inert substrates to stabilize compound I intermediates of P450s

In the widely accepted natural catalytic cycle, the highly reactive Fe(IV)=O porphyrin π-cation (**6**) radical or the so called compound I intermediate, which results from a proton assisted scission of the O-O bond has eluded spectroscopic characterization, presumably owing to its inherently short life time and has recently earned the "mystery" title.[81] In recent years several experimental approaches have been used to artificially produce compound I and investigate its electronic structure and reaction kinetics.[82–91] The application of spectroscopic methods in the characterization of these species has been reviewed recently.[92,93] An artificially produced compound I form of CYP119 has been reported to be an Fe(IV)=O-porphryin π-cation radical, exhibiting a ferryl iron spin (S=1) that is antiferromagnetically coupled to the S` = ½ of the porphyrin radical, giving a total spin of ½, equivalent to the ground state of chloroperoxidase compound I.[85] The obvious interest in this highly reactive intermediate calls for the development of effective capture strategies (or trapping experiments), ideally in the natural catalytic cycle leading to the subsequent characterization of the "true" compound I form of these biological catalysts. The present work is focused on efforts to generate, trap and spectroscopically characterize the elusive potent compound I intermediate of P450s under turn over conditions. Specifically, utilization of chemically inert substrates of P450s were investigated as a possibly viable method of stabilizing the transient and highly oxidizing Fe(IV)=O porphyrin π-cation radical intermediate occurring in the P450 catalytic cycle (**6** in Figure 1.1.4) allowing for its characterization by RR methods. This strategy was initially applied to the P450cam system utilizing perfluoroadamantanone

(PFA) as a chemically inert substrate and later to the thermophilic bacterial P450, CYP119, where perfluorinated long chain fatty acids were employed as inert substrates.

1.4.2 NMR spectroscopy characterization of isotopically labeled P450s

This study aims at employing NMR methods to allow solution phase active site structure determination of P450s bearing isotopically labeled heme groups. Specifically, NOE experiments will be exploited to derive distances between heme reference points and substrate protons providing enhanced active site definition in the solution phase. NOE measurements will also be employed to establish spatial proximity between the heme reference points and active site residues. ^{13}C-enriched P450 active side residues will also be exploited as reference points for establishing spatial proximity to substrate protons. Employing different substrates and derivation of distances between substrate protons and active site reference points will provide information on the flexibility and/or rigidity of the P450 active site. An extension of this approach to important drug metabolizing enzymes such as CYP2D6 has the potential to furnish valuable experimental restrictions in docking routines, which are commonly employed in determining the relative affinities of drug candidates. A recent and novel approach for the isotopic labeling of the prosthetic group in heme proteins has been exploited to produce a ^{13}C analogue of the soluble bacterial cytochrome P450cam.[78] Briefly, the HU227 strain of E. coli that lacks the δ-aminolevulinic acid (δ-ALA) synthase gene was employed in the heterologous expression of P450cam harboring a prosthetic group ^{13}C labeled at the Cm and Cα positions (Figure 1.3.3) by growing cells in the presence of [5-^{13}C] δ-ALA synthesized in four steps from [2-^{13}C] glycine.[94,95] This system has been employed in a

“proof of principle” exercise for the strategy of defining active site structure using NMR methods.

CHAPTER 2 UTILIZATION OF FLUORINATED SUBSTRATES TO STABILIZE COMPOUND I INTERMEDIATES OF CYTOCHROME P450

2.1 Perfluorinated substrates of P450cam

2.1.1 Introduction

Initial efforts to employ chemically inert substrates as a possible strategy to stabilize and capture the compound I forms of P450s were performed using perfluoroadamantanone (PFA) [96] and the bacterial cytochrome P450cam.The major pitfall of using PFA as a P450cam substrate is its apparent lack of solubility in aqueous buffer. The alcohol derivative of PFA denoted PFA-ol, however has been reported to be soluble in a 1:1 methanol-water solution.[97] Owing to limited quantities of PFA, optimization of the reduction procedure to obtain PFA-ol was done using 2-adamantanone. The product of 2-adamantanone reduction, 2-adamantanol, dissolved in a methanol/water solution (1:1 ratio by volume), was shown to bind substrate-free P450cam with almost 100% spin state conversion of the heme from low spin to high spin (Figure 2.1.1). It was also established that reduction of PFA resulted in an impure product, which exhibited partial binding to substrate-free P450cam (Figure 2.1.2). The suggested reasons for the partial binding observed were thought to be false substrate stock concentration (due to the impure substrate) and that possibly PFA-ol only binds partially to P450cam as an inherent characteristic (thus not achieving 100% spin state conversion, see Figure 2.1.2). This required further optimization of the PFA reduction procedure; however the major setback was the dwindling quantities of stock starting material. In view of this drawback, 2-adamantanone was used for further optimization of the reduction reaction and the results of such efforts are discussed in the following sections.

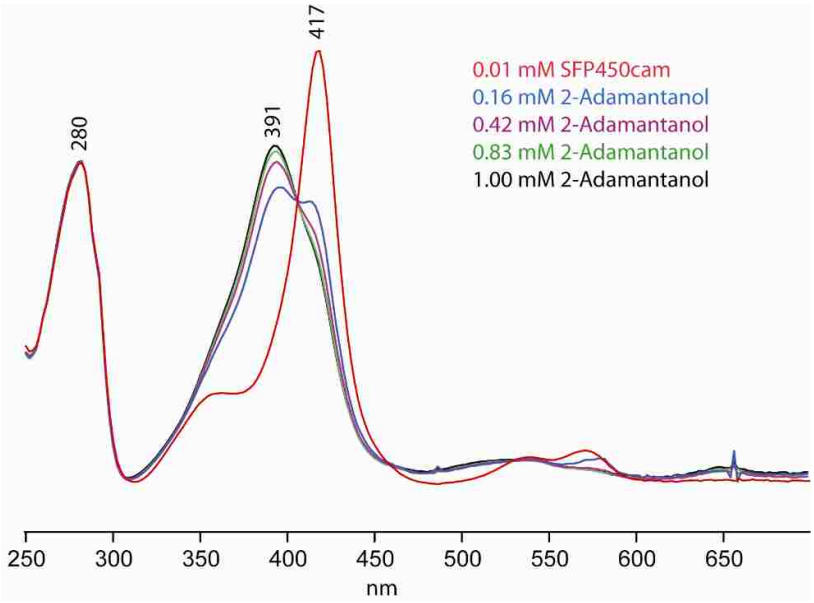

Figure 2.1.1 The UV-Vis spectra of 2-adamantanol binding to substrate-free P450cam

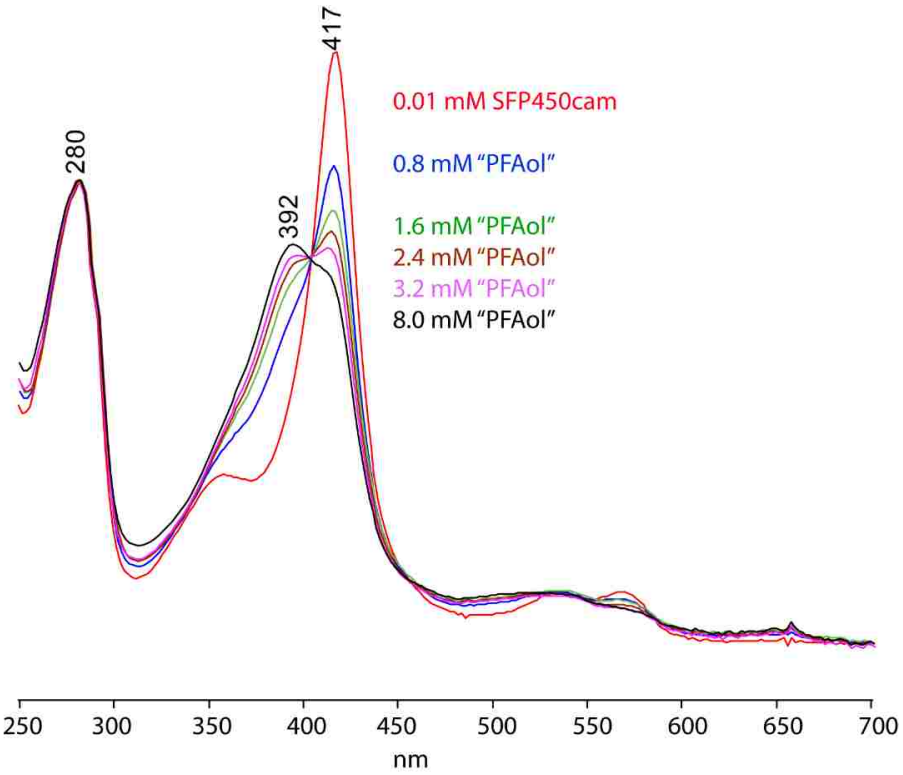

Figure 2.1.2 The UV-Vis spectra of F-adamantanol binding to substrate-free P450cam

2.1.2 Optimization of PFA reduction procedure

The optimization of PFA reduction was done using 2-adamantanone following the published procedure of Adcock *et al.* (1996).[97] Specifically, a 15 mg portion of 2-adamantanone was weighed and transferred to a glass vial. The vial was degassed by flushing with H_2O/O_2-free N_2 gas for about 10 minutes, followed by addition of 370 µL of diethyl ether under N_2 using a gas tight syringe. A solution of 1 M $LiAlH_4$ in diethyl ether (130 µL) was then added to the solution of 2-adamantanone in diethyl ether. The vial was stirred for 2 h at about -2 °C and at room temperature overnight followed by addition of 100 µL of absolute ethanol under N_2. The mixture was stirred for another 15 minutes and then poured into a solution of 5 g of 98% H_2SO_4 (500 µL). The product was then extracted in diethyl ether and dried over P_2O_5 in a desiccator. The white product was sublimed at about 165 °C to give about 90% of pure 2-adamantanol (Figure 2.1.3). The improvement in the yield of 2-adamantanol (75 to 90%) suggests that an inert environment may be a required condition for PFA reduction.

Reduction of PFA following the procedure just described gave transparent crystals stuck on the glass wall after evaporation of the ether extract (probably about 5 mg). Efforts to sublime this product were unsuccessful as nothing was recovered at the cold finger possibly due to the small amount used. Considering that when 150 mg of PFA was used, about 60 mg of impure product was obtained and when further scaled down to 60 mg only 15 mg was realized, utilizing 15 mg (as in the case described above) proved impractical for this deceivingly simple procedure. Also given that the reaction works excellently with 2-adamantanone giving yields of up to 90% pure 2-adamantanol even on the same small scale described, it may be argued at this point that 2-adamantanone has a different chemistry as compared to PFA and as such cannot be ideal for optimizing the

PFA reduction reaction. As mentioned previously, the dwindling quantities of PFA have proven to be challenge in these reactions. In an effort to advance the running aim of using chemically inert substrates to stabilize the compound I forms of P450s, an alternative route using CYP119 and perfluorinated fatty acids as possible inert substrates was adopted.

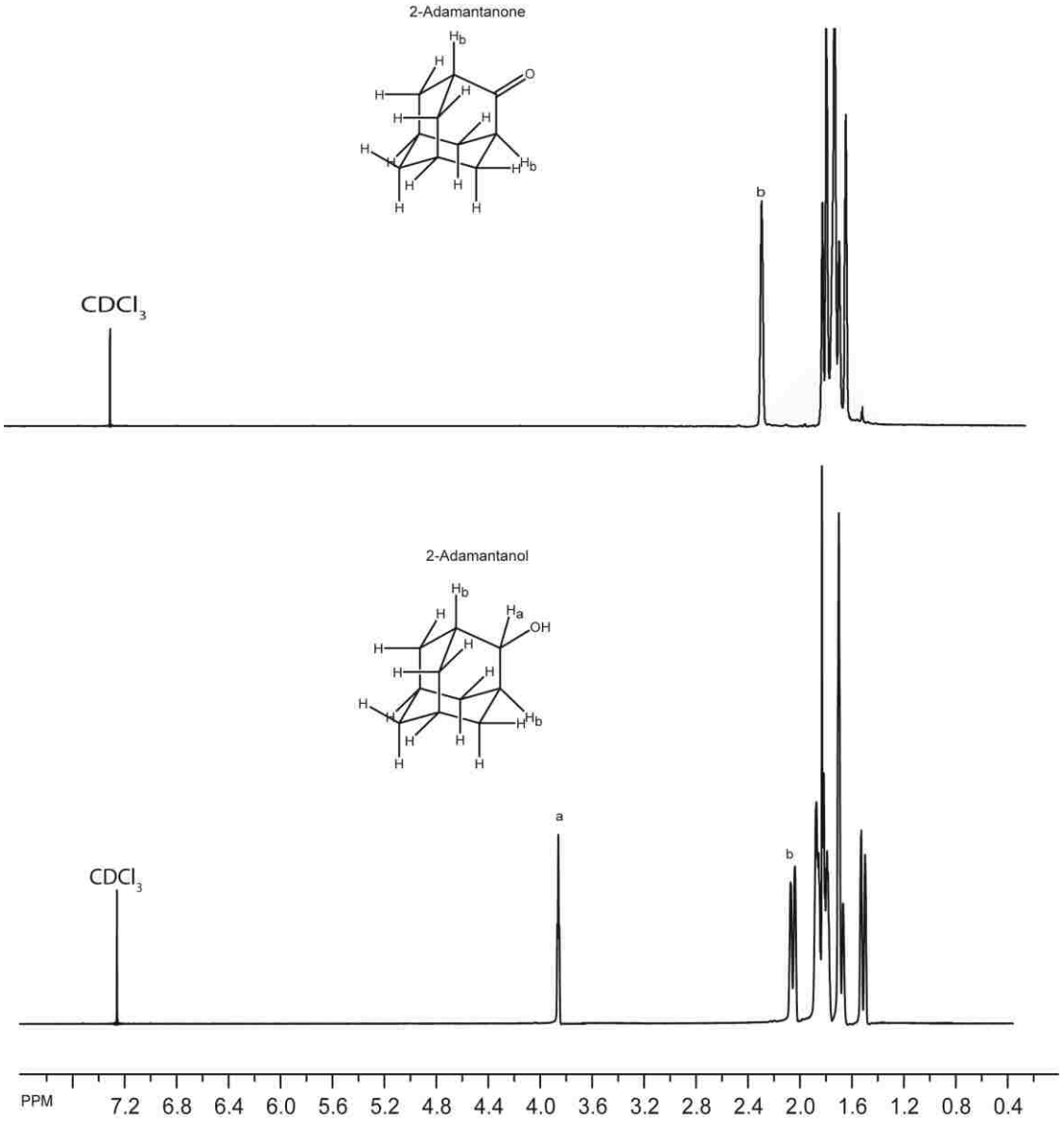

Figure 2.1.3 H NMR of 2-adamantanone (top trace) and 2-adamantanol (bottom trace) in $CDCl_3$

2.1.3 Cytochrome P450 119 (CYP119)

CYP119, a thermophilic protein from the archaebacteria *Sulfolobus solfataricus,* has been shown to be stable under extreme temperatures and pressure.[98] The reported melting temperature (90 °C) is 40 °C higher than the mesophilic P450cam and the enzyme has been demonstrated to exhibit hyperbaric stability, withstanding pressure of up to 200 MPa.[98–100] Crystal structure studies of CYP119 have documented the presence of extended aromatic clusters not observed in mesophilic proteins and have been thought to confer the inherent thermal and pressure stability (Figure 2.1.4).[99–102] The melting temperature was shown to decrease by approximately 10 °C when the aromatic clusters were disrupted by either a single or double mutation.[103]

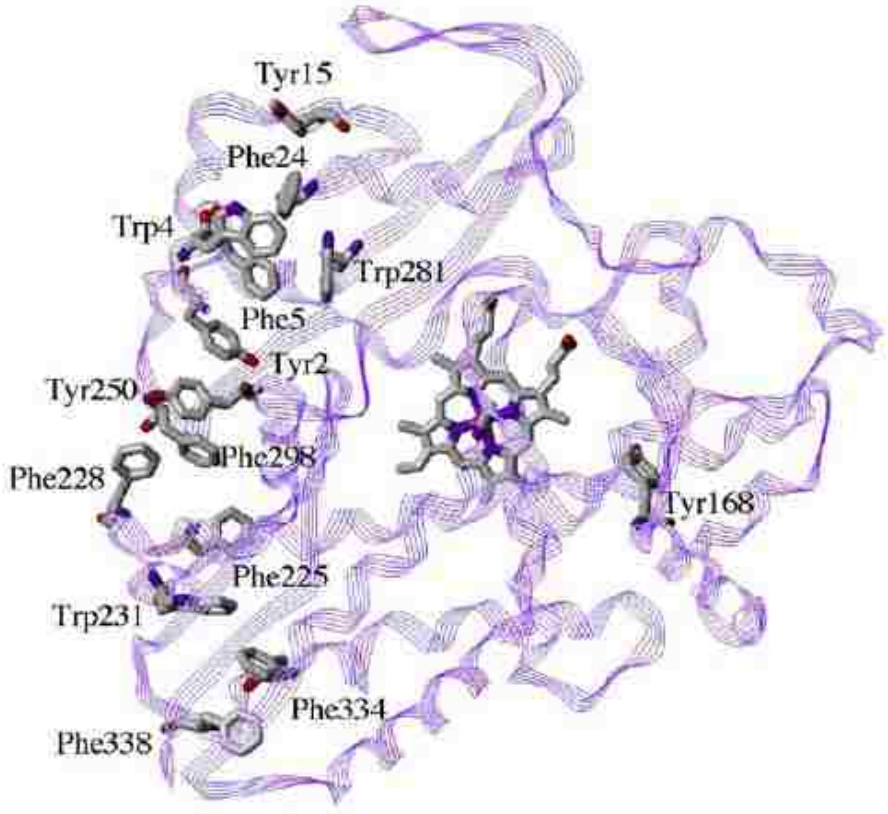

Figure 2.1.4 Crystal structure of CYP119 showing the aromatic residues thought to confer thermal stability[103]

Determination of the underlying factors conferring these unusual properties exhibited by thermophilic proteins can possibly be exploited in the engineering of stable mesophilic biocatalysts. In addition, the demonstrated structural stability of these proteins allows for mechanistic investigations, which are otherwise almost impossible in mesophilic P450s. In fact, at room temperature, the active site of such thermostable enzymes is possibly rigid, resulting in a possible slowdown of individual steps in the catalytic cycle.[104] However, the dioxygen complex of the substrate free CYP119 was shown to be unusually unstable with an autoxidation rate of 0.08 s^{-1} at 5 °C.[105]As would be expected, the substrate free dioxygen adduct of P450s are less stable compared to species in complex with substrate. However the observation in CY119 has in addition, been linked to the active site architecture in which the heme iron is more in plane than in the bacterial P450cam. Moreover a large deviation of the Fe−S bond from the heme axis and unusual ruffling of the prosthetic group have been proposed to account for the observed fast autooxidation rate.[105] Structural investigations of the active sites of CYP119, P450cam and CYP102 showed that the thermophilic enzyme exhibits an open conformation with higher flexibility and greater solvent access than P450cam, but similar to CYP102.[98] On the other hand, the compound I form of CYP119 produced by laser flash photolysis of the corresponding compound II (a product of peroxynitrite oxidation of CYP119) species has been reported to be stable with a lifetime of ~ 200 ms at 20 °C.[91] However, later studies on peroxynitrite oxidation of CYP102 have shown that the intermediate generated is an iron-nitrosyl complex rather than the FeIVoxo.[106] More recently, however, Green *et al* have utilized *meta*-chloroperoxybenzoic acid *(m*-CPBA) to generate the compound I intermediate in 75% yield permitting its spectroscopic and kinetic as discussed briefly

under Section 1.4.1.[85] These findings make the thermophilic protein an attractive alternative to the ongoing work of using chemically inert substrates to stabilize what has been referred to as the Holy Grail of P450 intermediates or the so-called compound I.[91]

The natural substrate for CYP119 remains unknown. However it has been shown to bind fatty acids ranging from C8-C20 in carbon chain length with lauric acid considered as a surrogate substrate exhibiting the highest binding affinity (Table 2.1.1).[107,108]

Table 2.1.1 The binding affinities of various surrogate substrates of CYP119[107]

substrate	K_s (μM)
capric acid (C10)	28 ± 2
lauric acid (C12)	1.2 ± 0.2
myristic acid (C14)	1.0 ± 0.2
palmitic acid (C16)	0.7 ± 0.2
stearic acid (C18)	1.3 ± 0.2
arachidic acid (C20)	5 ± 1

Lauric hydroxylation at 37 °C with chemically produced compound I species of CYP119 have been reported to occur at positions ω1, ω2 & ω3.[107] Based on these observations, it is now being postulated that the perfluorinated analogues of these long chain fatty acids, which are commercially available, might possibly act as chemically inert substrates of CYP119. Chemical reduction of the ferric substrate-bound CYP119 (using perfluorinated fatty acids as inert substrates) was followed by binding oxygen to form the dioxygen adduct (**4** in Figure 1.1.4). Cryoradiolysis of the dioxygen adducts of substrate bound CYP119 was employed in an attempt to generate, stabilize and spectroscopically

characterize the subsequent intermediates occurring in the catalytic cycle, of particular interest being the compound I form (**6**) of CYP119.

2.2 Materials and Methods

The plasmid encoding the CYP119 gene was kindly provided by the Sligar group and competent BL21 *E.coli* cells were purchased from Biolabs. Tryptone, yeast extract and Lauria-Bertani (LB) agar, used in the expression procedure described below, were purchased from Mo Bio Laboratories Inc. Lauric acid and ethylene glycol were obtained from Sigma Aldrich. Perfluorododecanoic acid (PFLA), perfluorodecanoic acid (PFDA) and perfluorooctanoic acid (PFOA) were purchased from Alfa Aesar and used without further purification. Ethylene glycol-d4 and D_2O were purchased from Cambridge Isotopes.

2.2.1 CYP119 Expression and Purification

P450s are routinely produced by heterologous expression utilizing *E.coli* cells.[109] Basically, a self-replicating circular DNA, called a plasmid, bearing the sequences coding for the P450 of interest is introduced into *E. coli* competent cells (cells treated with $CaCl_2$ to make them porous; so they can take up foreign DNA) by a process known as transformation. The cells are then exploited to amplify the plasmid to produce large quantities of it. Usually, the plasmid contains sequences that code for an antibiotic resistance protein, such that only competent cells containing the foreign plasmid can grow on media supplemented with the respective antibiotic. Most commonly, the expression vectors (plasmids) contain inducible sequences upstream of the gene of interest, for example, the pCWori+ vector,[110] which is widely used for P450

expression,[111] exhibits sequences of a lac operon. The lac operon is involved in lactose metabolism in bacteria and its transcription is shutdown by a DNA binding protein known as a lac repressor protein, the operon is turned on in the presence of a lactose metabolite, allolactose, which binds the lac repressor protein. In the pCWori+, the lac operon, situated upstream of the P450 gene in the promoter region, is induced by addition of isopropyl β-D-1-thiogalactopyranoside (IPTG), an allolactose mimic, which binds to the lac repressor protein and turns on the lac operon. Thus, it induces expression of the downstream P450 protein.

The CYP119-containing plasmid (provided by Sligar group at Urbana Champagne, IL) was transformed into BL21 cells (Biolabs) following the manufacturer's protocol. A single colony from the overnight grown CYP119/BL21-LB agar plate was used to inoculate 10 mL of LB broth (supplemented with 100 μg/mL ampicillin) as a starter culture for the expression of CYP119 performed according to a previously published procedure with minor modifications.[98] Briefly, cells were grown overnight at 37 °C and 250 rpm and used as 1 % inoculum in 10 mL of 2YT media (16 g tryptone, 10 g yeast extract and 5 g NaCl per 1L) supplemented with 100 μg/ml ampicillin. The 10 mL culture was incubated at 37 °C and 250 rpm until the OD at 600 nm was about 0.3 (about 2-3 h). This early log phase culture was used to inoculate 1L of 2YT media (also supplemented with 100 μg/mL ampicillin) grown at 37 °C and 250 rpm for 20 h. The cells were harvested by centrifugation at 8000 rpm for 10 minutes at 4 °C, giving an average of 12.5 g/L of wet cells. Cells were stored at -80 °C until needed.

Cells were thawed and resuspended in 4 volumes (4 mL/g of wet cells) of lysis buffer (50 mM Tris/HCl pH 8.0, 1mM EDTA, 4 mg/mL lysozyme, 16 U/mL DNase, 4 U/mL

RNase) and stirred gently for 4 h at 4 °C followed by centrifugation at 20 000 rpm for 1 h to remove cell debris. The supernatant was incubated at 75 °C for 15 minutes to remove some of the contaminating bacterial proteins. The precipitated bacterial proteins were spun down at 8000 rpm for 30 minutes and the supernatant slowly saturated to 40 % $(NH_4)_2SO_4$ (243 g/L) and stirred gently for an hour at 4 °C. The precipitated proteins were removed by centrifugation at 8000 rpm for 30 minutes and the crude soluble CYP119 was precipitated following 100 % saturation with $(NH_4)_2SO_4$ (469 g/L). The CYP119 pellet was resuspended in a minimum volume (~ 5mL) of 10 mM phosphate buffer (KPi), pH 7.2) and loaded onto Bio-gel P-100 column (3 x 40 cm) equilibrated and resolved in the same buffer. Fractions with R_z (A_{416}/A_{280}) values greater than 0.5 were pooled, concentrated and loaded onto DEAE 53 anion exchange column (3 x 12 cm) equilibrated in 10 mM KPi, pH 7.2. The column was washed with 6 column volumes (CV) of 10 mM KPi, pH 7.2 and the protein was eluted with a 10-100 mM KPi gradient at pH 7.0. Fractions with $R_z > 1.5$ were pooled and concentrated giving an average of 0.5 mL of ~ 0.4 mM (per L of culture) of pure substrate free CYP119 (SFCYP119) with a low spin state heme iron (Figure 2.2.1).

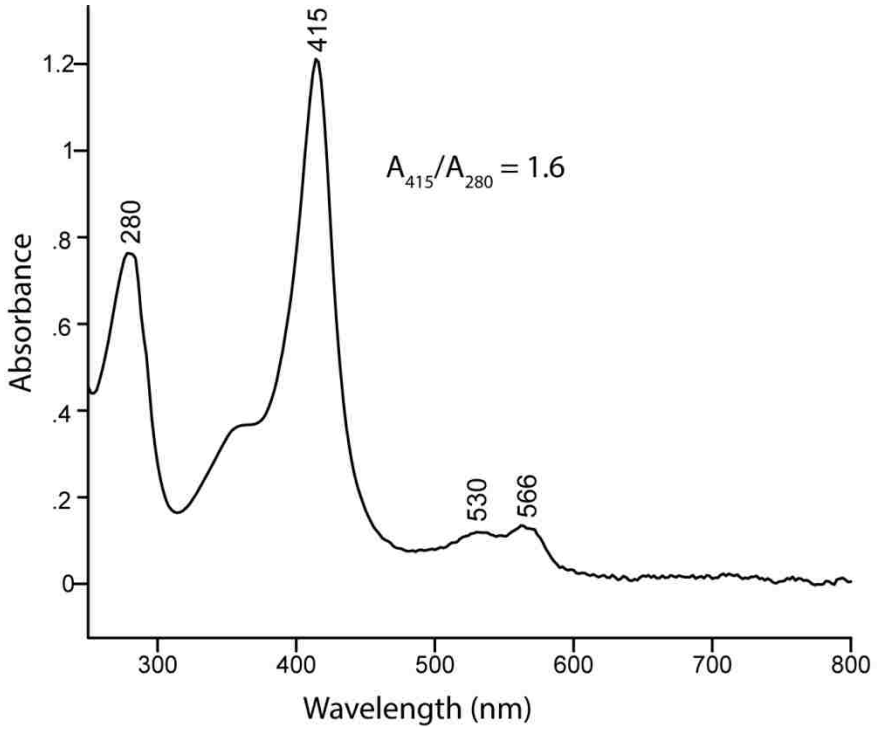

Figure 2.2.1 The absorption spectra of the ferric substrate free form of CYP119

2.2.2 Identification of a suitable inert substrate

Lauric acid and its perfluorinated analogue were the first candidates due to the reported high binding affinity of lauric acid.[108] Concentrated (12 mM) substrate stock solutions were dissolved in methanol and used to titrate substrate-free CYP119 (SFCYP119). Substrate binding to SFCYP119 was monitored by spin state associated shifts of the Soret band from around 416 nm down to 392 for the substrate free (low spin) and bound (high spin) forms, respectively. UV-Visble spectra were obtained using a Hewlett-Packard Model 8452 Diode Array Spectrophotometer.

2.2.3 Preparation of Oxy complexes

Protein samples were prepared by mixing 20 μL of 1 mM SFCYP119 (in 100 mM KPi, pH 8.0, 0.3 M NaCl), 7 μL of glycerol (v/v) and 3 μL of 25 mM PFDA (or Lauric acid) dissolved in ethylene glycol and transferred to an NMR tube. Deuterium substitution was achieved by equilibrating protein samples in D_2O KPi buffer, pD 8.0, 0.3 M NaCl for 2 days at 4 °C. Preparation of protein samples was essentially the same as above, with the only exception being utilization of deuterated glycerol and ethylene glycol. An in-house vacuum line assembly shown below was used in the preparation of dioxygen adducts of CYP119 (Figure 2.2.2). The NMR tube containing the sample was frozen in liquid N_2 and evacuated by opening valve1, while valves 2 and 3 remained closed. Small amounts of argon were added to the frozen sample by closing valve 1 and opening valve 2. The liquid N_2 bath was removed from the sample and the sample was thawed and vortexed. This evacuation process was done 4 times. While the sample is still immersed in liquid N_2, in the 4^{th} evacuation cycle, valves 2 and 3 are both opened, such that a positive pressure is maintained. This is followed by dismantling of the removable part allowing addition of $Na_2S_2O_4$ and O_2 saturated buffer. The ferrous form of PFDA-CYP119 was prepared by incubating the respective ferric form with 1 μL of 12 mg/mL $Na_2S_2O_4$ for about 30 minutes under argon atmosphere while formation of ferrous LA-CYP119 required 45 minutes incubation with 2 μL of the dithionite solution. Reduction was monitored by changes in the Q-band region of the absorption spectra, the band near 550 nm is characteristic of the ferrous form of the heme protein (Figure 2.2.3).

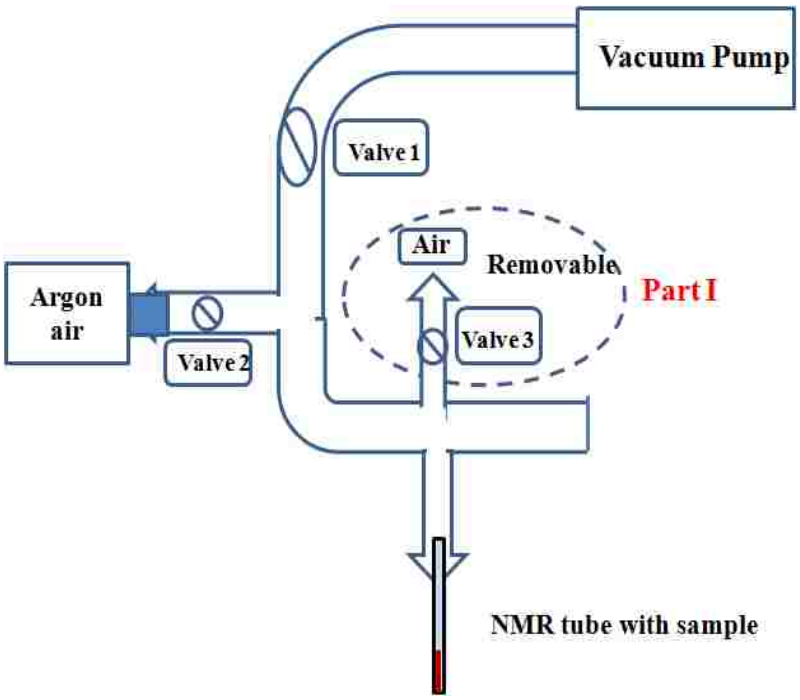

Figure 2.2.2 Schematic of the vacuum line assembly utilized in the preparation of dioxygen adducts of CYP119

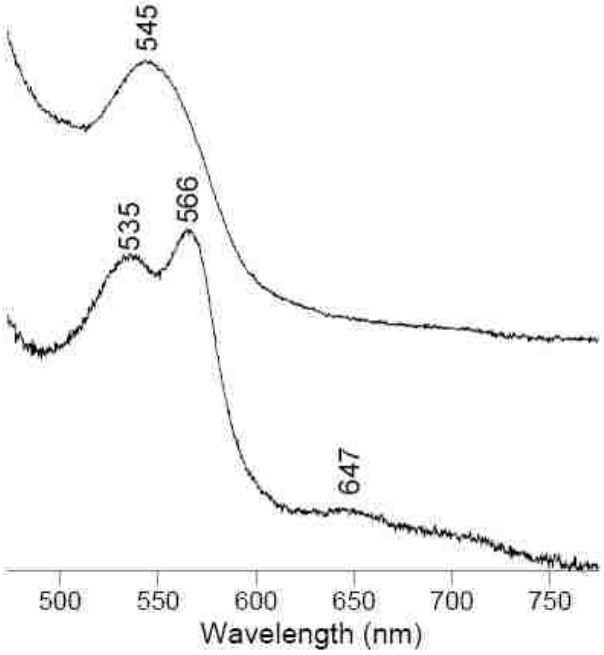

Figure 2.2.3 The absorption spectra of ferric (bottom trace) and ferrous (top trace) lauric acid bound CYP119

The reduced samples were cooled down to – 20 °C by immersing the NMR tube in an ethanol/dry ice bath for 2 minutes while a positive argon pressure was maintained. Approximately 70 μL of cold (-20 °C) $^{16}O_2$-saturated buffer [100 mM KPi , pH 8.0, 30 % glycerol] was added to the cooled reduced protein followed by rapid mixing (using a vortex) for 10 s. The oxygenated samples were immediately frozen in liquid N_2. Preparation of $^{18}O_2$ adducts was achieved by rapidly mixing (10 s vortex) the reduced samples with ~ 100 μL of $^{18}O_2$-saturated buffer. The process was repeated for samples equilibrated in D_2O KPi buffer with $^{16}O_2/^{18}O_2$-saturated D_2O KPi buffer. The formation of the dioxygen complex of substrate bound CYP119 was verified by RR at liquid N_2 temperature (*vide infra*).

2.2.4 Cryoradiolytic reduction of CYP119 oxy complexes

Cryoradiolytic reduction of the oxy complexes of CYP119 was performed as reported earlier[112] with minor modifications. Specifically, frozen samples of oxy-ferrous CYP119 were irradiated with ^{60}Co γ rays at 77 K and a dose rate of 92 Gy/min. The total irradiation time was 330 minutes, which translates to a total dose of ~ 3 Mrad or 30 kGy. Samples were kept in liquid N_2 before, during and after irradiation. Irradiated and annealed (*vide infra*) irradiated samples were probed by EPR and RR spectroscopic methods

2.2.5 Resonance Raman Spectroscopy of CYP119 intermediates

Resonance Raman spectra were obtained using a Spex 1269 spectrometer equipped with a CCD detector (Spec 10 from Princeton Instruments), at liquid N_2 temperatures (77 K). The excitation lines employed for the oxyferrous samples before and after irradiation were 413 nm (Coherent Sabre Kr ion laser) and 441.6 nm (Kimmon Model IK4153RC He:Cd laser), respectively. Fenchone was used to calibrate all spectra, which were processed with Grams 32/AI (Galactic Industries, Salem, NH). Rayleigh scattering was removed by use of an appropriate Notch filter from Kaiser Optical. The power at the sample was approximately 1.5 mW. The NMR tube containing the sample was spun and the RR spectra were collected at liquid N_2 temperature using 180° (back scattering) geometry in combination with a cylindrical lens, which focuses the laser beam on the sample as a line image to avoid local heating (Figure 2.2.4).[113,114]

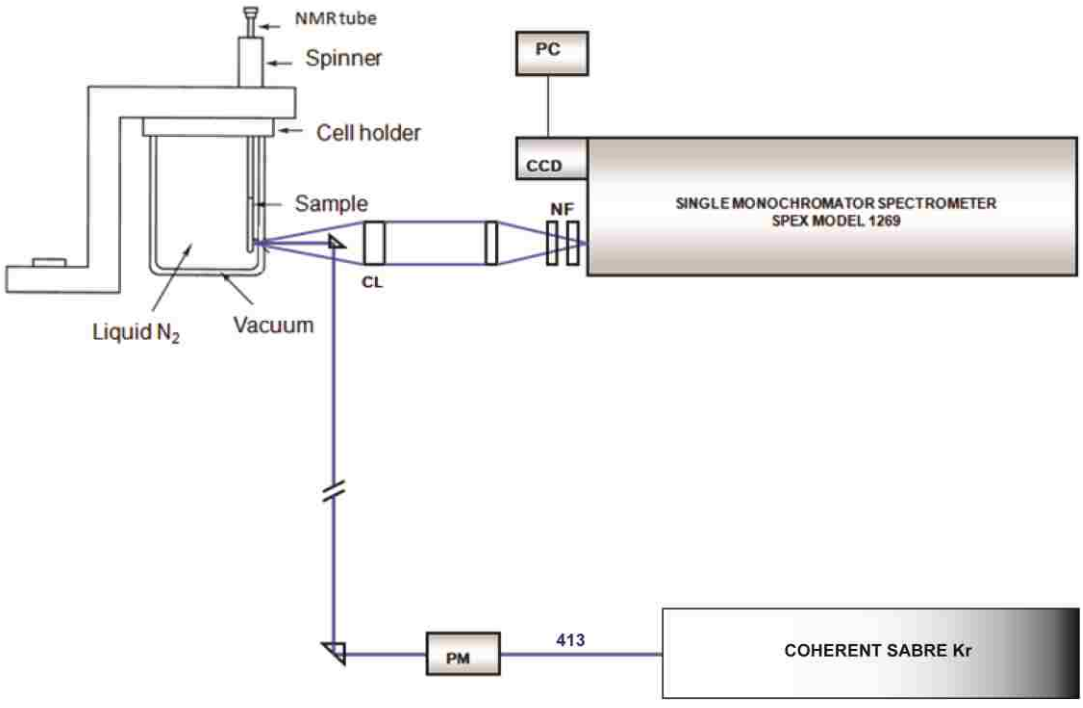

Figure 2.2.4 Schematic of RR instrumentation

2.3 Results and Discussion

2.3.1 Inert substrate-CYP119 binding titrations

As mentioned previously, substrate binding was monitored by observing shifts of the Soret band from 416 nm (for substrate free protein) to 391 nm (substrate bound). All the fatty acids employed were soluble in methanol; however, when the SFCYP119 was titrated using concentrated (12 mM) methanolic stock substrate solutions no significant spin state changes were observed in the absolute visible spectra of the protein even at elevated temperatures (37 °C) (Figure 2.3.1 and Figure 2.3.2). The difference spectra, however shows substrate binding associated spin state shifts [Figure 2.3.3 (data shown for lauric acid and its perfluorinated analogue)].

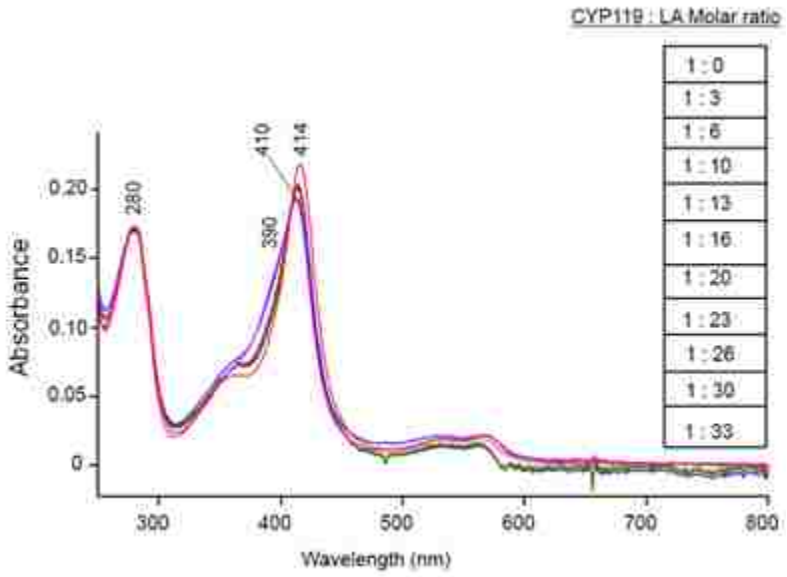

Figure 2.3.1 The absorption spectra of ~ 0.2 μM SFCYP119 titration with LA (12 mM in ethylene glycol) at 37 °C; insert shows the molar ratio

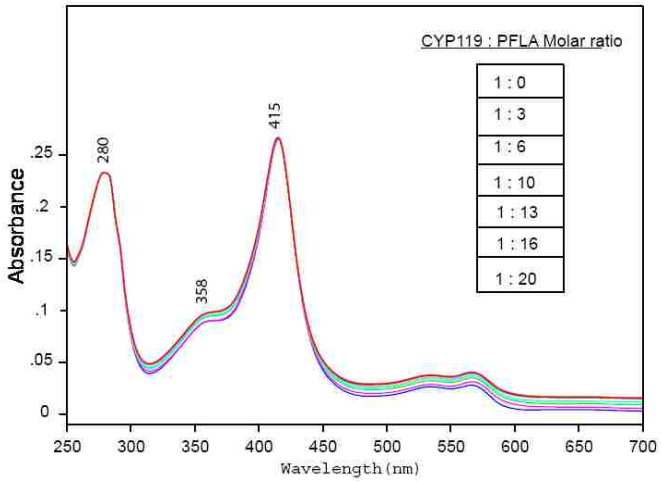

Figure 2.3.2 The absorption spectra of ~ 0.2 μM SFCYP119 titration with PFLA (12 mM in ethylene glycol) at 37 °C; insert shows the molar ratio

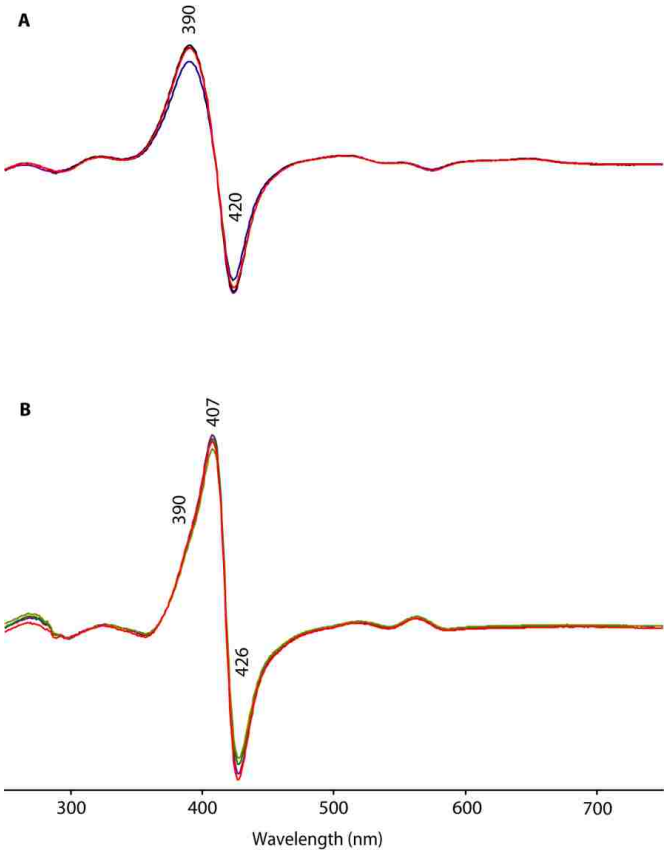

Figure 2.3.3 The difference spectra of SFCYP119 titration with 12mM LA (**A**) and PFLA (**B**) dissolved in methanol at 37 °C

As alluded to earlier, exogenous ligands coordinated to the heme iron on the distal site can be exploited to spectroscopically investigate structural details in the active site. The CO ligand was employed as a spectroscopic probe to monitor structural changes associated with substrate binding in heme proteins. Specifically, changes in the ν(Fe−CO) stretching frequency of the ferrous CO bound form of the enzyme can be used as evidence of substrate binding. The substrate free and bound samples of CYP119 were bubbled with CO, reduced by sodium dithionite and the ν(Fe−CO) frequency monitored by resonance Raman spectroscopy. Only slight changes in the ν(Fe−CO) mode were observed for CYP119 "bound" to lauric acid (LA), its perfluorinated analogue (PFLA) and perfluorodecanoic acid (PFDA), suggesting that the substrates may not be in close enough proximity to the heme group to cause any significant perturbation in the ν(Fe−CO) stretching mode (Figure 2.3.4). This is in contrast to the spectroscopic changes observed for the bacterial protein, P450cam, where the ν(Fe−CO) stretching mode exhibits a 20 cm^{-1} shift from 464 to 484 cm^{-1} upon binding of substrate.[36,115] On the other hand, the ν(C-O) modes of PFLA and PFDA bound CYP119 occurring at 1950 and 1953 cm^{-1} are upshifted by about 4 and 6 cm^{-1} respectively, suggesting slightly different substrate structure effects on the CO fragment (Figure 2.3.4).

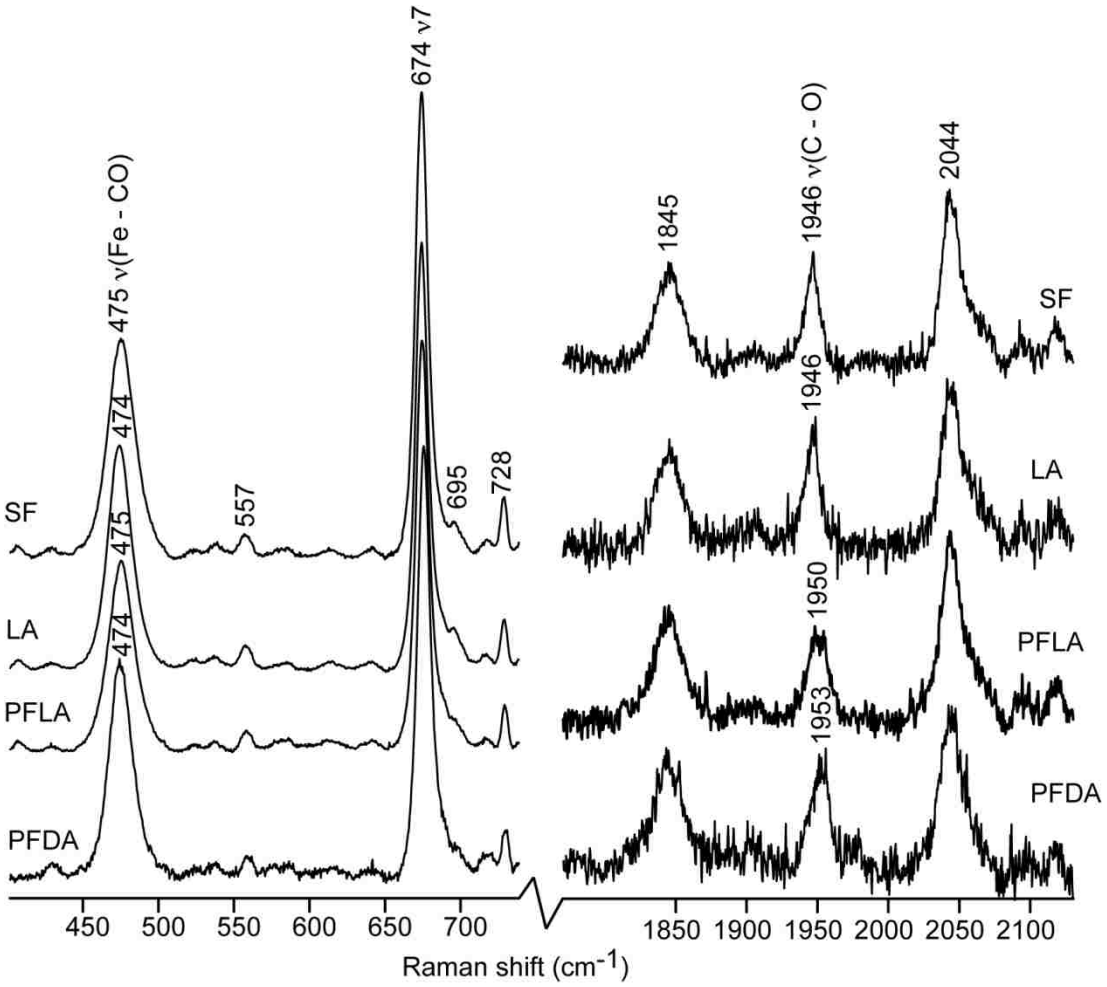

Figure 2.3.4 RR spectra in the Low (left traces) and high (right traces) frequency regions of the ferrous CYP119-CO forms. SF; substrate free, LA; lauric acid bound, PFLA; perfluoro lauric acid bound and PFDA; perfluorodecanoic acid bound.

Significant spin state changes were however observed when ~ 0.6 μM SFCYP119 was incubated in 100 mM KPi, pH 7.0, 60% glycerol and ~2.5 mM LA at 50 °C (Figure 2.3.5). PFLA on the other hand was not soluble in glycerol, but dissolved in ethylene glycol; however spectral changes were observed for the SFCYP119 incubated in 100 mM KPi with 30 % ethylene glycol (Figure 2.3.6), suggesting that ethylene glycol might be competing as a substrate. No significant spin state changes were observed when SFCYP119 (in 100 mM KPi with 60 % glycerol) was titrated with volumes of ethylene glycol not exceeding 3 % at 50 °C (Figure 2.3.7). Under these conditions

perfluorodecanoic acid (PFDA) “dissolved” (at 50 °C the fatty acid melts) in ethylene glycol was shown to bind SFCYP119 with observable spin state changes (Figure 2.3.8). Specifically, a concentrated stock solution (50 mM) of PFDA “dissolved” in ethylene glycol was used to titrate ~ 0.6 µM SFCYP119 in 100 mM KPi, pH 7.0, 60 % glycerol in 5 µL increments up to 20 µL, which translates to less than 1 % of ethylene glycol (v/v).

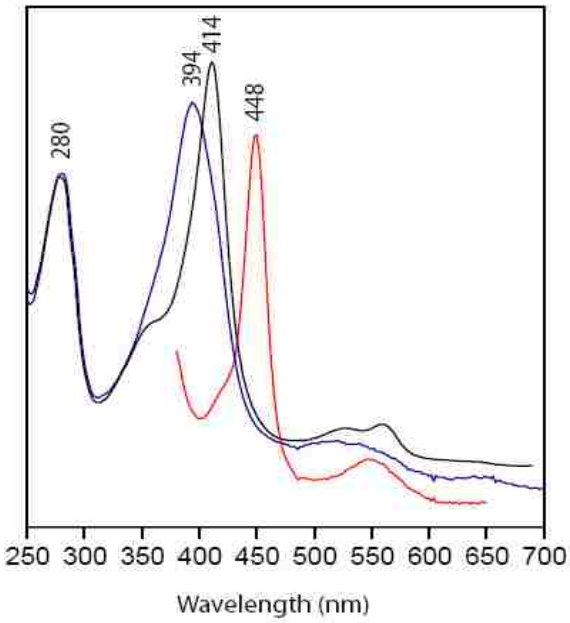

Figure 2.3.5 The absorption spectra of ferric substrate free (black trace), ferric LA bound (blue trace) and ferrous-CO (red trace) forms of CYP119

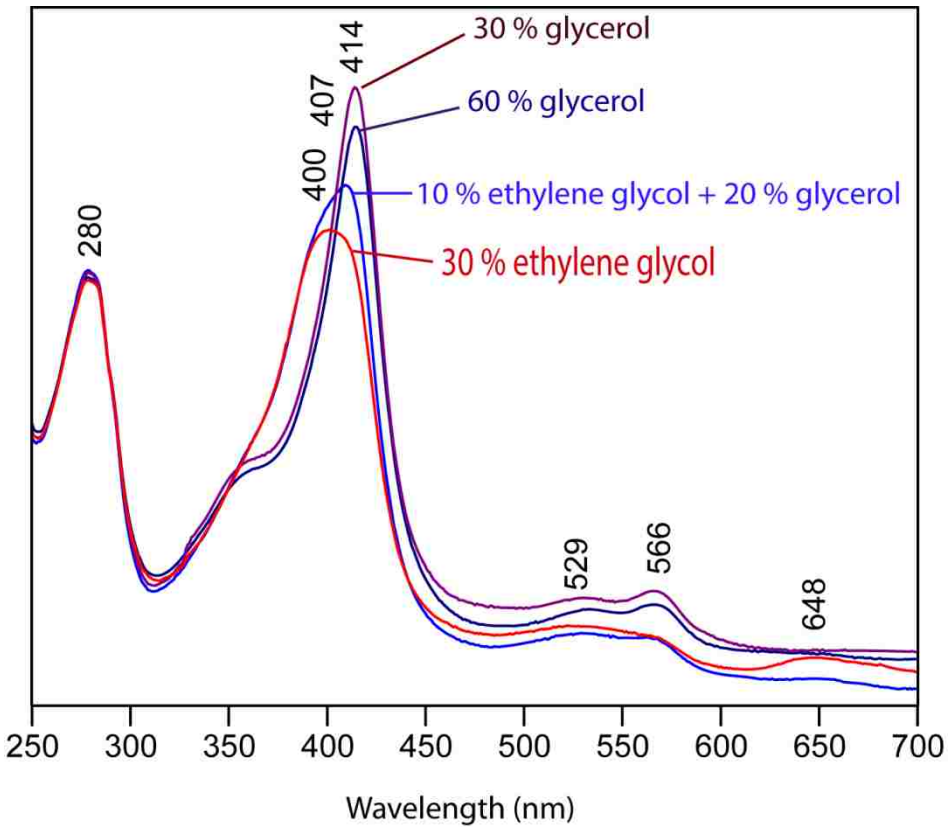

Figure 2.3.6 The effects of ethylene glycol and glycerol on the absorption spectra of ferric SFCYP119 at 50 °C

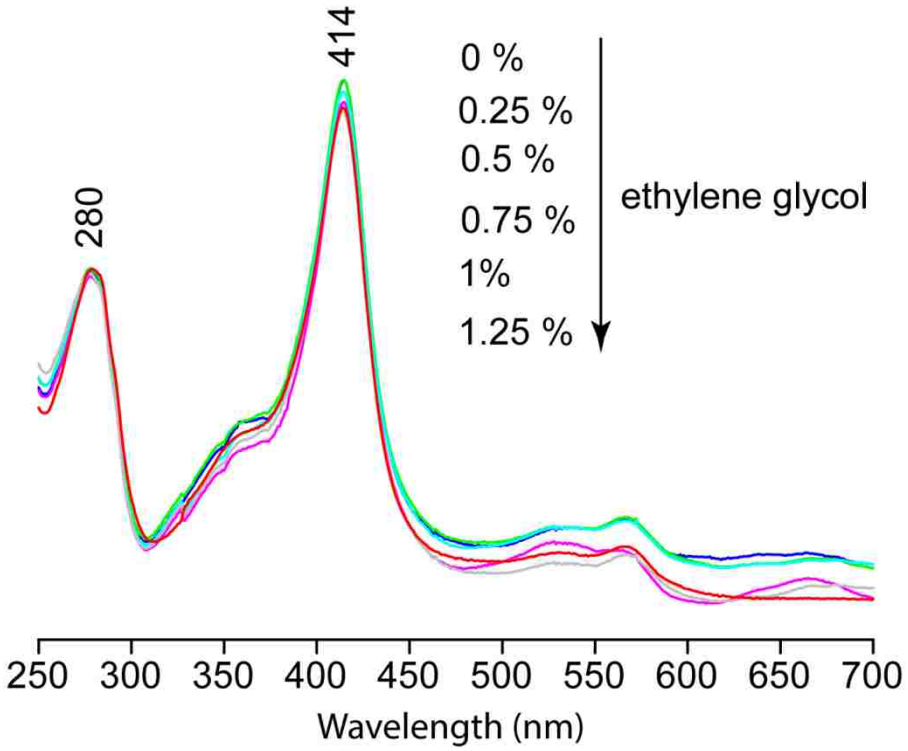

Figure 2.3.7 Absorption spectra of SFCYP119 titration with ethylene glycol obtained at 50 °C

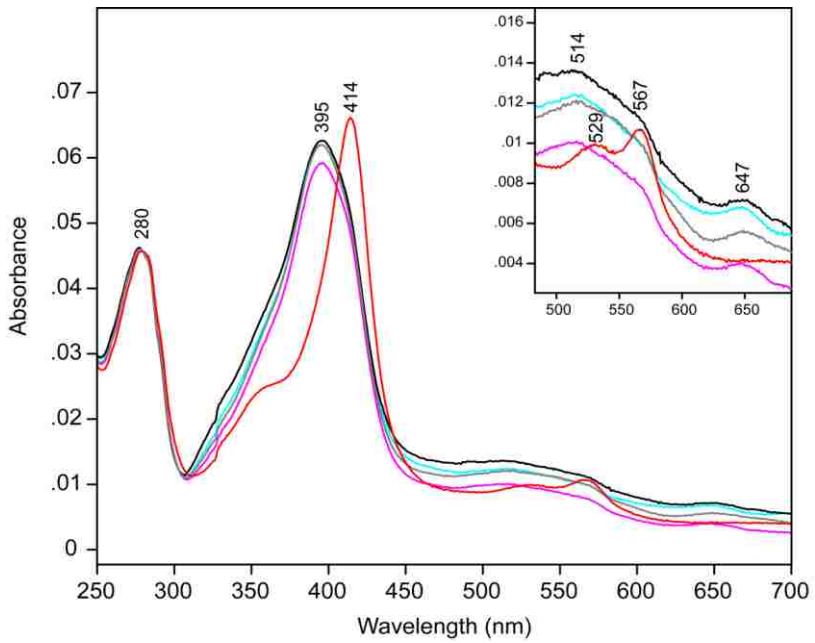

Figure 2.3.8 The absorption spectra of ferric SF (red trace) and PFDA bound CYP119 at 50 °C. The insert shows changes in the Q-bands region upon substrate binding.

2.3.2 RR spectroscopy of substrate bound CYP119

The high frequency resonance Raman spectra of the ferric substrate free and bound samples obtained at ~ 50 °C shows the corresponding partial spin state changes observed by absorption spectroscopy (Figure 2.3.9). The spin state marker ν_3 occurring at 1502 cm^{-1} for the low spin SFCYP119, exhibits a clear down shift to 1488 cm^{-1} (characteristic of a 5 coordinate high spin heme iron) upon substrate binding. As is evident in trace B of Figure 2.3.9, lauric acid binding causes the most significant (greater than 50%) spin state changes, a finding that is consistent with its high binding affinity (1.2 ± 0.2 μM).[107,108] In contrast PFDA results in a less significant spin state conversion, which may be due to the lower binding affinity of its non fluorinated analogue, decanoic acid (28 ± 2 μM).[107] However the spin state conversions in this current work observed at 50 °C are significantly higher as compared to those reported for styrene-bound CYP119 at 70 °C.[116] The observed recalcitrance of CYP119 to spin state changes upon substrate binding is thought to be due to an unusually strong hydrogen bonding network stabilizing the distal water ligand in addition to the active site architecture discussed earlier[101]

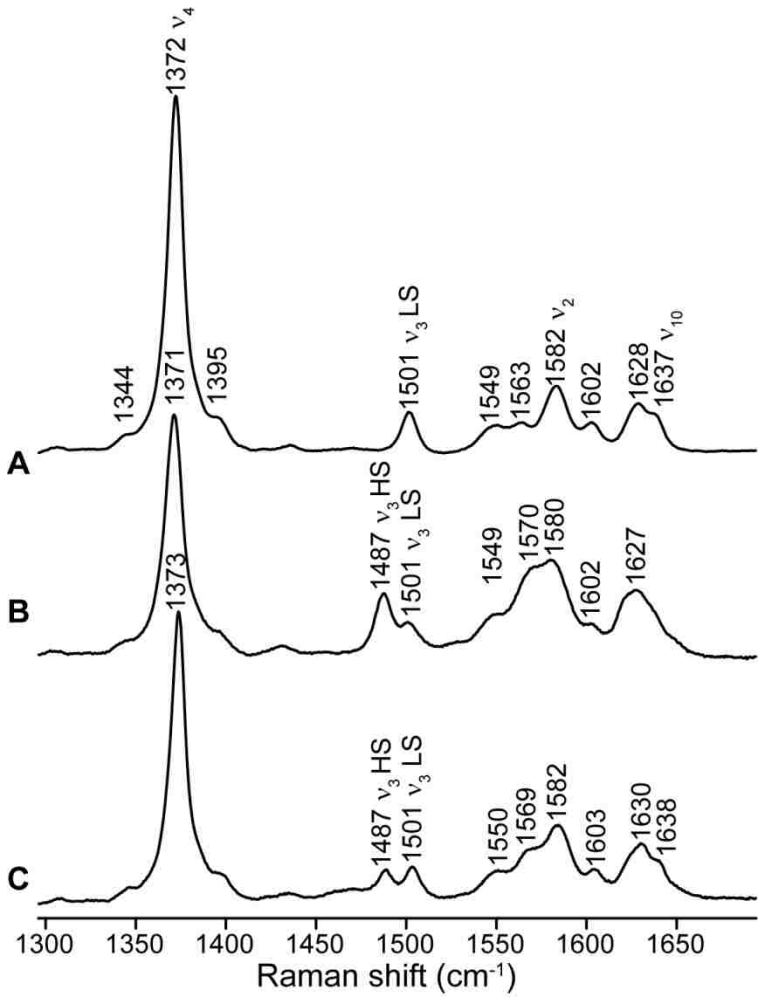

Figure 2.3.9 The high frequency region of resonance Raman spectra obtained with 406.7nm excitation at ~50°Cfor the SFCYP119 (**A**), Lauric acid bound CYP119 (**B)** and PFDA bound CYP119 (**C**).

Given that the optimal growth temperature for the thermophilic bacteria from which the CYP119 gene was cloned is between78-86 °C, [98,117,118] it may be possible to obtain 100% spin state conversion with lauric acid binding at temperatures greater than 70 °C (assuming that lauric acid does not decompose). Although this might be crucial in explaining substrate binding in this thermophilic P450, it offers no advantage to our current efforts to stabilize and capture the elusive compound I form of CYP119, both which are performed at cryogenic temperatures.

The corresponding low frequency region spectra indicate changes to the modes associated with propionate and vinyl groups upon substrate binding. Specifically, lauric acid binding activates a second propionate bending mode occurring at 371 cm^{-1} (Figure 2.3.10, trace B), which have been documented recently (in P450cam) to be degenerate with an out of plane γ_6 mode.[22] The lower frequency vinyl bending mode (rather accurately described as pyrrole I or II deformations with vinyl contributions) occurring around 405 cm^{-1} is activated and up shifted with 2 and 3 cm^{-1} upon binding of LA and PFDA respectively. Consistent with the spin state conversion observed in the high frequency region upon binding of PFDA, activation of the lower frequency "vinyl bending mode" is less significant as compared to binding of LA.

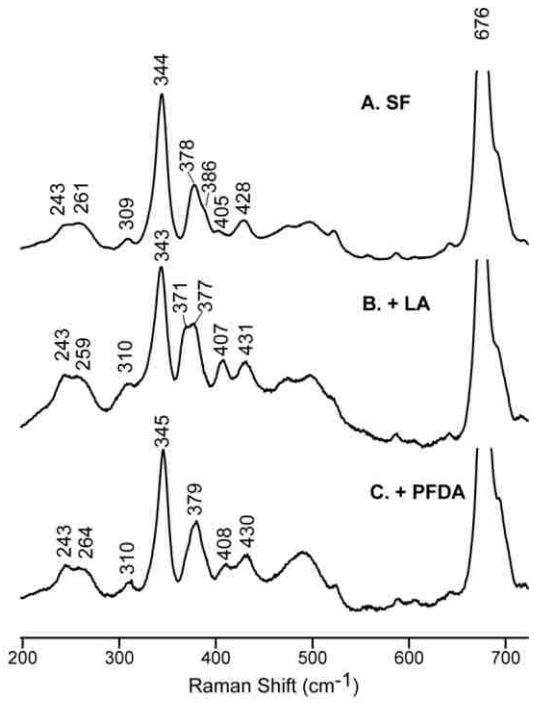

Figure 2.3.10 The low frequency resonance Raman spectra of ferric SF (A), LA bound (B) and PFDA bound (C) forms of CYP119 at ~50 °C

Interestingly, even with the observed spin state changes at 50 °C, no significant changes were observed in the ν(Fe-CO) upon substrate binding as noted earlier (Figure 2.3.11). Similar behavior has been observed in another bacterial cytochrome P450 isolated from *Bacillus megaterium,* the so-called $P450_{BM3}$.[33]

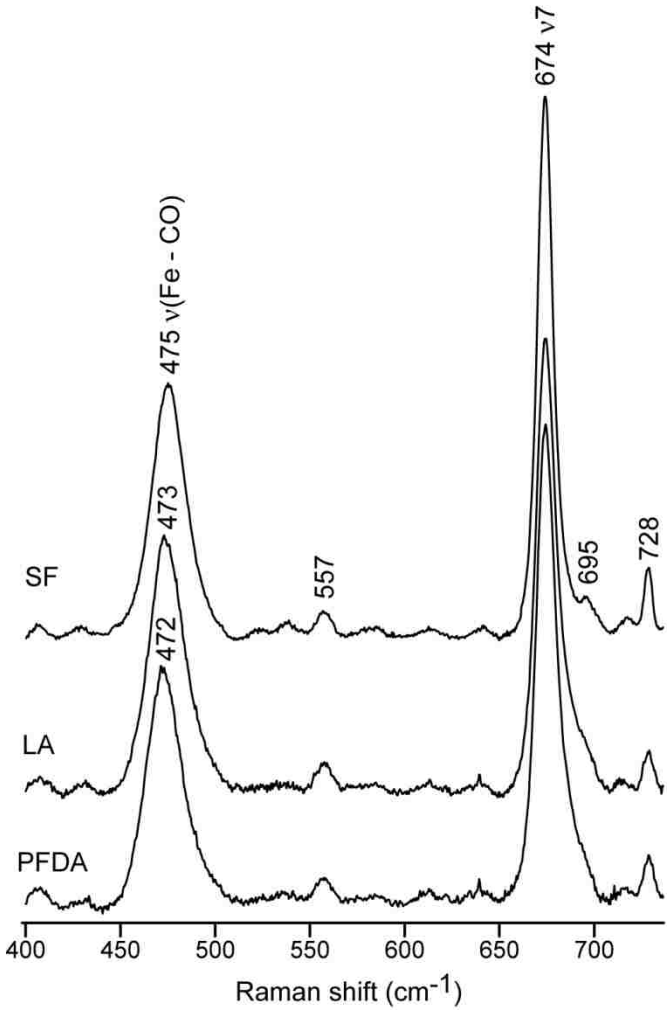

Figure 2.3.11 The resonance Raman spectra of the ferrous-CO for the substrate free (**A**), LA bound (**B**) and PFDA bound (**C**) CYP119 at 50 °C.

Although substrate binding in CYP119 does not result in a full spin state conversion to the high spin as observed in the mesophilic P450cam, T1 NMR experiments of CYP119 with bound styrene has shown it to be within 4.4-4.5 Å of the

heme iron.[116] On the other hand, the reported binding affinity of styrene is significantly lower than that of lauric acid, and indeed the hydroxylation of lauric acid, which has been studied extensively, suggests that it sits within reaction distance to the heme iron.[107,108]

2.3.2.1 RR characterization of CYP119 dioxygen adducts before cryoradiolytic reduction

The formation of oxy ferrous complexes of substrate bound (LA/PFDA) CYP119 were confirmed by RR spectroscopy at 77 K. The high frequency spectra of the oxy complex of LA bound CYP119 shown in Figure 2.3.12, exhibits a broad band centered around 1135 cm^{-1}, which has previously been interpreted as arising from the $\nu(^{16}O\text{-}^{16}O)$ stretching frequencies of different conformers of the Fe-O-O fragment. Indeed this mode exhibits isotope sensitivity shifting down by about 64 cm^{-1} upon $^{18}O_2$ substitution, as can be clearly seen in the difference spectrum in the top trace of Figure 2.3.12, a finding that is consistent with previously reported spectra of trapped O_2 adducts.[20,119] The corresponding RR spectra of LA bound CYP119 in D_2O buffer (Figure 2.3.13) suggests hydrogen bond interactions in the distal pocket between the bound dioxygen with either side chain residues or water molecules as evidenced by the H/D shift (2-3 cm^{-1}) of the both $^{18}O_2$ and $^{16}O_2$ stretching modes. The dioxygen adduct of CYP119 in complex with the fluorinated substrate, PFDA exhibited similar RR spectral behavior in the high frequency region, with both $\nu(^{16}O–^{16}O)$ and $\nu(^{18}O–^{18}O)$ only slightly shifted down (2 cm^{-1}) and centered around 1133 and 1068 cm^{-1} respectively (Figure 2.3.14). As observed for the LA bound dioxygen adduct of CYP119, both the $^{16}O_2$ and $^{18}O_2$ stretching frequencies also demonstrated isotope sensitivity upon deuterium substitution of exchangeable protons (Figure 2.3.15), suggesting an H-bonded dioxygen species in the

distal pocket. A calculated model structure of the dioxygen adduct of CYP119 in the absence of substrate revealed similarities with the oxygenated intermediate of CYP101 with the conserved threonine residue at position 213 within hydrogen bonding distance to the bound oxygen.[105] In addition ,the active site water molecules, visualized in the high resolution crystal structure of ligand free CYP119, are possible hydrogen bond donors, these have been proposed to play a role in the catalytic scission of the bound dioxygen.[101]

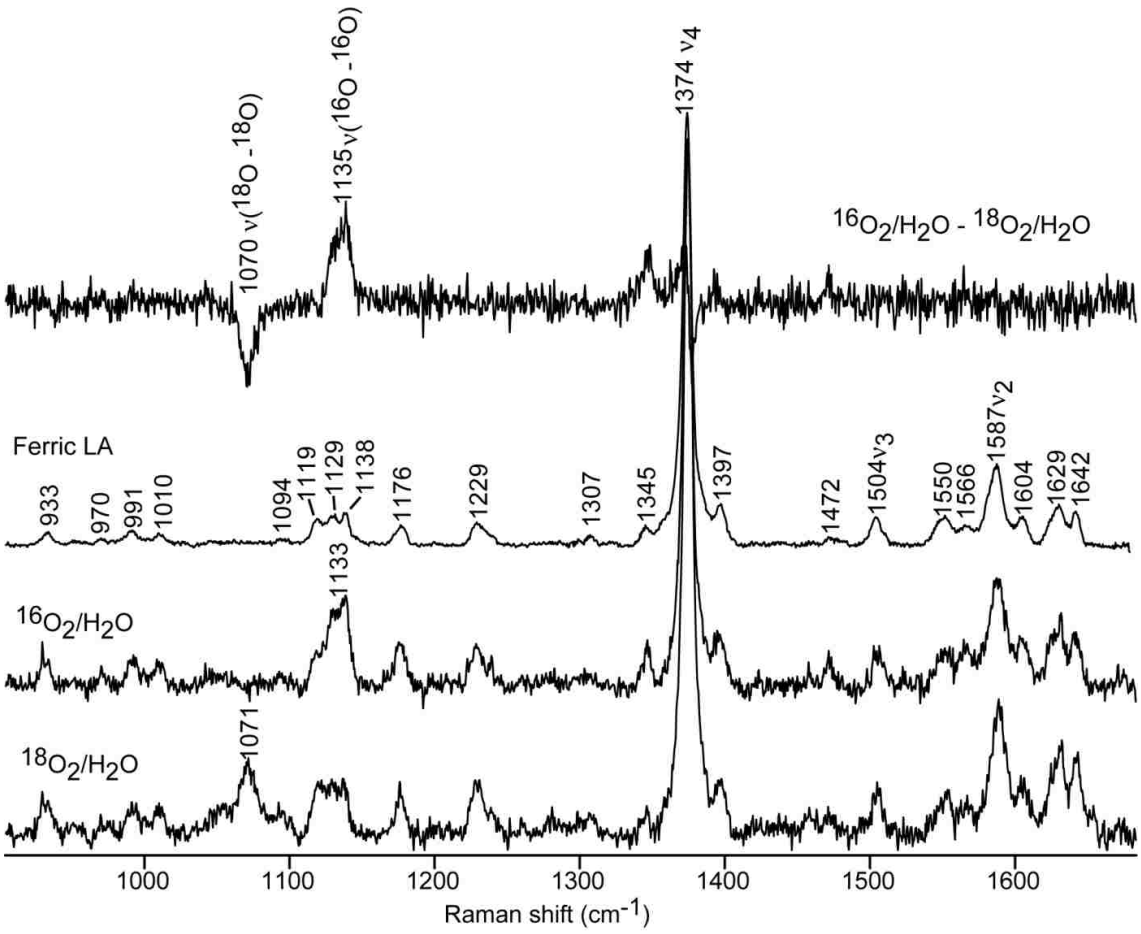

Figure 2.3.12 The high frequency RR spectra of the oxy ferrous complex of LA bound CYP119 in H_2O buffer collected using the 413 nm excitation line at 77K

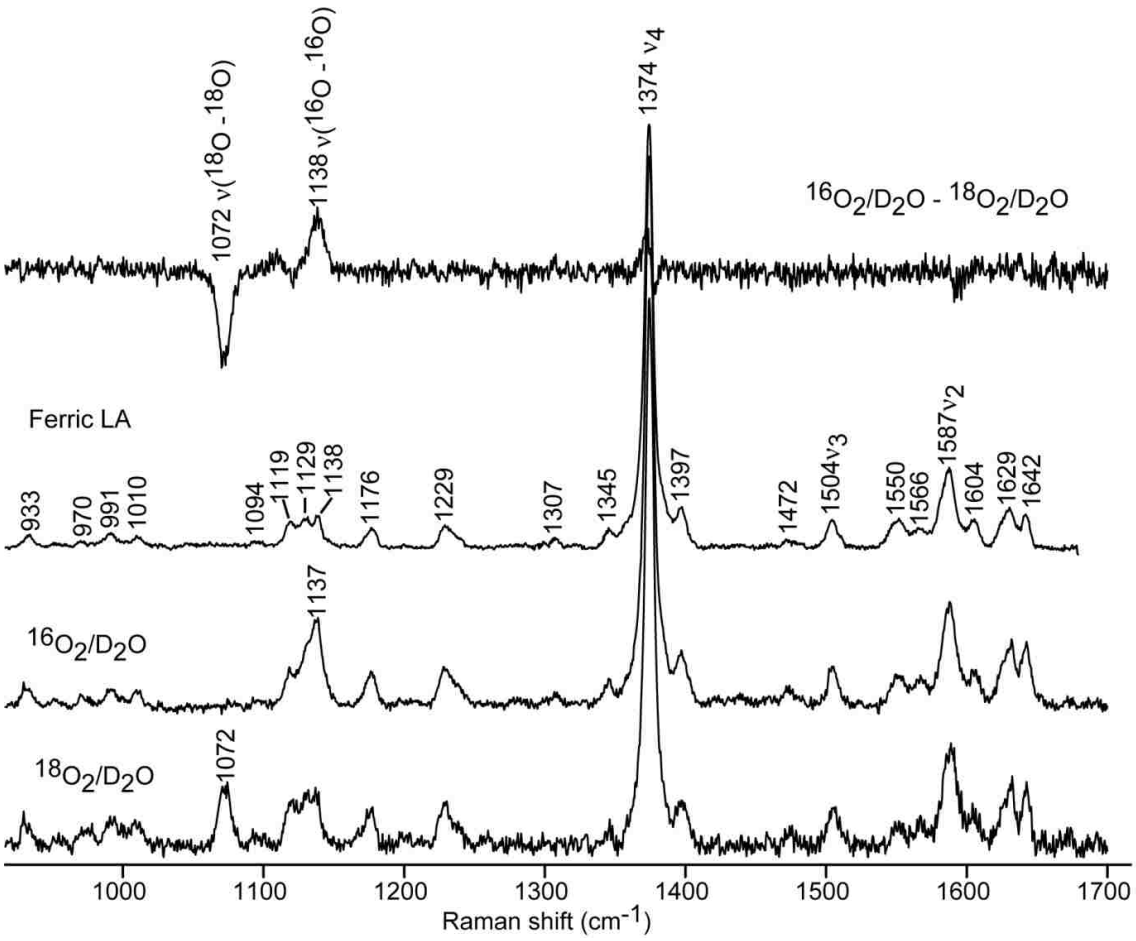

Figure 2.3.13 The high frequency RR spectra of the oxy ferrous complex of LA bound CYP119 in D_2O buffer collected using the 413 nm excitation line at 77K

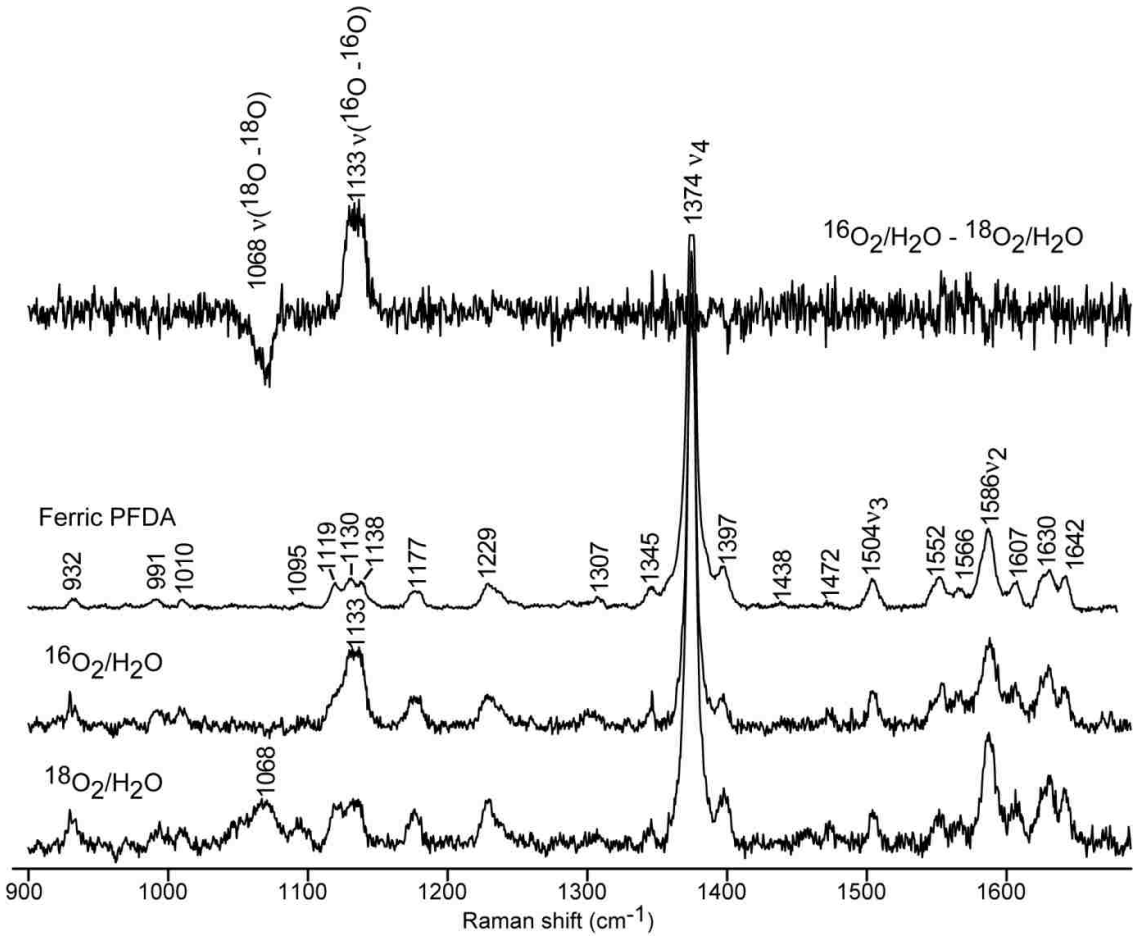

Figure 2.3.14 The high frequency RR spectra of the oxy ferrous complex of PFDA bound CYP119 in H_2O buffer collected using the 413 nm excitation line at 77K

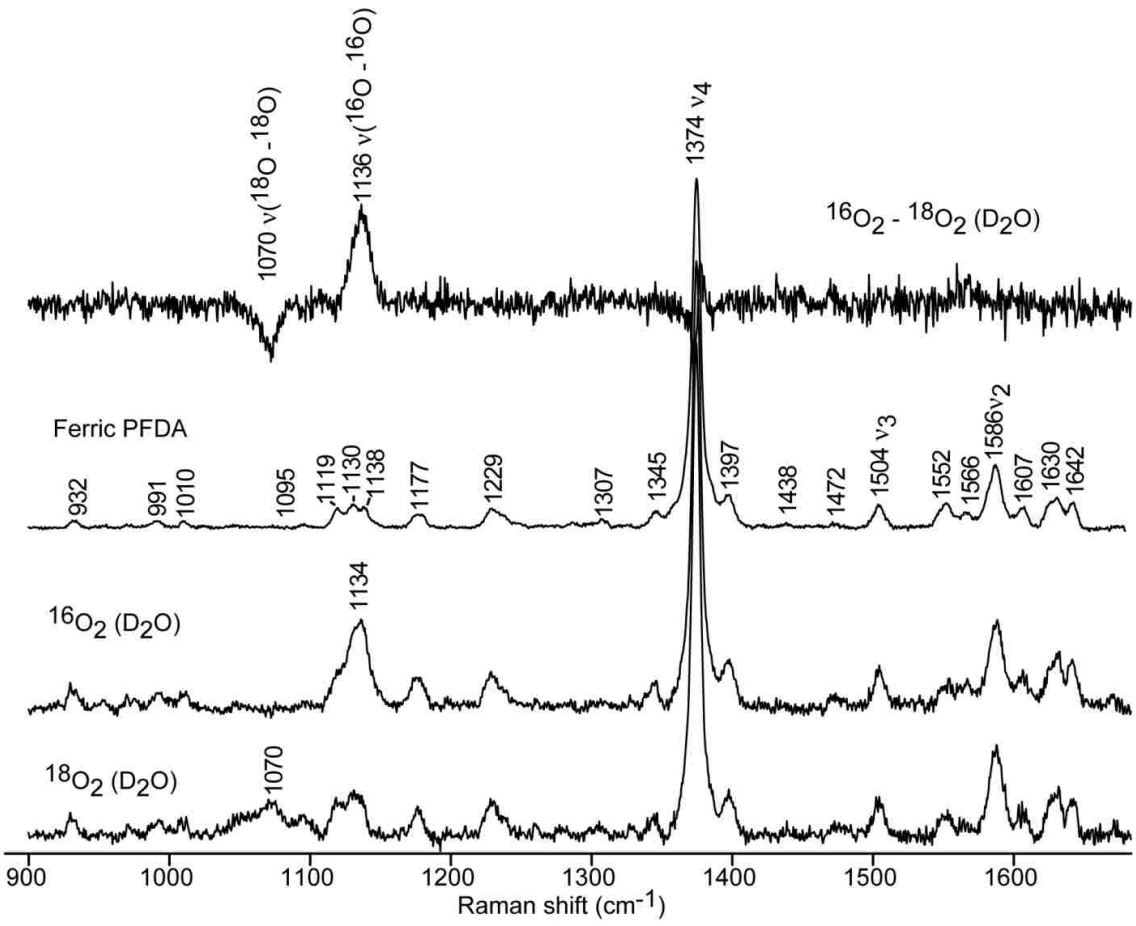

Figure 2.3.15 The high frequency RR spectra of the oxy ferrous complex of PFDA bound CYP119 in D_2O buffer collected using the 413 nm excitation line at 77K

The low frequency RR spectra of the dioxygen adduct of LA and PFDA bound CYP119 in H_2O and D_2O buffers are shown in Figures 2.3.16-2.3.19. Although spectral noise complicates identification of the $\nu(Fe{-}O_2)$ mode, the difference spectrum of $^{16}O_2{-}^{18}O_2$ provides some evidence for the $\nu(Fe{-}^{16}O_2)$ and $\nu(Fe{-}^{18}O_2)$ modes in the range expected for thiolate ligated heme proteins.[62] The LA bound CYP119 $\nu(Fe{-}^{16}O_2)$ occurs around 533 cm^{-1} and exhibits sensitivity to $^{18}O_2$ isotopic substitution, shifting with about 34 cm^{-1} as expected (Figure 2.3.16). Interestingly, the difference spectrum of $^{16}O_2{-}^{18}O_2$ in D_2O reveals an unusual distinct H/D shift, with both the $\nu(Fe{-}^{16}O_2)$ and $\nu(Fe{-}^{18}O_2)$

modes shifting up by about 3 cm^{-1} upon deuterium substitution (top trace in Figure 2.3.17), possibly suggesting H-bonding to the proximal oxygen. This observation is unusual in as much as such H/D shifts are reportedly small and normally not observable for the $\nu(M-O_2)$ modes.[28,29,120–122] The difference spectra of $^{16}O_2-^{18}O_2$ of the PFDA bound CYP119 dioxygen complex in H_2O buffer, shown in Figure 2.3.18, exhibits positive and negative broad bands centered around 524 and 490 cm^{-1}, which makes it almost impossible to assign them to the stretching Fe –O modes. On the other hand, the dioxygen adduct of PFDA bound CYP119 in D_2O buffer show similar behavior to the LA bound dioxygen species in the Fe−O stretching frequency region (Figure 2.3.19), with the $^{16}O_2$ and $^{18}O_2$ slightly upshifted by 3 and 5 cm^{-1} respectively, suggesting sensitivity of the bound ligand to different substrates. This observation has been reported earlier for CYP101, in which the $\nu(Fe-^{16}O)$ mode for the camphor bound enzyme, occurring around 541 cm^{-1} was down shifted to 537 cm^{-1}in the dioxygen complex of adamantanone-bound P450cam.[62] In summary, the RR data in both the high and low frequency spectral regions, document the successful formation of the dioxygen species of substrate bound CYP119 at liquid N_2 temperature. Cryoradiolytic reduction of this species is expected to yield the peroxo/hydroperoxo intermediates (*vide infra*), which precedes the proton assisted scission of the O-O bond resulting in the generation of the compound I.

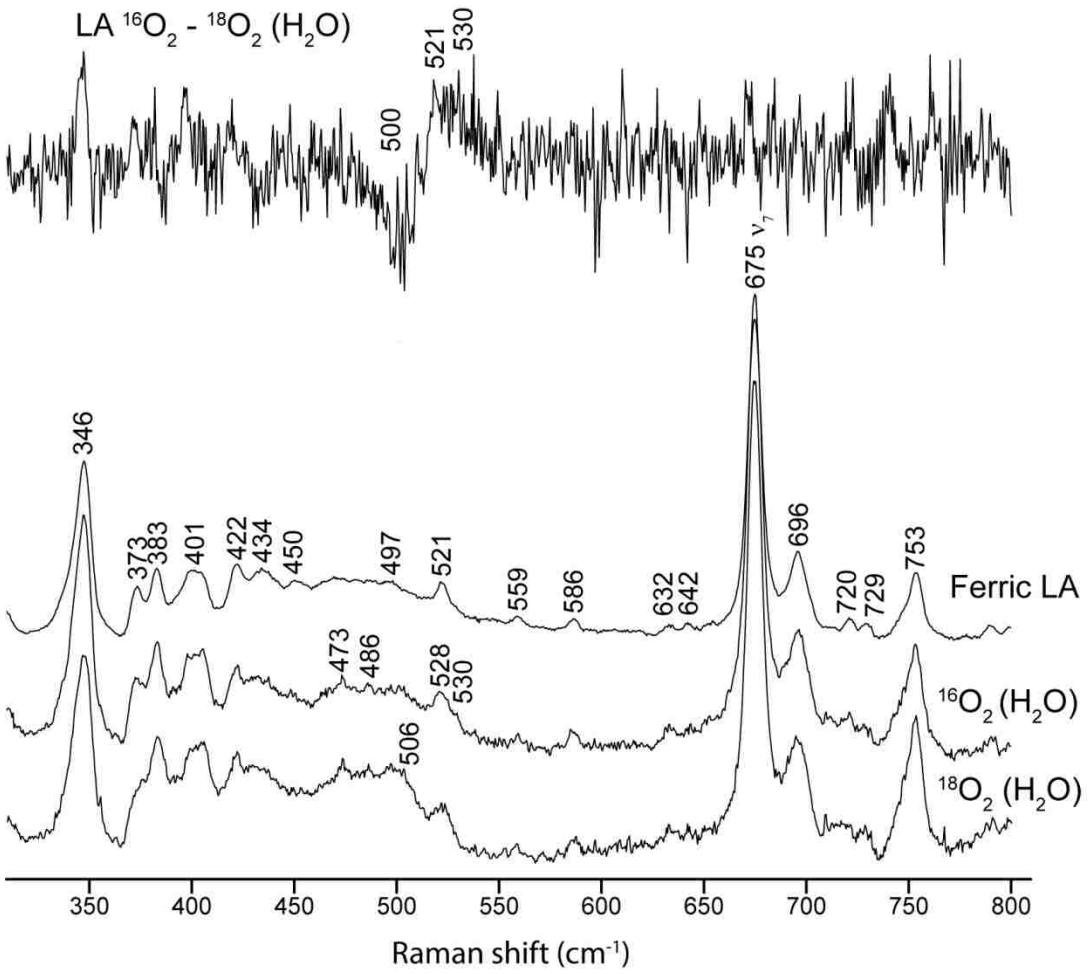

Figure 2.3.16 The low frequency RR spectra of the oxy ferrous complex of LA bound CYP119 in H_2O buffer collected using the 413 nm excitation line at 77K

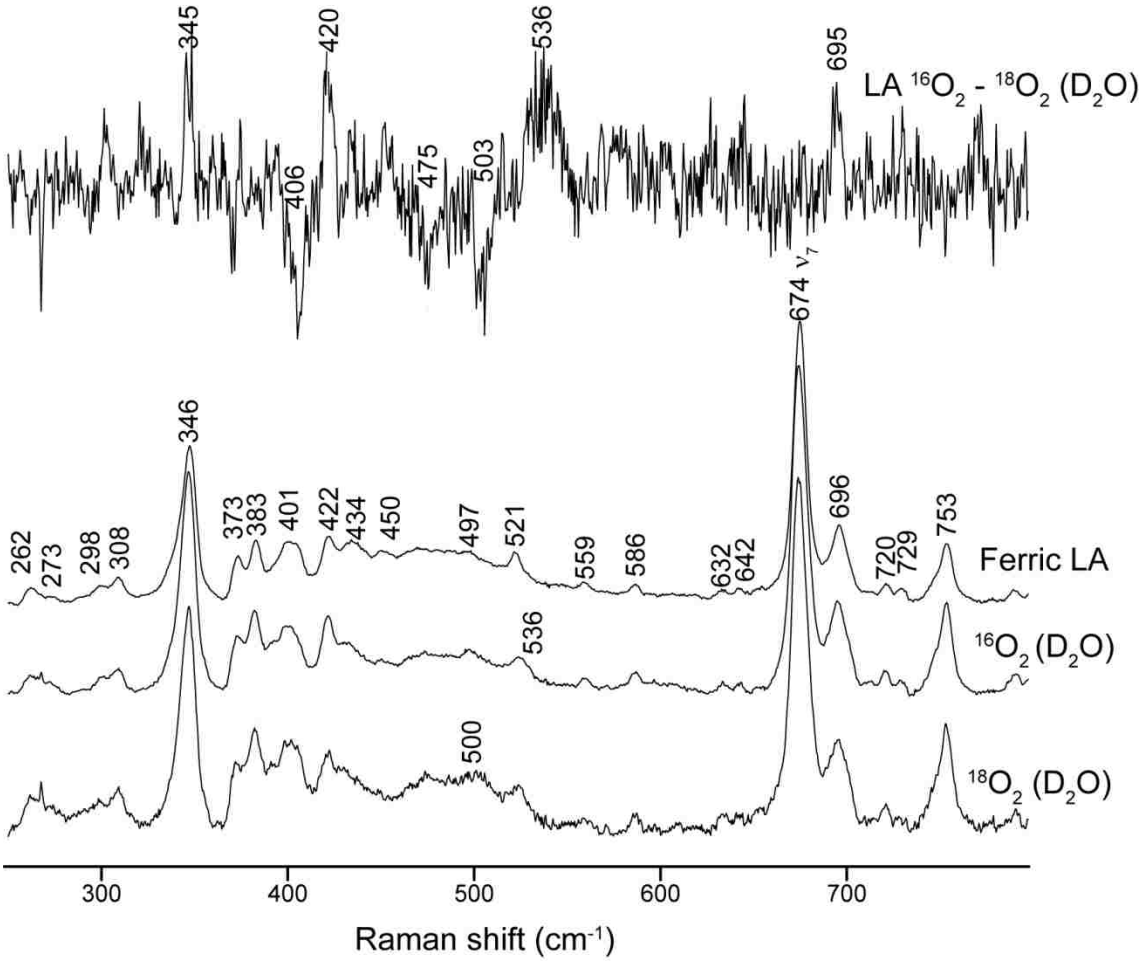

Figure 2.3.17 The low frequency RR spectra of the oxy ferrous complex of LA bound CYP119 in D_2O buffer collected using the 413 nm excitation line at 77K

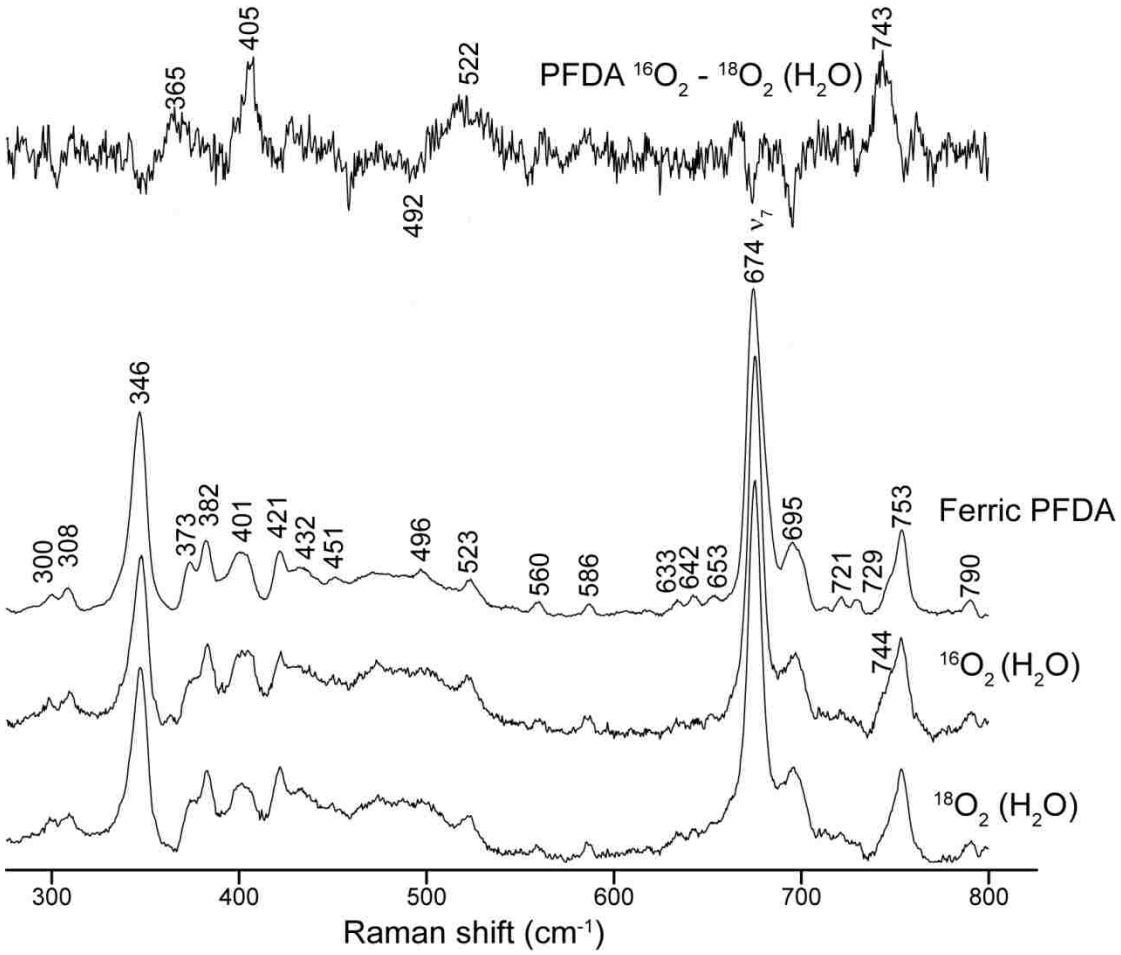

Figure 2.3.18 The low frequency RR spectra of ferric PFDA bound CYP119 and its $^{16}O_2$ and $^{18}O_2$ adducts in H_2O buffer

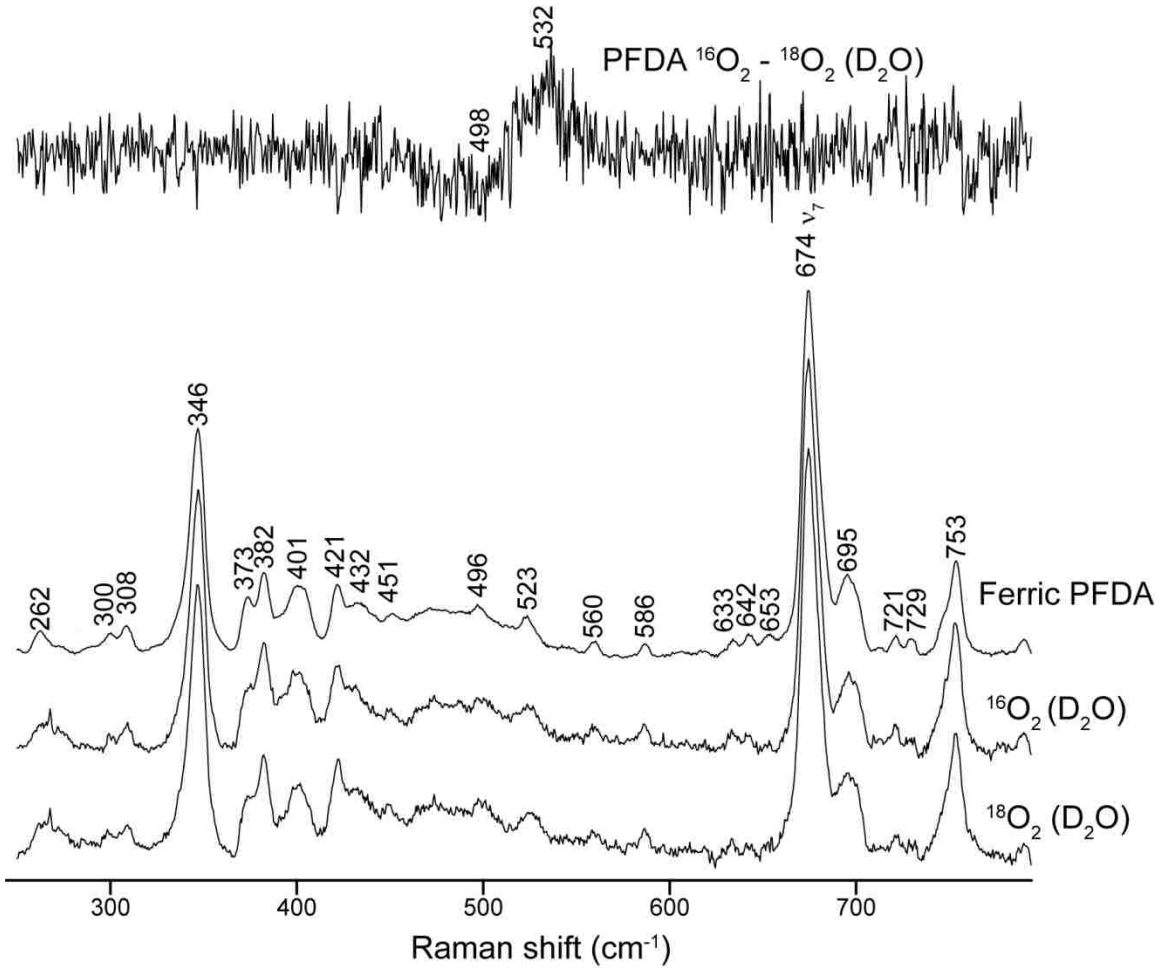

Figure 2.3.19 The low frequency RR spectra of the oxy ferrous complex of PFDA bound CYP119 in D_2O buffer collected using the 413 nm excitation line at 77K.

2.3.2.2 RR characterization of irradiated dioxygen adducts of CYP119

Cryoradiolytic reduction was employed to deliver another electron to the dioxygen adducts of substrate-bound CYP119 in an attempt to generate the subsequent intermediates occurring in the P450s catalytic cycle. Briefly, oxy-ferrous samples of LA- and PFDA-bound CYP119 were irradiated, using ^{60}Co, at a dose rate of 92 Gy/min for 330 minutes. The irradiated substrate-bound CYP119 samples were characterized by RR at 77 K using the 442 nm excitation line, which is expected to selectively enhance the

peroxo- and hydroperoxo- intermediates. The low-frequency RR spectra of irradiated dioxygen adducts of LA-bound CYP119, in H_2O and D_2O buffers, are shown below (Figures 2.3.20 and 2.3.21). The difference spectra of $^{16}O_2$-$^{18}O_2$, in both H_2O and D_2O buffers, shows residual oxy-ferrous complex of LA-bound CYP119 (top spectra in Figures 2.3.20 and 2.3.21). This is attributable to incomplete reduction of the oxy-ferrous samples during irradiation, probably because of weakening of the ^{60}Co radiation source. Additionally, a negative band around 752 cm^{-1}, is observed in both H_2O and D_2O samples. On the other hand, the $^{16}O_2$-$^{18}O_2$ difference spectra of irradiated samples of PFDA-bound oxy-ferrous CYP119 show no evidence of residual dioxygen adducts; neither, unfortunately, is there any evidence for the expected peroxo/hydroperoxo intermediates (top trace of Figures 2.3.22 and 2.2.23). The band around 752 cm^{-1}, for the LA-bound samples, might possibly be arising from the $\nu(^{18}O–^{18}O)$ mode, however, no corresponding $\nu(^{16}O–^{16}O)$ positive bands, expected in the 750-800 cm^{-1} region,[20] were detected, making unequivocal assignment impossible. In fact, this band might be a heme mode coming from residual ferric form as observed in the low-frequency region of the spectra before irradiation (Figure 2.3.16). In addition, no isotopic sensitive bands were observed in the 520-580cm^{-1} region, where the $\nu(Fe–O_2)$ mode is expected for the peroxo/hydroperoxo intermediates of P450s.[20] The inability to detect either the peroxo/hydroperoxo intermediates, by RR at 77 K, might be due to warming, by the laser beam, at the surface of the sample. This, presumably, results in the decay of peroxo/hydroperoxo intermediates, through proton transfer and O-O bond cleavage leading to compound I and hydroxylation of LA. On the other hand, warming up irradiated samples of the dioxygen adducts of CYP119 in complex with a chemically inert substrate, PFDA, might result in accumulation of compound I on the surface of the

sample, however, to possibly undetectable levels. Low levels of oxy-ferrous in the samples may also explain the lack of accumulation of these intermediates to detectable levels. Noting that no ferrous form of the enzyme was detected following addition of oxygenated buffer (see Figures 2.3.12-2.3.15) during preparation of dioxygen adducts, it may be possible that the ferric form accumulated due to autooxidation. Further RR investigation of irradiated samples in the high-frequency region showed high content of the ferrous form, presumably arising from radiolytic reduction of the ferric form, which accumulated during oxy-ferrous preparation by autooxidation (Figure 2.3.24)

In an earlier study,[105] Denisov *et al.* utilized EPR spectroscopy to characterize the intermediates produced following radiolytic reduction of the oxy-ferrous complex of substrate-free CYP119. The authors observed a species with an EPR signature characteristic of the hydroperoxo intermediate (g-values = 2.29, 2.20, 1.95), which decays to the low-spin ferric form, via a 'peroxide shunt' pathway, upon gradual annealing at 170-195 K.[105] Interestingly, when EPR spectroscopy was employed in the investigation of irradiated samples of the dioxygen adducts of LA- and PFDA-bound CYP119 (Figure 2.3.25), the respective spectra exhibited rhombic features (g = 2.28, 2.16, 1.95) characteristic of the hydroperoxo intermediate of P450s.[20,30,105] Unfortunately, a high content of the low-spin ferric form was also observed with g-values [2.40, 2.24, 1.916], possibly formed during oxy-ferrous preparation, by autooxidation, as mentioned above. As can be seen in the EPR spectra (Figure 2.3.25 top trace) at 77 K, the low spin ferric content is higher in the PFDA-bound CYP119 samples; this may be attributed to the lower binding affinity of PFDA as compared to LA, such that autooxidation is possibly faster for the corresponding dioxygen adduct. Based on the EPR data, discussed above, it can be confirmed that input of one electron into the oxygenated intermediate

resulted in the formation of the hydroperoxo intermediate, however, to levels not detectable by RR at 77 K inasmuch as the only scattered light collected, is from the surface of the frozen samples. Annealing of the irradiated samples of LA- and PFDA-bound CYP119 oxy-ferrous complexes resulted in the attenuation of the hydroperoxo signal (Figures 2.3.26 and 2.3.27), as previously observed in the substrate-free samples,[105] however, both tubes reportedly broke during annealing, which explains the low S/N ratio in the spectra from 183-198 K. Interestingly, the hydroperoxo signal for the LA-bound sample is still present at 198 K, consistent with the higher initial content of oxygenated LA sample compared to the PFDA-bound sample as discussed above. Noting that these EPR studies were performed at 15 K, it may be possible that the signal of the compound I form of CYP119 could not be detected due to fast relaxation at this temperature.[123] Rittle and Green,[85] who utilized *m*-CPBA to artificially produce the compound I form of CYP119, were able to detect the EPR signals consistent with an S = 1 Fe(IV)=O that is exchange coupled with an S = ½ ligand based radical at 7.5 K. The authors utilized high microwave power to fully saturate signals from contaminating paramagnetic species and obtained the CYP119 compound I spectrum by difference. In any case, the detection of the hydroperoxo intermediate, in this present work, is especially encouraging in that there is a reasonable probability of trapping and spectroscopically characterizing the compound I by EPR at 7.5 K, using the approach outlined by Rittle and Green[85] and possibly even by RR, provided sufficiently oxygenated ferrous forms of substrate bound CYP119 can be produced.

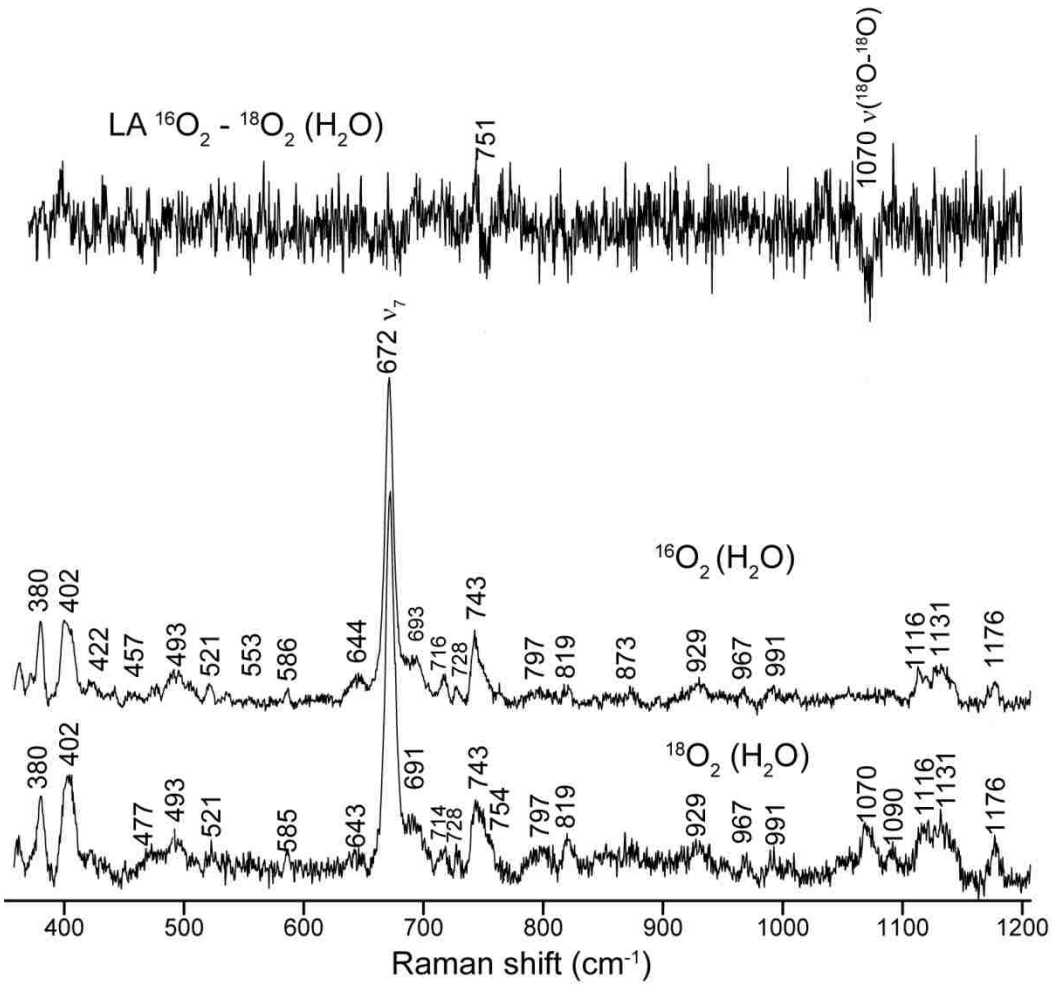

Figure 2.3.20 RR spectra of irradiated dioxygen adducts of LA-bound CYP119 in H_2O buffer [$^{16}O_2$ (H_2O) and $^{18}O_2$ (H_2O)] collected using the 442 excitation line at 77 K. The top trace shows the difference spectra of $^{16}O_2$ – $^{18}O_2$.

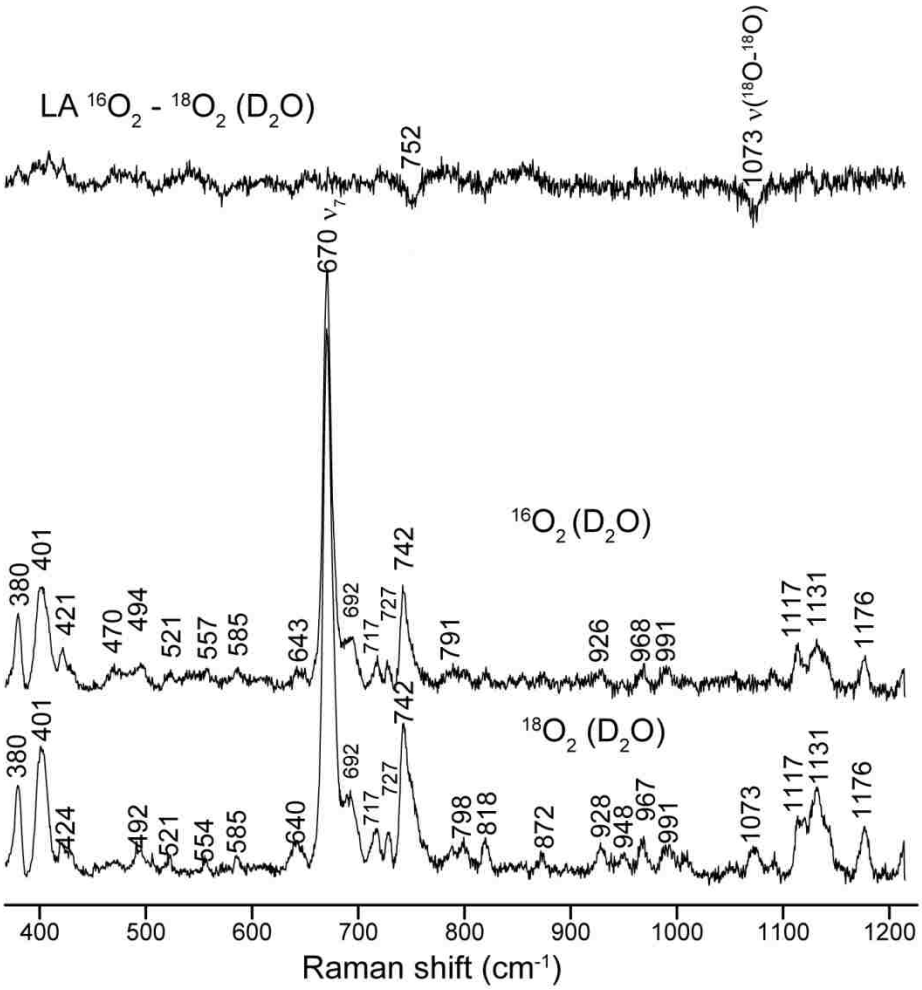

Figure 2.3.21 RR spectra of irradiated dioxygen adducts of LA-bound CYP119 in D_2O buffer [$^{16}O_2$ (D_2O) and $^{18}O_2$ (D_2O)] collected using the 442 excitation line at 77 K. The top trace shows the difference spectra of $^{16}O_2$ – $^{18}O_2$.

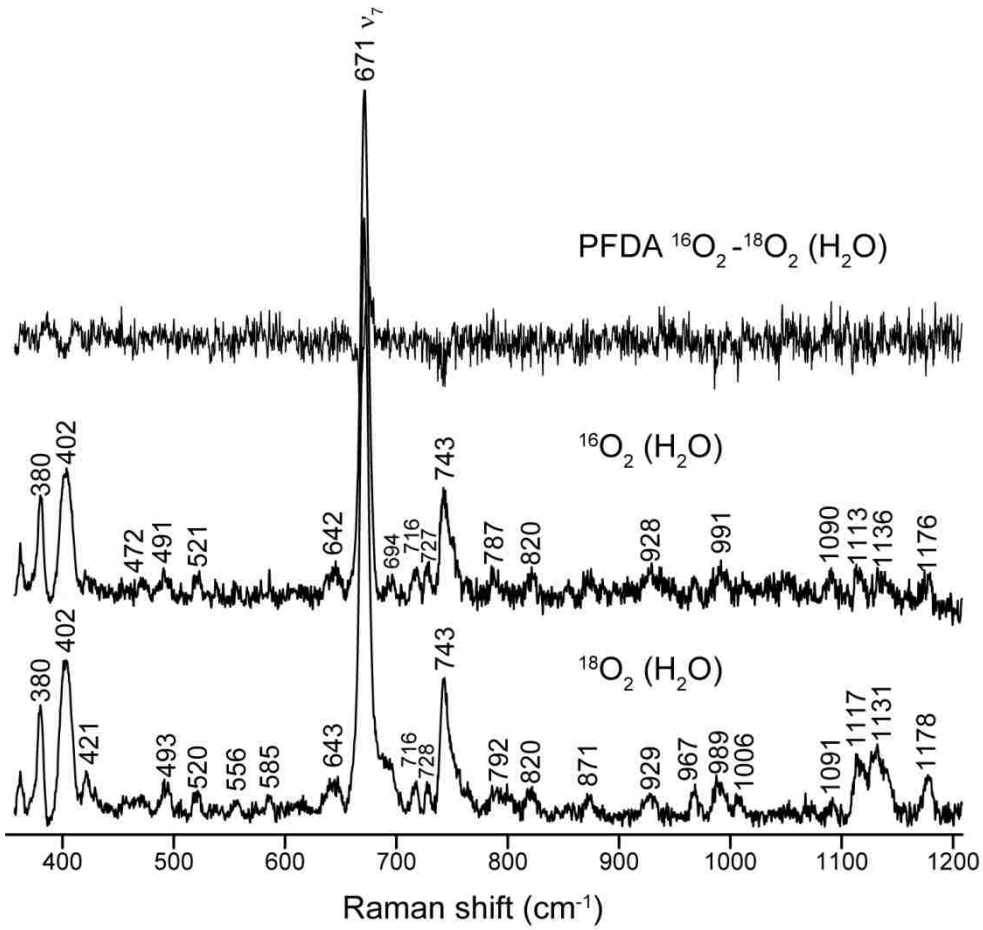

Figure 2.3.22 RR spectra of irradiated dioxygen adducts of PFDA-bound CYP119 in H_2O buffer [$^{16}O_2$ (H_2O) and $^{18}O_2$ (H_2O)] collected using the 442 excitation line at 77 K. The top trace shows the difference spectra of $^{16}O_2 - {}^{18}O_2$.

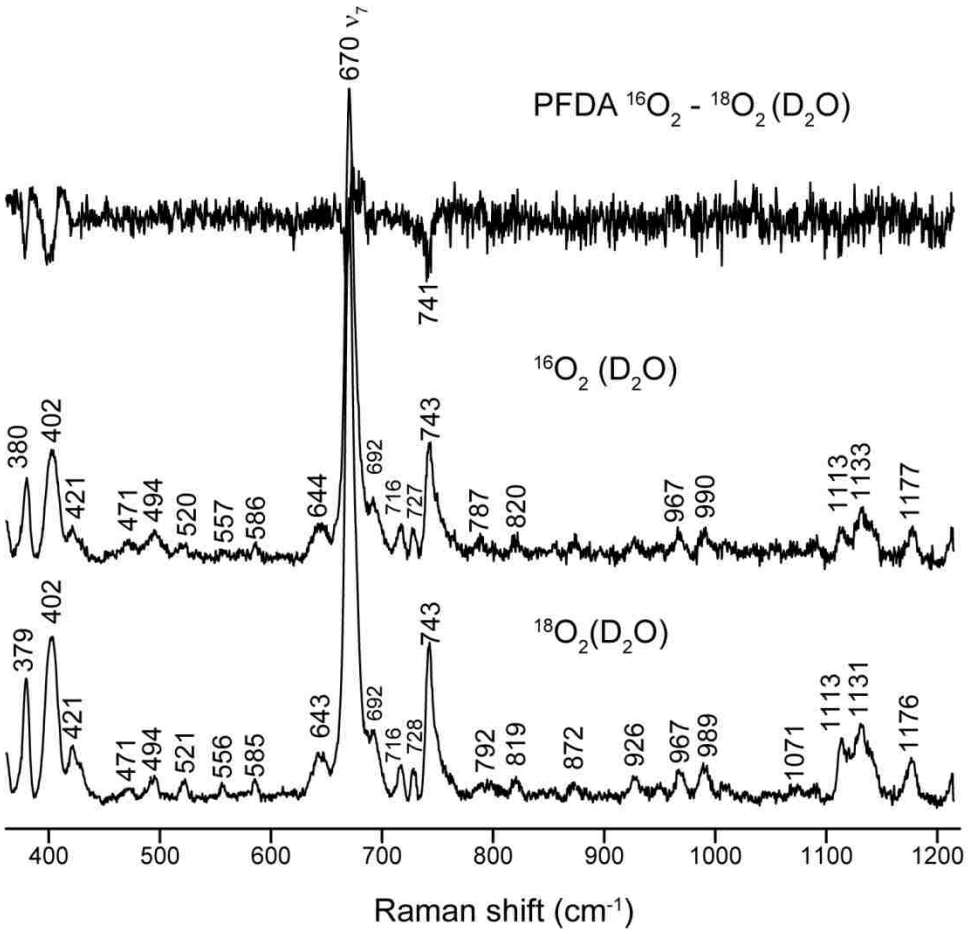

Figure 2.3.23 RR spectra of irradiated dioxygen adducts of PFDA-bound CYP119 in D_2O buffer [$^{16}O_2$ (D_2O) and $^{18}O_2$ (D_2O)] collected using the 442 excitation line at 77 K. The top trace shows the difference spectra of $^{16}O_2 - {}^{18}O_2$.

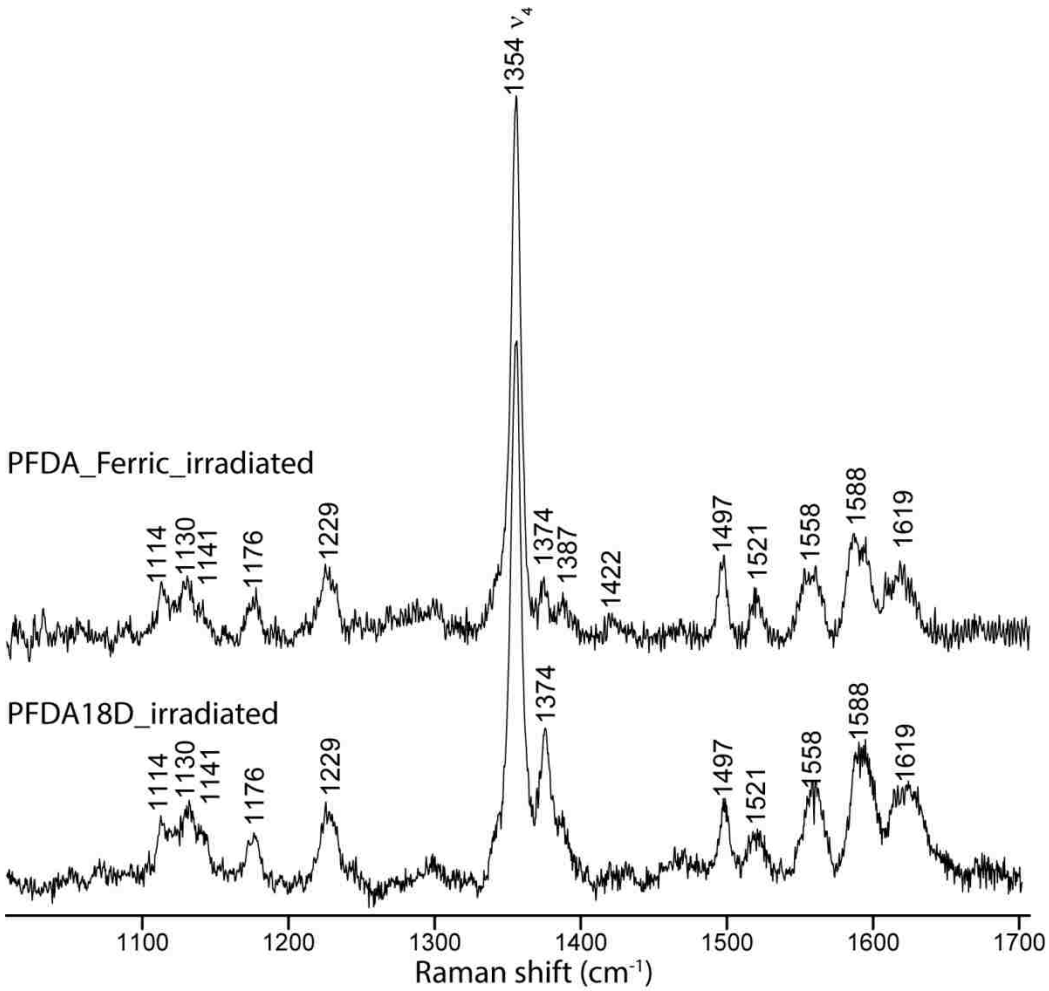

Figure 2.3.24 High-frequency RR spectra of irradiated ferric (top trace) and $^{18}O_2$ (bottom trace) complex of PFDA-bound CYP119 in D_2O buffer

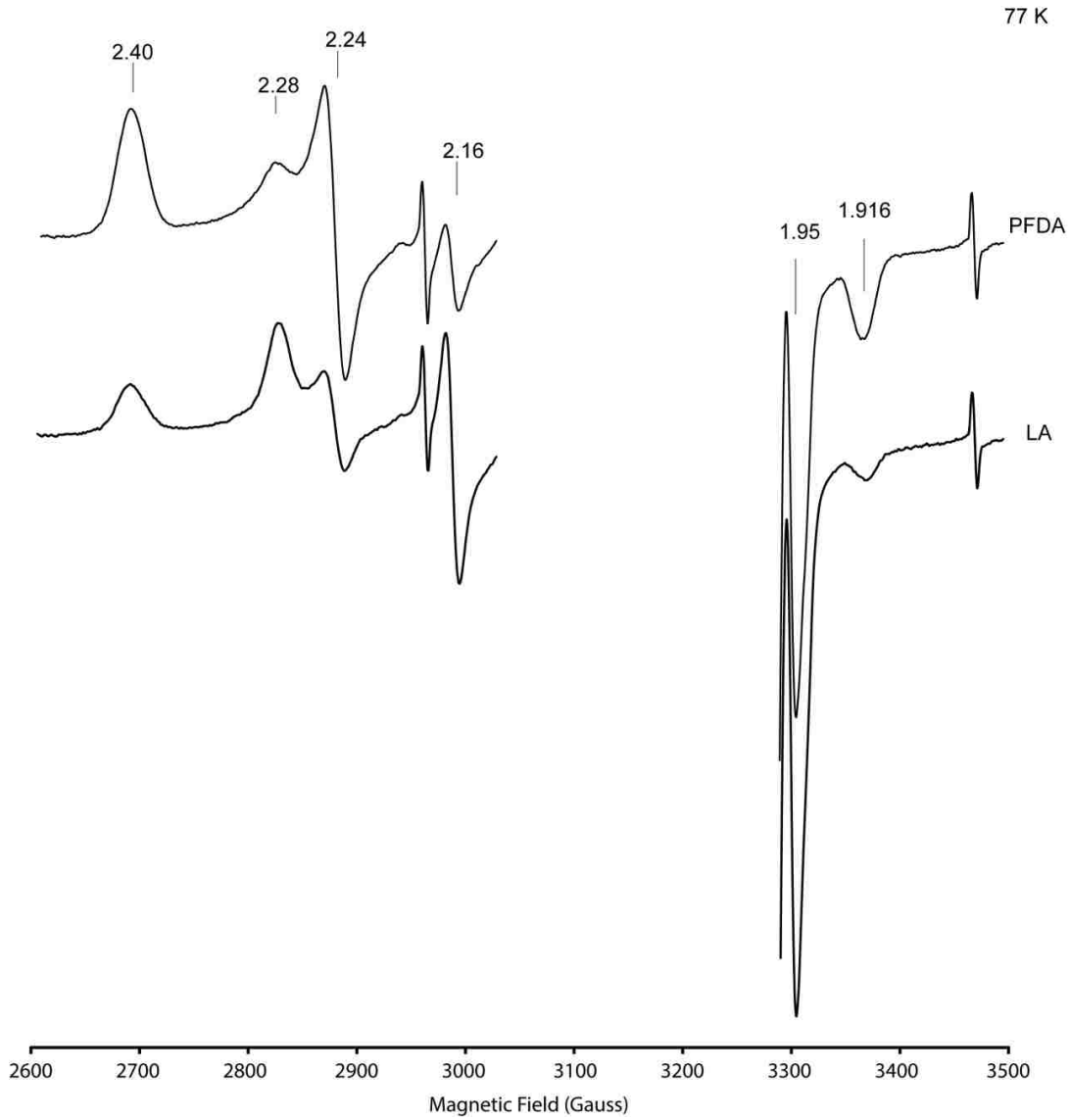

Figure 2.3.25 EPR spectra of irradiated oxy-ferrous samples of PFDA-(top trace) and LA-bound (bottom trace) CYP119 at 77 K. The strong signal at g = 2 not shown

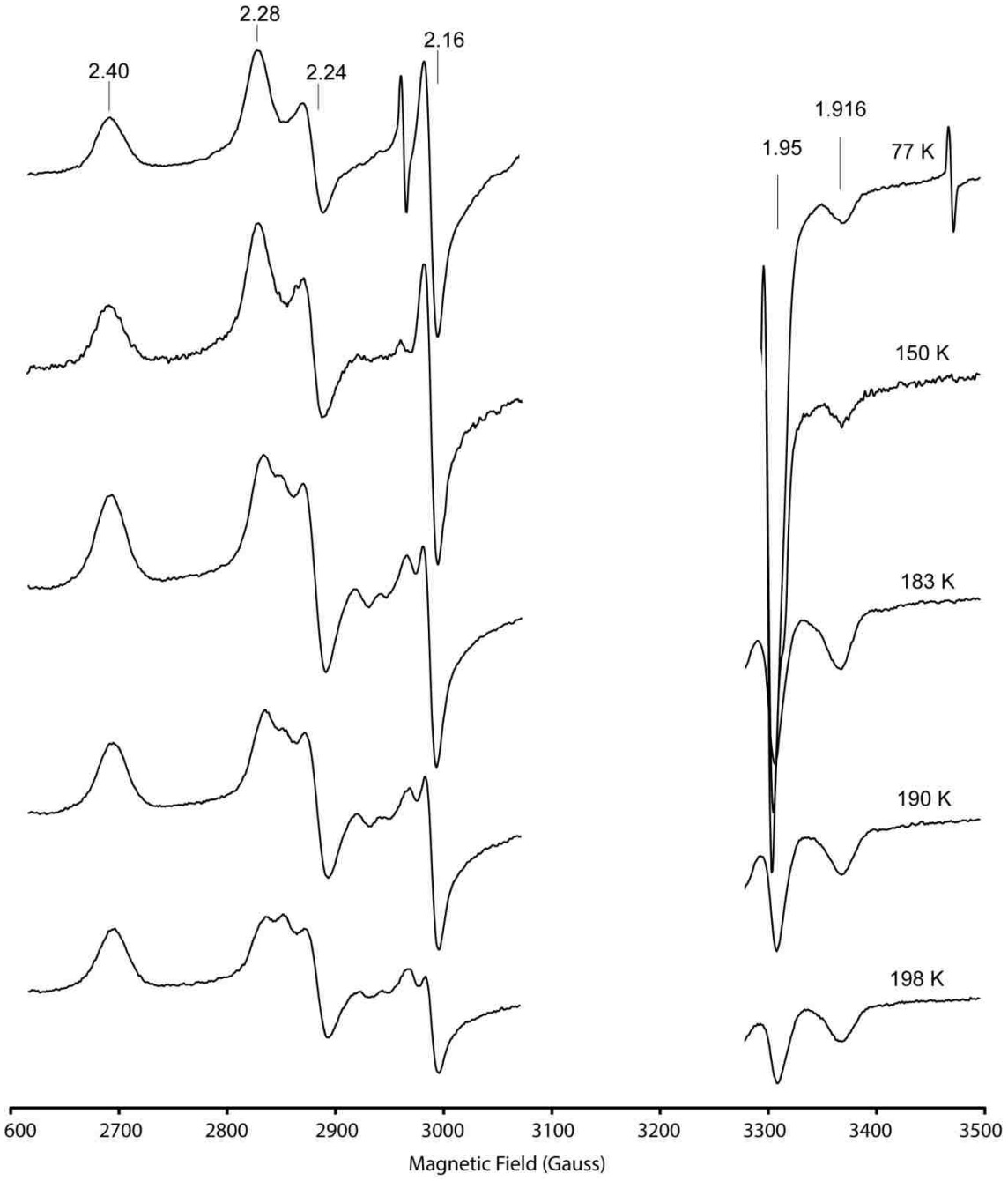

Figure 2.3.26 EPR spectra of irradiated samples of the dioxygen adduct of LA-bound CYP119 at different annealing temperatures. The strong signal at g = 2 is not shown

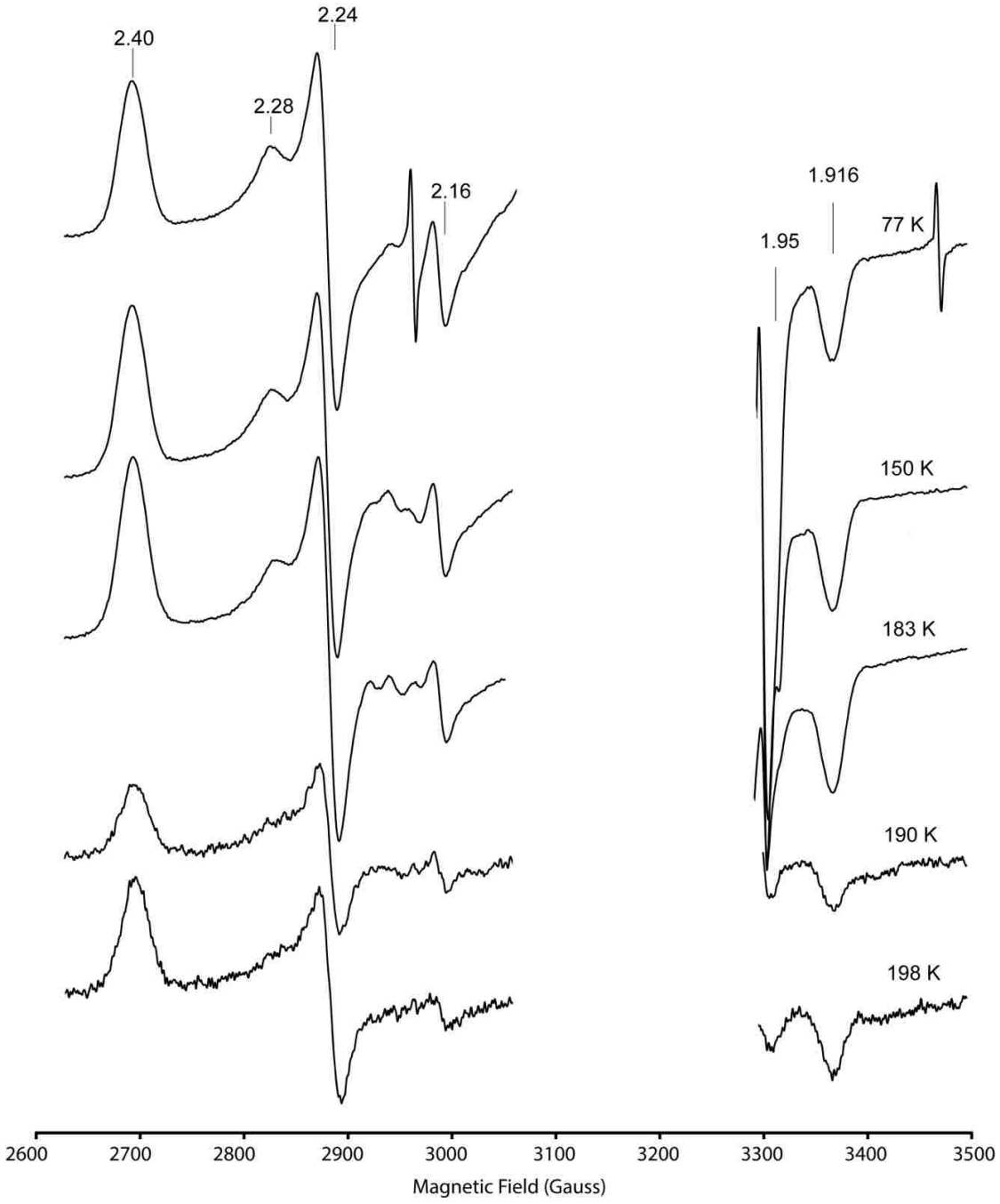

Figure 2.3.27 EPR spectra of irradiated samples of the dioxygen adduct of PFDA-bound CYP119 at different annealing temperatures. The strong signal at g = 2 is not shown

2.4 Summary

The present work employed PFDA as an inert substrate of the thermophilic CYP119 in an attempt to generate, capture and spectroscopically characterize the compound I intermediate. CYP119 was shown, by absorption and RR spectroscopic methods, to bind LA and PFDA, inducing significant spin state changes at elevated temperatures (70 °C). However, no substantial substrate-binding associated shifts were observed in the ν(Fe−CO) for both substrates, possibly due to the open active site conformation of the thermophilic enzyme. Dioxygen adducts of substrate-bound samples of CYP119 were prepared at -20 °C, by rapidly mixing oxygen-saturated buffer with the ferrous form of the enzyme. Formation of the oxy-ferrous complex was confirmed by RR at 77 K where isotopic sensitive modes, consistent with the O−O bond stretching frequency, were observed. Cryoradiolysis was employed to generate the subsequent intermediates in the P450 catalytic cycle, specifically, the peroxo or hydroperoxo intermediates. RR investigation of the irradiated samples at 77 K, however, could not detect isotope sensitive bands in the regions expected for either peroxo/hydroperoxo intermediates. Residual oxy-ferrous form was observed in the $^{18}O_2$ samples of LA-bound, possibly indicating inefficient reduction. On the other hand, EPR spectroscopy of irradiated samples confirmed generation of the hydroperoxo intermediate (g = 2.28, 2.16, 1.95), however with a high content of the low-spin ferric form, possibly due to autooxidation (during oxy-ferrous preparation). The hydroperoxo species EPR signal was observed to decrease during stepwise warming from 77 to 198 K, however, tubes broke during annealing, making interpretation of the data difficult. Noting that the high content of the ferric low spin form in the irradiate samples could be due to autooxidation, production of sufficiently oxygenated ferrous substrate-bound CYP119 could be achieved

by reducing the mixing time (from 10 s to 5 s, for example) following addition of the oxygenated buffer. In addition, autooxidation may be decreased by reducing the cooling temperature from – 20 to – 30 ° C. This will however require increasing the glycerol content in the buffer. On the other hand, cryosolvents mixtures such a mixture of buffered ethylene glycol (20 %), methoxyethanol (70 %) could be employed to obtain less viscous protein solutions at – 50 °C.[124] Detection of the hydroperoxo intermediate by EPR at 15 K provides proof of reduction of the dioxygen adduct. Inasmuch as EPR detection of the artificially produced compound I was achieved at temperatures below 8 K, performing the above experiments at 7.5 K with irradiated samples containing an initial high content of the oxy-ferrous form, may possibly lead to the detection of the compound I form of CYP119 in complex to PFDA under turnover conditions for the first time.

CHAPTER 3 NMR DERIVED PARAMETERS FOR DOCKING SUBSTRATES TO CYTOCHROMES P450

3.1 Introduction

Cytochrome P450 2D6 (CYP2D6) is an enzyme responsible for metabolizing at least 20% of all drugs in the market, trailing behind only CYP3A4, which metabolizes at least 50%. The rather promiscuous behavior of these important drug metabolizing proteins is physiologically efficient in that it eliminates the need for the body to produce specific enzymes for each of the multitudinous pharmaceutical products or other xenobiotic compounds encountered and is attributed to the malleability of their active sites, which allows binding of different substrates (Table 3.1.1).[125–127]

Table 3.1.1 List of CYP2D6 substrates[127]

Amitriptyline	Doxepin	Methylphenidate	Propranolol
Amoxapine	Doxorubicin	Metoprolol	Protriptyline
Aripiprazole	Duloxetine	Mexiletine	Risperidone
Atomoxetine	Flecainide	Mirtazapine	Sertraline
Betaxolol	Fluoxetine	Moclobemide	Tamoxifen
Captopril	Fluphenazine	Nefazodone	Tamsulosin
Carvedilol	Fluvoxamine	Nortriptyline	Thioridazine
Chloroquine	Haloperidol	Oxycodone	Timolol
Chlorpromazine	Hydrocodone	Paroxetine	Tolterodine
Clomipramine	Imipramine	Perphenazine	Tramadol
Codeine	Labetalol	Pindolol	Trimipramine
Desipramine	Lidocaine	Pipotiazine	Venlafaxine
Dextroamphetamine	Lomustine	Procainamide	Zuclopenthixol
Dextromethorphan	Maprotiline	Promethazine	
Dihydrocodeine	Methamphetamine	Propafenone	

The presence of a basic nitrogen and a planar aromatic ring is a structural feature common to all known CYP2D6 substrates, as shown below in some representative structures (Figure 3.1.1).[128,129]

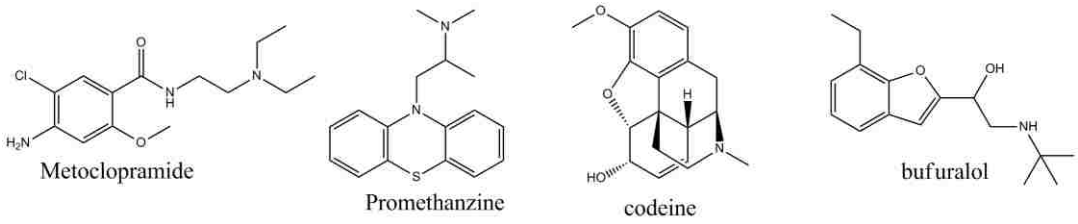

Figure 3.1.1 Four representative structures of CYP2D6 substrates with the typical basic nitrogen and a planar aromatic ring

Unfortunately, efficient and accurate prediction of protein-ligand interactions by computational docking methods,[130,131] which are routinely employed in determining the relative binding affinities of potential substrates and inhibitors, is compromised by the inherent flexibility of these binding sites. This, coupled to the fact that few crystal structures of protein-ligand complexes exist for these mammalian P450s, highlights the need for the development of strategies that can furnish valuable experimentally derived parameters for application in docking routines.

Another long time problem of studying mammalian membrane bound P450s is the difficulty in expression and their lack of solubility in aqueous buffers such that the use of detergents is required to solubilize the proteins. In recent years soluble forms of mammalian proteins have been heterologously expressed in *E. coli* strains transformed with plasmid constructs bearing truncated P450 gene fragments that lack the N-terminus (hydrophobic membrane spanning) region.[128,132] Rowland *et al* [128]reported the crystal structure of a ligand-free (Figure 3.1.2) truncated form of the human CYP2D6 in which the N terminus of the wild type protein had been truncated at residue 34 and replaced with a more hydrophilic 2C3d N –terminus (residue 2-10). In order to increase the solubility, site directed mutagenesis was used to replace leucine surface hydrophobic residues at position 230 and 231 with the more hydrophilic aspartate and arginine residues, respectively. [128]

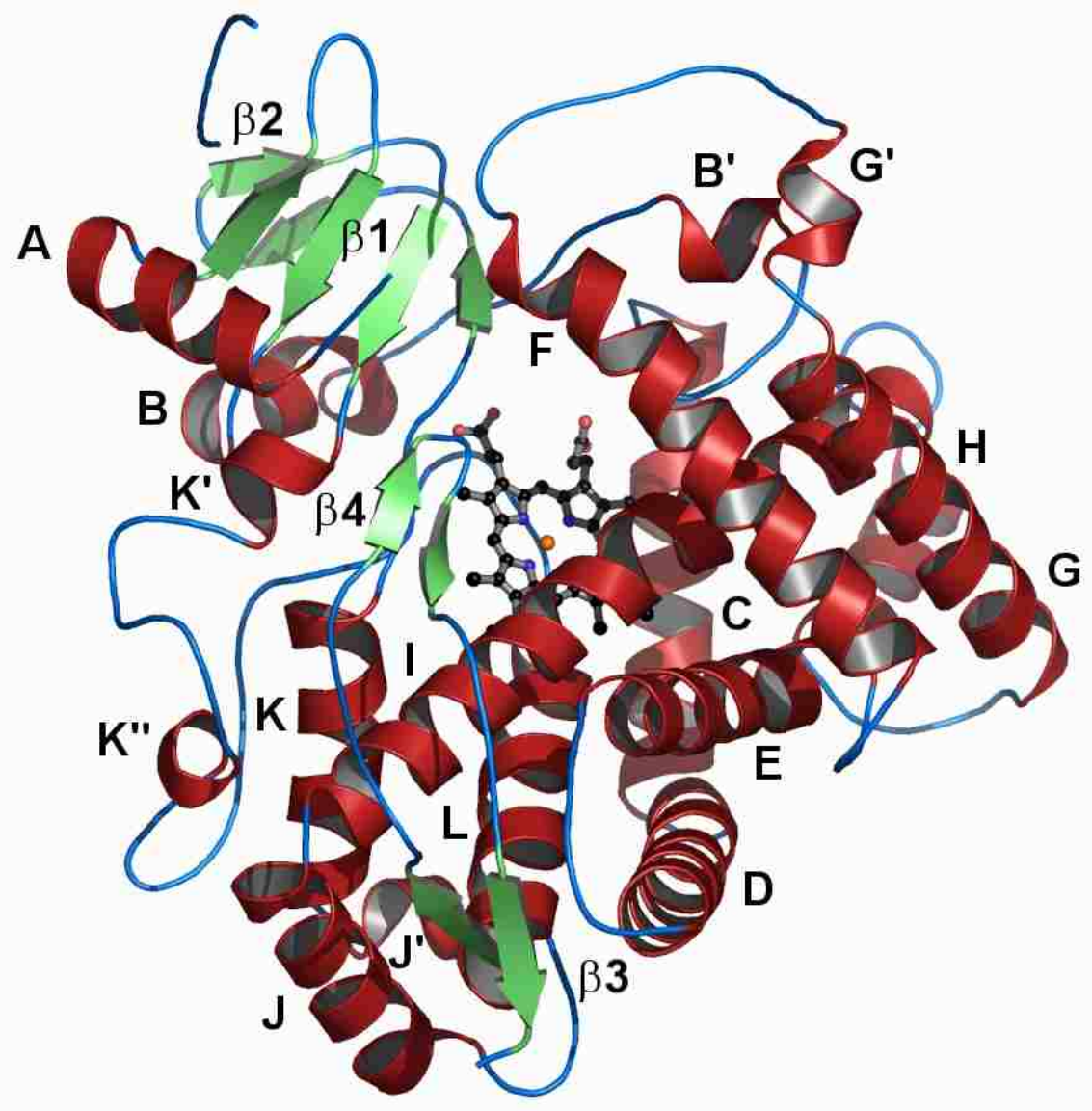

Figure 3.1.2 The crystal structure of ligand-free CYP2D6[128]

The ligand-free structure reported by Rowland *et al* differs significantly from the recently published structure of prinomastat (a substrate and potent inhibitor of CYP2D6) bound CYP2D6 (Figure 3.1.3).[132] Differences were evident in β sheet 1, helices A, F, F`, G", G and H as well as the helix B-C loop. Prinomastat bound CYP2D6 exhibits a closed cavity active site, which closely conforms to the substrate structure as compared to a rather open

active site of the ligand-free enzyme. This apparent induced fit model was attributed to a change in the direction and pitch of helix F and a turn at Gly-218, which is followed by a well defined helix F` not observed in the ligand-free structure (Figure 3.1.3).[132]

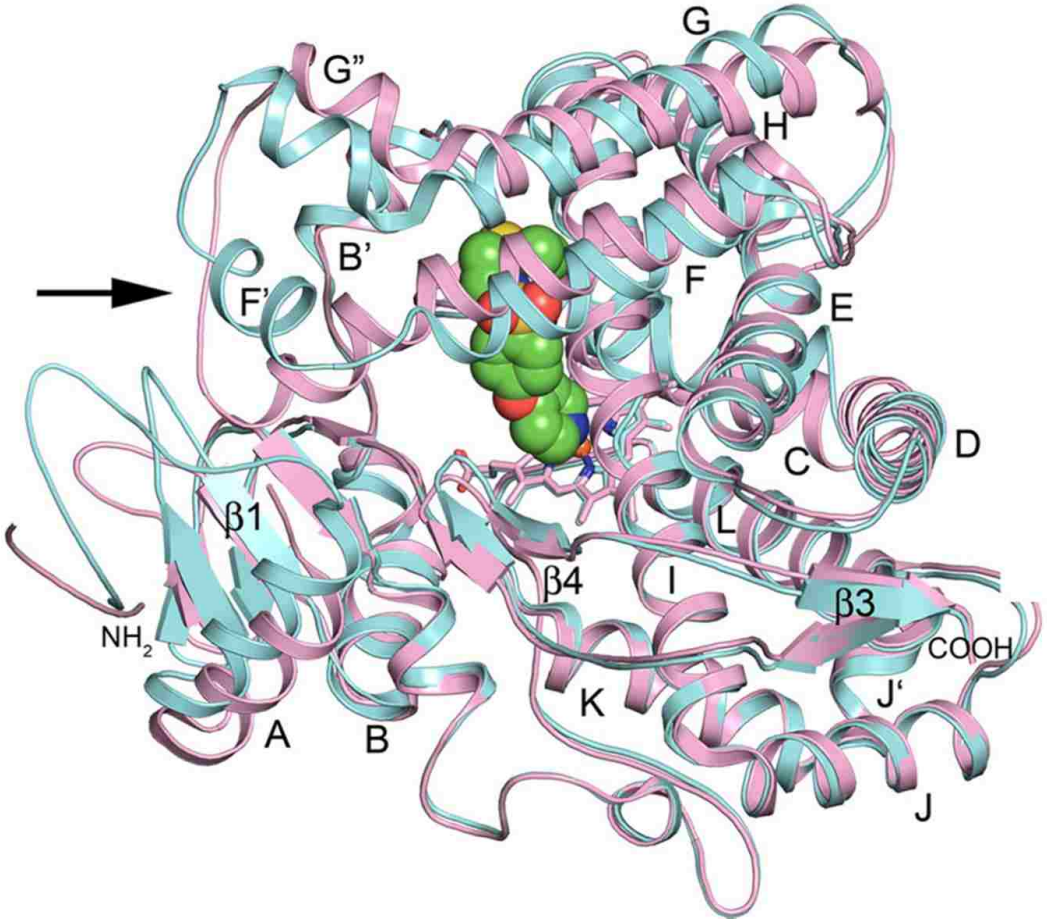

Figure 3.1.3 Superposition of the prinomastat-bound (cyan) and ligand-free (light magenta) crystal structures. The arrow indicates the F' helix present in the substrate bound structure.[132]

Inasmuch as the number of crystal structures of protein-ligand complexes is likely to increase with the advent of better methods to express soluble mammalian proteins, adequate representation of the flexible P450s active sites could still be a challenge. Thus the potentially tremendous value of solution structure determination by spectroscopic methods cannot be over emphasized. The present study aims at exploiting NMR

spectroscopic methods to define the solution active site architecture of P450s. Thus, NMR measurements of P450s bearing isotopically labeled heme will be used to derive distances between reference points on the heme prosthetic group and substrate protons. Isotopically labeled P450cam was employed as a proof of principle exercise for this strategy of defining active site structure in mammalian P450s using NMR methods. More specifically, P450cam containing a heme group ^{13}C-labeled at the methine carbons was heterologously expressed in *E-coli* cells grown on media supplemented with [5-^{13}C] δ-aminolevulinic acid ([5-^{13}C] δ-ALA, a precursor in the heme biosynthesis). It is noted that use of this particular labeled precursor results in labeling of C_α and C_m carbons on the heme group (Figure 3.1.4), the latter of which will be useful for application of the nuclear Overhauser effect (NOE), an NMR technique used to determine spatial proximity between nuclei. NOEs will be measured for the methine protons (using ^{13}C filter), providing needed data to determine relative distances from detectable substrate and active site amino acid residues protons. This will provide better definitions of substrate disposition in the active site and offer experimentally derived parameters, which are of potential value in docking calculations involving drug metabolizing enzymes. Incorporation of spectroscopically derived restrictions in docking routines will further refine these computational methods of defining the relative binding affinity and disposition of substrates in the active site of the protein

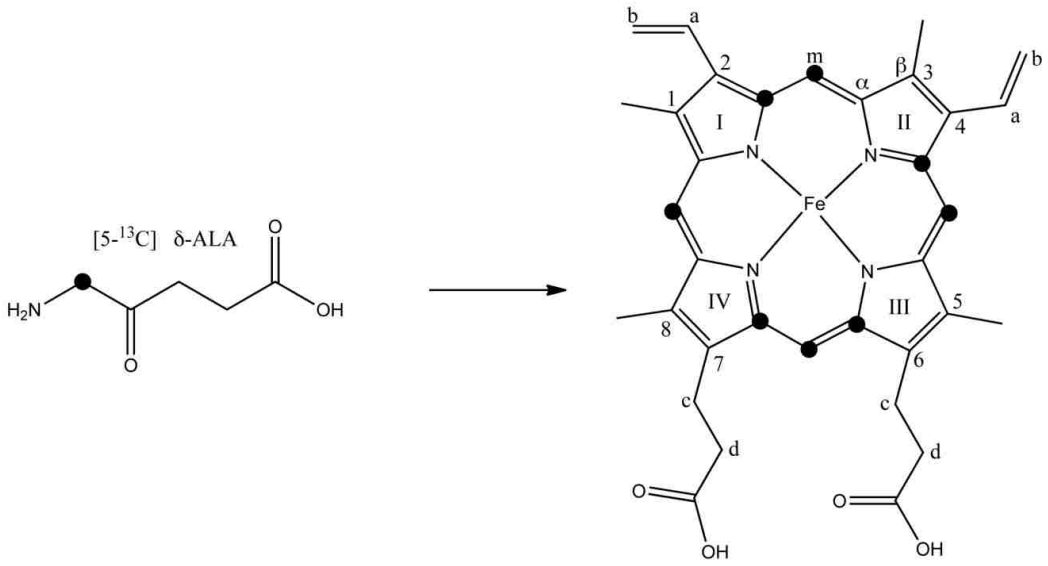

Figure 3.1.4 Supplementing bacterial media with [5-^{13}C] δ-ALA will result in the biosynthesis of heme labeled at the C_m and C_α positions; black dots mark the positions of ^{13}C enrichment[79]

3.2 Materials and Methods

The HU227strain of *E.coli* cells were kindly provided by Professor Gregory M. Raner of University of North Carolina Greensboro. CYP101 plasmids were isolated from *E. coli* BL21 cells using the Zippy plasmid prep kit (Zymo Research Corporation). The CYP2D6 construct was custom designed and synthesized by GenSript and cloned into pUC57. Subcloning of the CYP2D6 gene into the pCWori (from the CYP101 construct provided by Professor Paul R. Ortiz de Montellano of the University of California San Francisco) was also performed by GenSript. Phthalic anhydride and NaI were purchased from Sigma Aldrich while ethyl 3-bromopropionate, Zn-Cu couple and $Pd(PPh_3)_4$ were purchased from Alfa Aesar and used without further purification. The isotopically labeled [2-^{13}C] glycine was purchased from Cambridge Isotope Laboratories.

3.2.1 Synthesis of [5-^{13}C] δ-Aminolevulinic acid (ALA)

Synthesis of [5-^{13}C] δ-ALA with an average yield of 70% was achieved in four steps (Scheme 3.2.1) from [2-^{13}C] glycine following published procedures, with minor modifications.[94,95] Specific details of the procedure summarized are for the natural abundance δ-ALA. The ^{13}C enriched heme biosynthesis precursor was synthesized from [2-^{13}C] glycine after successful optimization of the procedure.

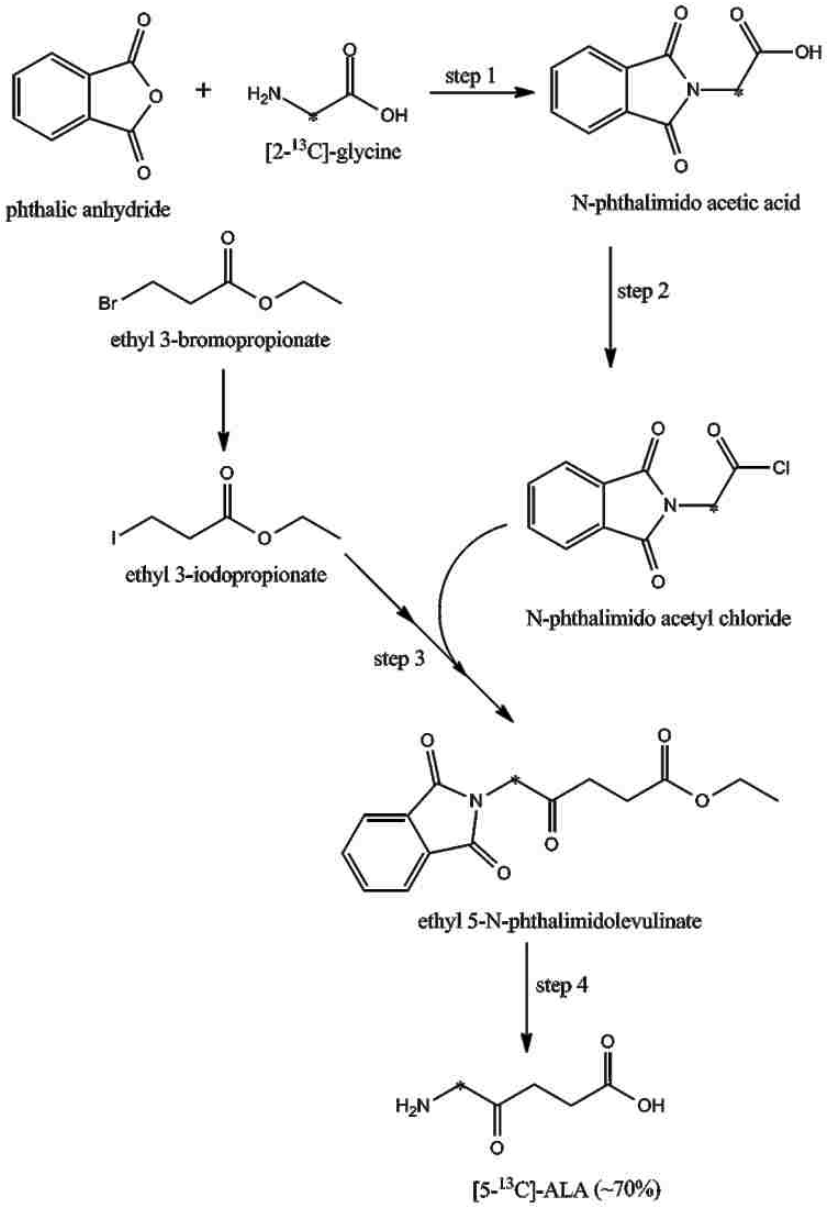

Scheme 3.2.1 Synthesis of [5-^{13}C] δ-ALA, the asterisk represents the ^{13}C enriched carbon

Step 1: Synthesis of N-phthalimido acetic acid

Well ground phthalic anhydride (~2 g, 13 mmol) and ~1 g (13 mmol) of natural abundance glycine were weighed and transferred to a 50 mL round bottom flask. The solids were mixed well before heating at ~180°C until the whole was melted (~ 5 min). This was followed by rigorous stirring for another 5 min, after which the mixture was cooled to give a yellow residue. The residue was dissolved in ~ 20 mL of hot water (~ 80°C) and left to recrystallize for about 2 h, after which needle-like transparent crystals had formed. The crystals were filtrated and allowed to dry in a desiccator containing P_2O_5. The procedure was repeated using [2-^{13}C] glycine to produce N-phthalimido [2-^{13}C] acetic acid. The ^{1}H- NMR of the recrystallized product matched the published spectra of N-phthalimido acetic acid.[94]

Synthesis of Ethyl 3-iodopropionate

About 17 g (~110 mmol) of NaI were transferred to a 250 mL flame dried 2-neck round bottom flask, to which was added 10 mL (78 mmol) of ethyl 3-bromopropionate and 100 mL of 2-butanone. The flask was purged with argon for about 10 minutes and then refluxed at 90 °C for 16 h under argon. After cooling the suspension was filtered, giving a reddish brown filtrate and a yellowish-white solid. The filtrate was evaporated using the rotary evaporator to remove 2-butanone, after which it was diluted with ~ 80 mL of diethyl ether. This organic solution was washed with brine (3 x ~50 mL washings), followed by distillation to give ethyl 3-iodoprionate in 61% yield.

Step 2: Phthalimido acetyl chloride

A 2.3 g (11 mmol) portion of natural abundance N-phthalimido acetic acid was weighed and transferred to a flame-dried 50 mL round bottom flask, to which 30 mL of $SOCl_2$ was added. The mixture was refluxed at 80°C for 18 h after which the reaction was cooled and the excess $SOCl_2$ was removed by rotary evaporator. The residue was dissolved in 5 mL of dry toluene and evaporated (this was done 3 times) to remove excess $SOCl_2$. Immediately before use in the coupling reaction, described below, the product was dissolved in 5 mL of anhydrous toluene under Ar.

Step 3: Ethyl phthalimido levulinate

A 1.0 g portion of Zn-Cu couple was weighed and transferred to a flame-dried 2-neck 50 mL round bottom flask. The flask was flushed with argon for 10 minutes followed by addition of dry toluene (1.2 mL) and 14 mL of N,N-dimethylacetamide (containing < 1% H_2O) under argon. Ethyl 3-iodopropionate (2.0 mL, 12.4 mmol) was added to this suspension and the mixture was stirred for 15 h at 60°C followed by addition of a suspension of $Pd(PPh_3)_4$ (~530 mg) in 5 mL of dry toluene under argon. The reaction flask was then stirred for 5 min at 60°C followed by the addition of a 5 mL of a suspension of partially dissolved phthalimido acetyl chloride in dry toluene. The reaction was stirred for an additional 25 min and then diluted with 300 ml ethyl acetate. This mixture was washed with 1 N HCl (250 mL), saturated $NaHCO_3$ (250 mL) and brine (250 mL), dried over $MgSO_4$, filtered and evaporated. The resulting reddish-brown residue containing the desired product, as judged by ^1H NMR,[94] was passed through a silica gel (60) column (15″ x 1.8″) using ethyl acetate: hexane (1: 1) solvent system. The fractions

were checked by TLC; those with a single spot were pooled and the presence of the desired product verified by ^{1}H NMR and melting point measurements (*vide infra*).

Step: 4 Aminolevulinic acid (ALA)

A 480 mg (1.60 mmol) portion of ethyl phthalimido levulinate was transferred to a 25 mL round bottom flask followed by addition of ~ 6 mL of 6 N HCl. The mixture was refluxed at 110 °C for ~24 h. After cooling to room temperature, the reaction mixture was filtered (crystals of phthalic acid, ~180 mg) and the resulting aqueous filtrate was washed 3 times with diethyl ether (10 mL). The aqueous filtrate was evaporated giving a brown residue, which was recrystallized from an ethanol-ether solution (3 mL). This procedure was repeated using ethyl 5-N phthalimido [5-^{13}C] levulinate to yield [5-^{13}C] δ-ALA in ~ 70% yield.

3.2.2 Expression of [5-^{13}C] δ-ALA P450cam

Viability of HU227 E-coli cells

The cells of the δ-ALA synthase-deficient *E-coli* strain, HU227 obtained as a gift from Dr. Raner (University of North Carolina Greensboro) require $CaCl_2$ treatment[133] to render them competent prior to transformation with the P450cam gene. The viability of the cells was tested by aseptically growing them overnight on LB plates supplemented with the natural abundance δ-ALA. After 12 h of incubation at 37 °C, several colonies appeared in LB plates supplemented with 20 mg/L δ-ALA whilst no growth was observed in plates without δ-ALA (negative control plates). Single colonies were picked

to inoculate 50 mL of LB medium containing 20 mg/L ALA. The cells were shaken (250 rpm) at 37 °C until an OD_{600} of 0.5 (~3 h). The cells were diluted further by spreading 10 µL on LB plates supplemented with ALA and grown overnight at 37 °C. Single colonies were picked and the process repeated as described above. Plates with well separated colonies were stored at 4 °C prior to preparation of competent cells.

Preparation of Competent cells

A single colony of HU227 cells was picked and used to inoculate 100 mL LB medium containing 20 mg/L ALA. The cells were grown (at 225 rpm and 37 °C) to an OD_{600} of 0.5. Ideally for normal *E. coli* strain, cells should reach an OD_{600} of 0.5 after 3h of vigorous shaking; however the cultures in this work reached an OD_{600} of less than 0.1 after ~5h of incubation, possibly indicating high level of cell deaths of this fragile strain of *E. coli*. The cells were left at 4 °C overnight and then transferred to the shaking incubator at 37 °C, finally reaching an OD_{600} of 0.5 after about 2 h. The cells were transferred to ice cold 50 mL polypropylene tubes and incubated on ice for about 10 minutes. The cells were recovered by centrifugation at 4100 rpm for 10 min and the medium decanted. The tubes were inverted on a wad of paper towel to drain away all traces of media. Each pellet was resuspended in 30 mL of ice-cold $MgCl_2$-$CaCl_2$ solution (80 mM Mg Cl_2, 20 mM $CaCl_2$) and mixed by gently swirling. The cells were recovered again by centrifuging at 4100 rpm for 10 minutes followed by decantation of the medium. All traces of the media were drained away by inverting the tubes on a wad of paper towel for about a minute. Each pellet from the original 50 mL culture was resuspended by gently swirling in 2 mL of ice-cold 0.1M $CaCl_2$. Frozen stocks of HU227 competent cells were prepared by gently mixing each 2mL suspension with 70 µL of DMSO and

incubating on ice for 15 min followed by an additional 70 µL of DMSO. Aliquots of 50 µL were transferred to pre-chilled microcentrifuge tubes using sterile chilled pipette tips and immediately frozen using liquid nitrogen. Cells were stored at -80 °C overnight prior to transformation as described below.

Transformation of HU227 cells and expression P450cam

The $CaCl_2$ treated HU227 competent cells were transformed with the pCWori plasmid harboring the P450cam gene and selected for ampicillin resistance on Luria-Bertani (LB) agar plates supplemented with δ-ALA (20 mg/L). A single colony was utilized to initiate expression of P450cam. Specifically, transformed HU227cells were grown (from a single colony) overnight at 37 °C in 10 mL LB broth supplemented with ampicillin and δ-ALA (20 mg/L). About 1% of the overnight culture was used as inoculum in 100 mL of 2YT medium (16 g tryptone, 10 g yeast extract and 5 g NaCl per 1L) also supplemented with ampicillin and δ-ALA. The cells were grown to OD_{600} = 0.8 at 37 °C and 250 rpm followed by addition of 1 mM isopropyl β-D-1-thiogalactopyranoside (IPTG) and 0.5 mM δ-ALA. Induction was allowed to proceed for 24 h at room temperature and shaking at 190 rpm. After 22 h of induction, solid camphor was added to the culture to a final of concentration of 1 mM. The cells were harvested after 24 h of induction by centrifugation at 8000 rpm for 10 min, weighed (12 g/L of culture) and frozen at -80°C. Cells were thawed, resuspended in 3 volumes (3 mL/g of wet cells) of lysis buffer [50 mM Tris-Cl (pH 7.4), 25 mM KCl, 1 mM PMSF, 1 mM camphor, 1 mM EDTA, 1 mg/mL lysozyme, 1 µg/mL leupeptin, 1 mg/mL pepstatin, 1 mg/mL antipain, 32 Units/mL DNase I, 3 Units/mL RNase A)] and incubated at 4 °C for 30 min followed by sonication. Cells were centrifuged at 20 000 rpm for 2 h and the

clarified lysate was concentrated to about 5 mL and loaded onto an anion exchange (DEAE-cellulose) column (3 x 15 cm) equilibrated with 50 mM Tris-HCl (pH 7.4), 25 mM KCl, 1 mM camphor (running buffer). The bound protein band was washed with 6 column volumes (CVs) of the running buffer and eluted by a linear gradient using 50 mM Tris-HCl (pH 7.4), 300 mM KCl, and 1 mM camphor as the elution buffer. Fractions with an Rz (A_{391}/A_{280}) > 0.5 were pooled and concentrated (to about 5 mL) followed by addition of ammonium sulfate (75 mg/mL) The pooled fractions were loaded onto a hydrophobic interaction (Phenyl Sepharose) column equilibrated with 50 mM Tris-HCl (pH 7.4), 25 mM KCl, 1 mM camphor, 25% $(NH_4)_2SO_4$ and washed with 6 CVs of the same buffer. The elution buffer contained 50 mM Tris-HCl (pH 7.4), 25 mM KCl and1 mM camphor. Elution of the bound protein was achieved by applying a linear salt gradient 25-0% $(NH_4)_2SO_4$ and fractions exhibiting Rz > 1.4 were pooled and concentrated to about 2 mL. Ammonium sulfate was removed by exchanging the buffer to 30 mM KPi (pH 7.4), 100 mM KCl, 1 mM camphor D_2O using microsep centrifugal devices. Equilibration of samples in D_2O buffer was performed as an initial step for preparing samples for NMR measurements. When expression was scaled up to 1 liter of 2YT medium, 0.3 mL of ~ 0.4 mM pure P450cam (Rz = 1.5) was obtained. Protein concentration was calculated from the absorption spectra, using an extinction coefficient of ε_{391} = 102 $mM^{-1}cm^{-1}$ for the camphor bound CYP101.[134] The preceding procedure was repeated using [5-^{13}C] δ-ALA resulting in the expression of ^{13}C-labeled P450cam (0.5 mL of ~ 0.2 mM, Rz 1.5; Figure 3.2.1).

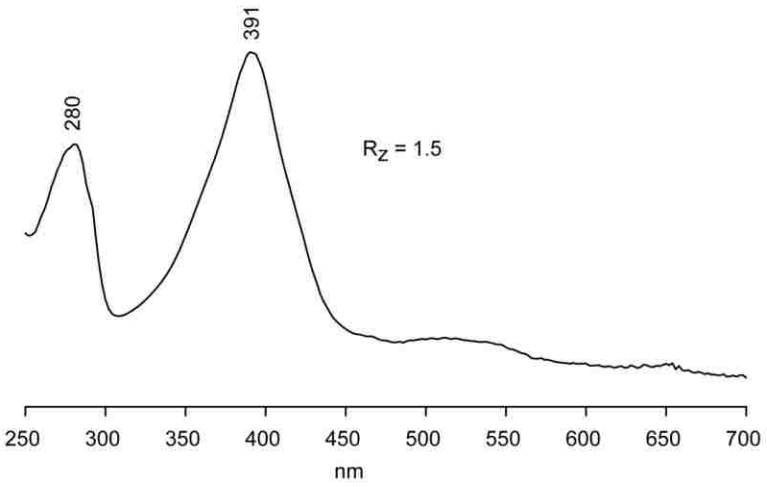

Figure 3.2.1 The absorption spectrum of high spin ferric cytochrome P450cam

3.2.3 CYP2D6 expression

Rowland *et al* (2006)[128] described modifications for the CYP2D6 construct, which included N-terminus truncation (truncated at residue 34 and residues 2-10 of 2C3d inserted at the N terminus), addition of 4 histidines at the C-terminus and mutations of the hydrophobic residues at positions 230 and 231. They reported high level expression of soluble holo-CYP2D6 using this truncate (truncate 5) in *E. coli* (DH10B strain).[128] These modifications described above were used to design a replica of truncate 5 using the wild type gene sequence (NCBI Gene bank: ADF36476.1). Codons for the modifications were derived from reverse translation of the amino acid sequence of 2C3d (for the N terminus) and L230D/L231R mutations and optimized for the *E.coli* expression system (see Figure 3.2.2 for the gene and protein sequences below). NdeI and XbaI restriction endonuclease recognition sites where introduced at the N and C termini respectively to allow subloning into the pCWori+ expression vector.

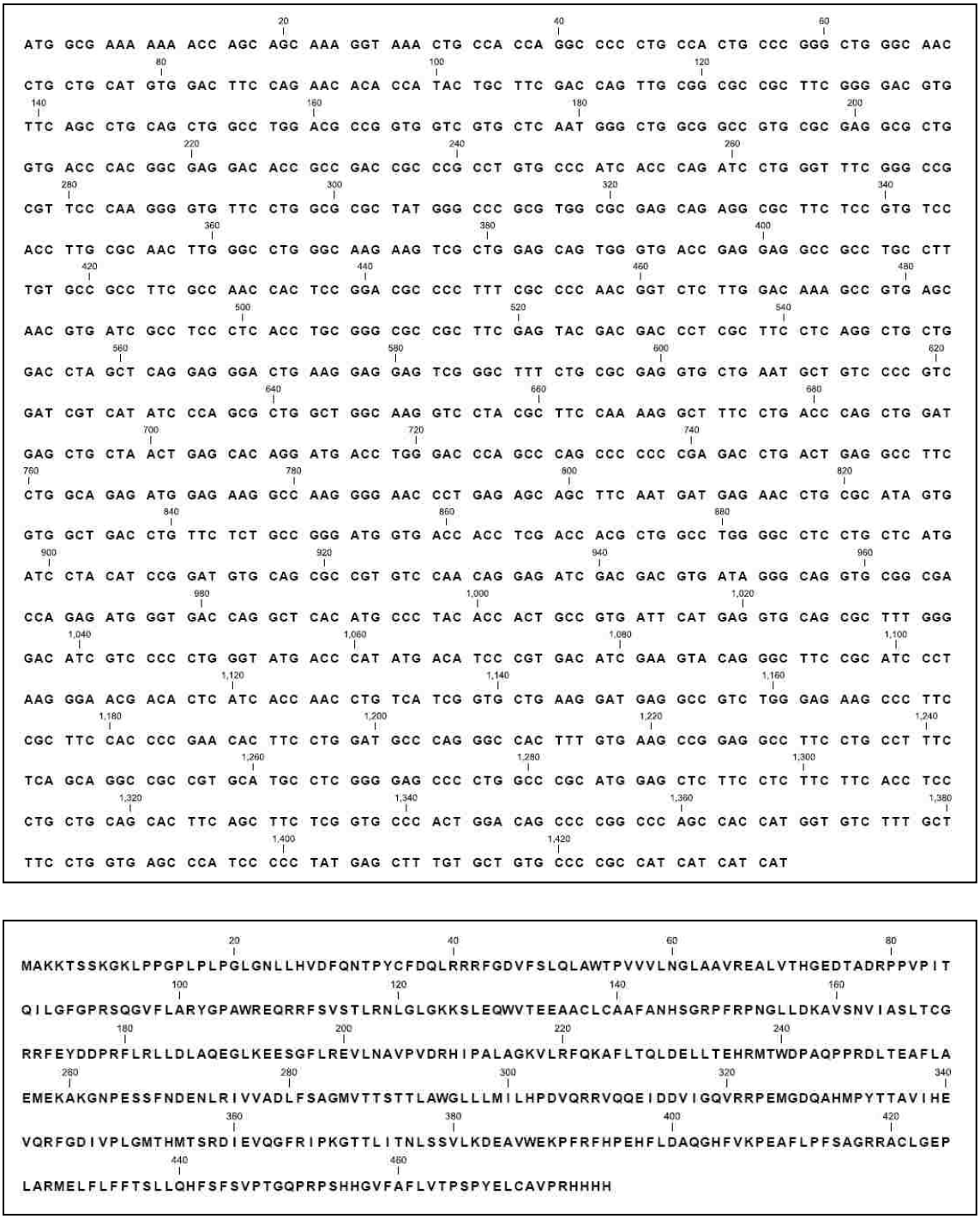

Figure 3.2.2 The gene (top) and protein (bottom) sequences of truncated CYP2D6

The construct was commercially synthesized (by GenSrcipt) and delivered as a lyophilized pUC57 plasmid. The gene was subcloned into pCWori (also by GenSript) and transformed into BL21 and competent HU227 cells for production of the natural

abundance and [5-^{13}C] δ-ALA labeled CYP2D6 respectively. The detailed expression procedure is outlined below. This procedure (with slight variations) has been used to successfully produce [5-^{13}C] δ-ALA CYP101 as already discussed earlier.

Transformed BL21cells were grown (from a single colony) overnight at 37 °C in 10 mL LB broth supplemented with 100 mg/L ampicillin. 1% of the overnight culture was used as inoculum in 100 mL of TB medium [(12 g tryptone, 24 g yeast, 9.4 g K_2PO_4, 2.2 g $KHPO_4$, 4 mL glycerol)/L] supplemented with ampicillin (100 mg/L), 20 mg/L δ-ALA, 1 mM thiamine and trace elements [(27 g $FeCl_3 \cdot 6H_2O$, 2 g $ZnCl_2 \cdot 4H_2O$, 2 g $CoCl_2 \cdot 6H_2O$, 2 g $Na_2MoO_4 \cdot 2H_2O$, 2 g $CaCl_2 \cdot 2H_2O$, 1 g $CuCl_2$, 0.5 g H_3BO_3, 100 mL HCl conc)/L] solution (3 mL per liter of culture).[135] The cells were grown at 30 °C with shaking at 250 rpm to an OD_{600} = 0.6, followed by addition of 1 mM IPTG. Induction was allowed to proceed for 24 h at room temperature and shaking at 190 rpm. The cells were harvested by centrifugation at 8000 rpm for 10 min, weighed (12 g/L of culture) and frozen at − 80°C. Expression of CYP2D6 was checked by CO difference spectra of the total cell lysate. Briefly, cells (~ 1 g) were freeze-thawed twice and resuspended in 4 mL of 400 mM KPi buffer (pH 7.6), 20 % glycerol, and 1 mM CHAPS. The lysate (~ 4 mL) was clarified by centrifugation at 20 000 rpm for 10 min. The clarified solution (~ 3 mL) was transferred to a gas tight 10 mm cuvette, bubbled with CO gas for ~ 20 min and treated with excess $Na_2S_2O_4$ (10 μL of 50 mM dithionite solution). The absorption spectrum was collected using the Hewlett-Packard Model 8452 Diode Array Spectrophotometer. The supernatant, presumably containing the cytosolic fraction of the truncated CYP2D6, was obtained following cell lysis performed according to a published procedure.[128] The cytosolic fraction in 400 mM KPi, pH 7.4, 20% glycerol and 10 mM β-mercaptoethanol buffer, was loaded onto a Ni^{2+}-nitrilotriacetic acid column equilibrated

with the same buffer and washed with 6 CVs washing buffer containing 400 mM KPi, pH 7.4, 20% glycerol, 10 mM β-mercaptoethanol, 50 mM glycine and 100 mM NaCl. The bound fraction was eluted using a linear gradient 0-100 mM EDTA (and simultaneously glycine concentration of 50 to 0 mM) of elution buffer (400 mM KPi, pH 7.4, 20% glycerol, 10 mM β-mercaptoethanol, 100 mM EDTA), as previously reported.[128] Fractions exhibiting spectral characteristics of CYP2D6 (Soret band at 415 nm) were pooled, concentrated and checked for P450 (and any P420) by CO difference spectra. The procedure described above was scaled up and applied to BL21 cells transformed with the pCWori+ plasmid bearing the truncated gene of CYP2D6.

3.2.4 Resonance Raman Spectroscopy of [5-^{13}C] δ-ALA P450cam

RR measurements of ferric forms of the natural abundance and ^{13}C enriched P450cam were essentially the same as described earlier except that the 406 nm excitation line from the Kr+ laser (Coherent Sabre) was used with ~ 15 mW at the sample and that spectra were collected at room temperature.

3.2.5 NMR spectroscopy

^{1}H and ^{1}H-^{13}C heteronuclear single/multiple-quantum correlation (HSQC/HMQC) NMR measurements were performed using Varian 600 MHz equipped with a triple-resonance cryoprobe while 1 D ^{13}C NMR experiments were done on the Varian 400 MHz instrument. NMR samples contained ~0.4-1 mM P450cam (both for the natural isotopic abundance and ^{13}C enriched camphor bound P450cam), 30 mM KPi, pD 7.4, 100 mM KCl, 1 mM camphor. The protein concentration was determined spectrophotometrically

using an extinction coefficient of ε_{391} =102 $mM^{-1}cm^{-1}$ for the camphor bound P450cam.[136] Substrate free samples were prepared by passing the camphor bound protein through a sephadex G25 column equilibrated with 50 mM MOPS buffer followed by equilibration with 30 mM KPi, pD 7.4, 100 mM KCl. One dimensional ^{1}H NMR experiments were performed using 0.1 s acquisition time, 20 ms relaxation delay with a total of 256 scans at 25 °C and were collected before and after ^{13}C and 2 D NMR measurements to verify sample integrity. A total of 400 000 scans were collected for the ^{13}C NMR experiment at 20 °C for both the natural abundance and ^{13}C enriched substrate bound P450cam. The 1 D version of ^{1}H-^{13}C HSQC measurements for the natural abundance and ^{13}C enriched substrate bound and free P450cam were performed at 20 °C using 23 ms acquisition time, 0.2 s relaxation delay and J_{CH} = 200 Hz; a total of 240 000 scans were collected. ^{1}H-^{13}C HMQC experiments, with the decoupler turned off, were performed using 50 ms acquisition time, 10 ms relaxation delay and J_{CH} = 300. ^{1}H-^{1}H NOESY was obtained with pre-saturation delay of 100 ms, acquisition time of 43 ms, 10 ms mixing time, J_{CH} = 600 and 7200 number of scans. All 1D NMR data were processed with the MestReNova NMR processing software with 10 Hz exponential line broadening while 2D spectra were processed using the NMRPipe software.

3.3 Results and Discussion

3.3.1 Synthesis of [5-^{13}] δ-ALA

Step 1: Synthesis of N-phthalimido acetic acid

The first step in the synthesis of ALA was relatively straightforward and complete in 5 min giving pure (see ^{1}H NMR in Figure 3.3.1) N-phthalimido acetic acid in ~86% yield (~2.3 g, 11.2 mmol) with a melting point between 192-197 °C (reported mp is between 193-195 °C)[94] after recrystallization from hot water

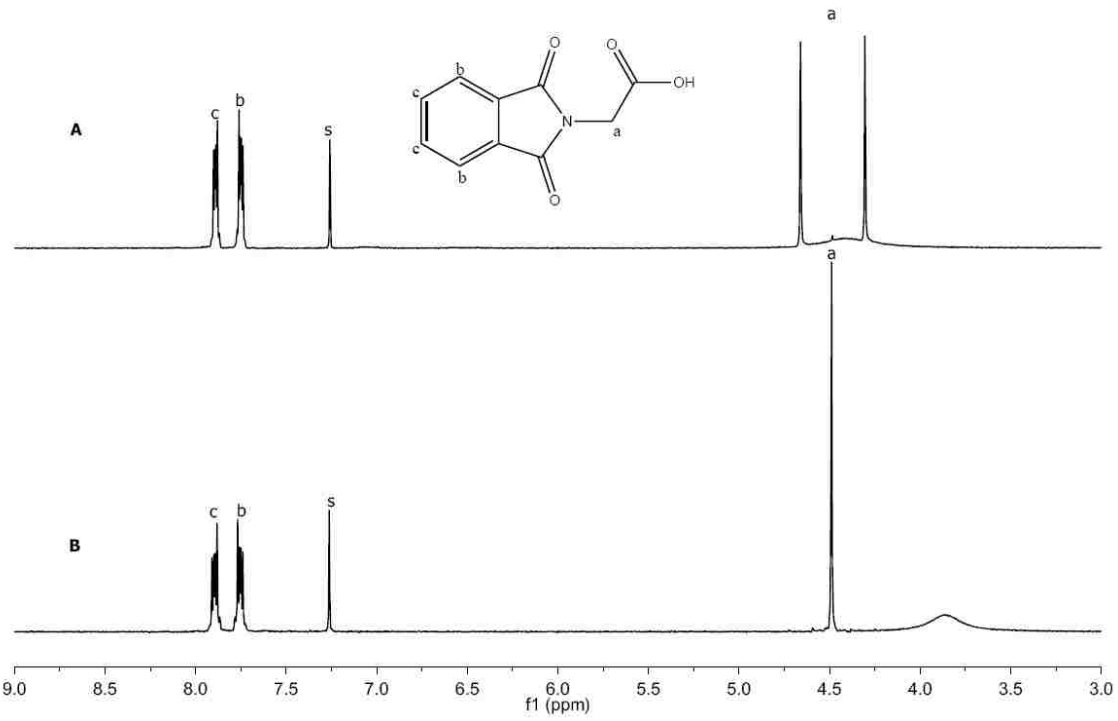

Figure 3.3.1 ^{1}H NMR of natural abundance (**B**) and ^{13}C enriched (**A**) N-phthalimido acetic acid dissolved in $CDCl_3$

Synthesis of Ethyl 3-iodopropionate

Distillation of the reaction mixture of NaI and 3-bromopropionate (in 2-butanone), after refluxing for 16 h at 90 °C, resulted in 61% yield (10.93 g) of 3-iodopropionate. The ^{1}H NMR (Figure Figure 3.3.2) shows a slight down-shift of the proton signals (a) located on C3 that is directly bonded to the halogen, indicating the success of the transhalogenation reaction.

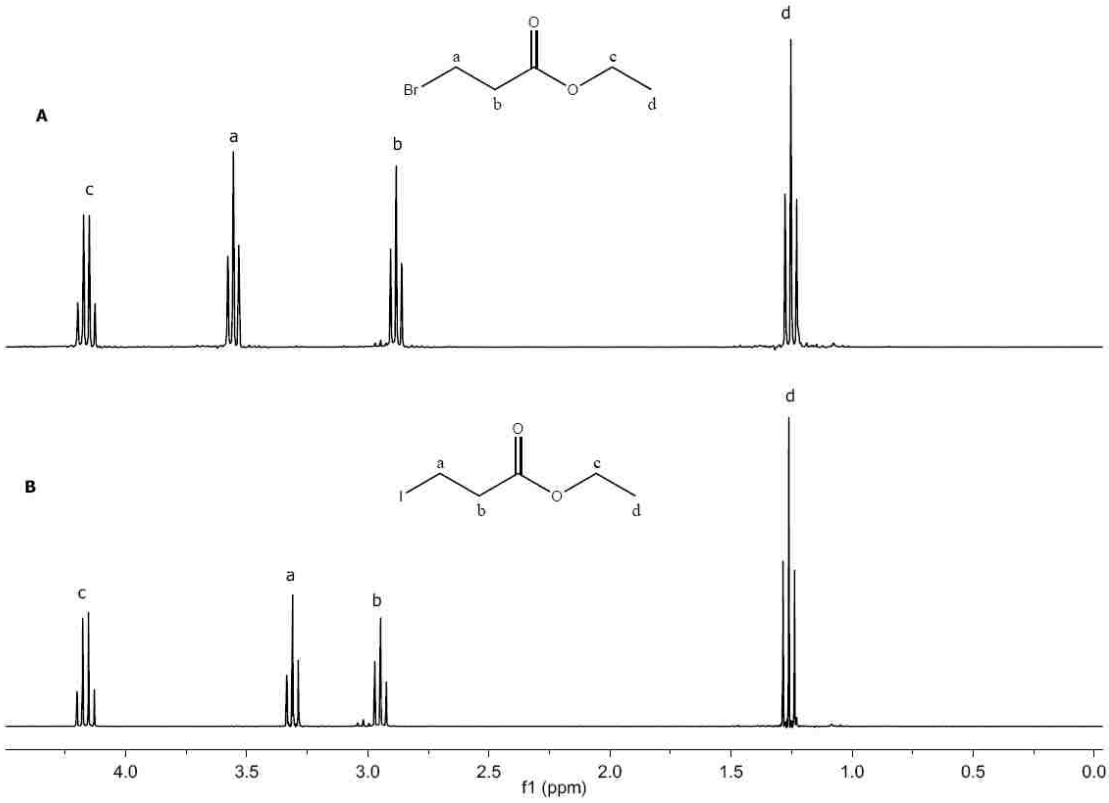

Figure 3.3.2 ^{1}H NMR of ethyl 3-bromopropionate (**A**) and ethyl 3-iodopropionate (**B**) in $CDCl_3$

Step 2: Phthalimido acetyl chloride

(a) Initial attempts

Initial attempts to synthesize phthalimido acetyl chloride following the methods of Kajiwara and Iida[94], resulted in a product that dissolved partially in anhydrous toluene, which was used to remove traces of $SOCl_2$. Removal of the solvent resulted in a dirty-yellowish-white solid. Noting that, in addition to the desired product, acetyl chloride, gaseous SO_2 and HCl are produced in this reflux, these may possibly react with rubber septa (the reaction was initially set up as a closed system under Ar) resulting in the dirty yellowish-white color observed. When an open system was used, the residue obtained after removal of $SOCl_2$ dissolved in dry toluene and was yellowish-white in color. The average yield from the three trials performed on this reaction was ~ 95 % (2.1 g, 2.2 g, 2.2 g) and the purity improved on the third trial as judged by ^{1}H NMR and melting point measurements. The product was left to dry in a desiccator containing P_2O_5. The acetyl chloride was flushed with argon for ~ 10 min and dissolved in 5 mL (the dissolution was only partial) dry toluene immediately before being coupled with 2-ethoxycarbonylethylzinc iodide as described in the following section (*Step 3*). It was noted (by ^{1}H and ^{13}C NMR, Figure 3.3.3) after failed repeated attempts to dissolve phthalimido acetyl chloride (obtained after refluxing phthalimido acetic acid and $SOCl_2$ at 80 °C for 18 h[94]), that when left for ~3 days contained about 25% phthalimido acetic acid, which suggests it is not stable. Phthalimido acetic acid is not soluble in toluene, which may explain the partial solubility mentioned above.

(b) Revised procedure for the synthesis of phthalimido acetyl chloride

This same reaction was reported by Deng *et al*., 2008[137] to be complete in about 3 h at a lower temperature of 60 °C, followed by removal of excess $SOCl_2$ at 55 °C (~ 70 °C was used in the reactions described above). They found that the product was partially decomposed at higher temperatures, which might explain the lower yields obtained in the coupling reactions (*vide infra*). In addition, they pointed out the need to use the product immediately after dissolution in an anhydrous solvent.[147] When this procedure (of Deng *et al*)[137] was followed (10 mlL of $SOCl_2$ was used in the reflux), the reaction was incomplete after 3 h as judged by ^{1}H NMR. It was noted that the reaction is almost done after 2 h when heated to 75 °C and complete after 3 h. Removal of the excess $SOCl_2$ was done under reduced pressure at ~ 55 °C. The resulting yellow crystalline product was dissolved in 3 mL of dry toluene and evaporated (done twice). A few mg of the product was dissolved in $CDCl_3$ for ^{1}H & ^{13}C NMR measurements and the rest of the sample was left to dry in a desiccator overnight to check its stability. The product was found to be stable overnight (by ^{1}H and ^{13}C NMR, see Figure 3.3.4), giving enough time to couple with the 2-ethoxycarbonylethylzinc iodide reaction, which runs overnight for 15 h.

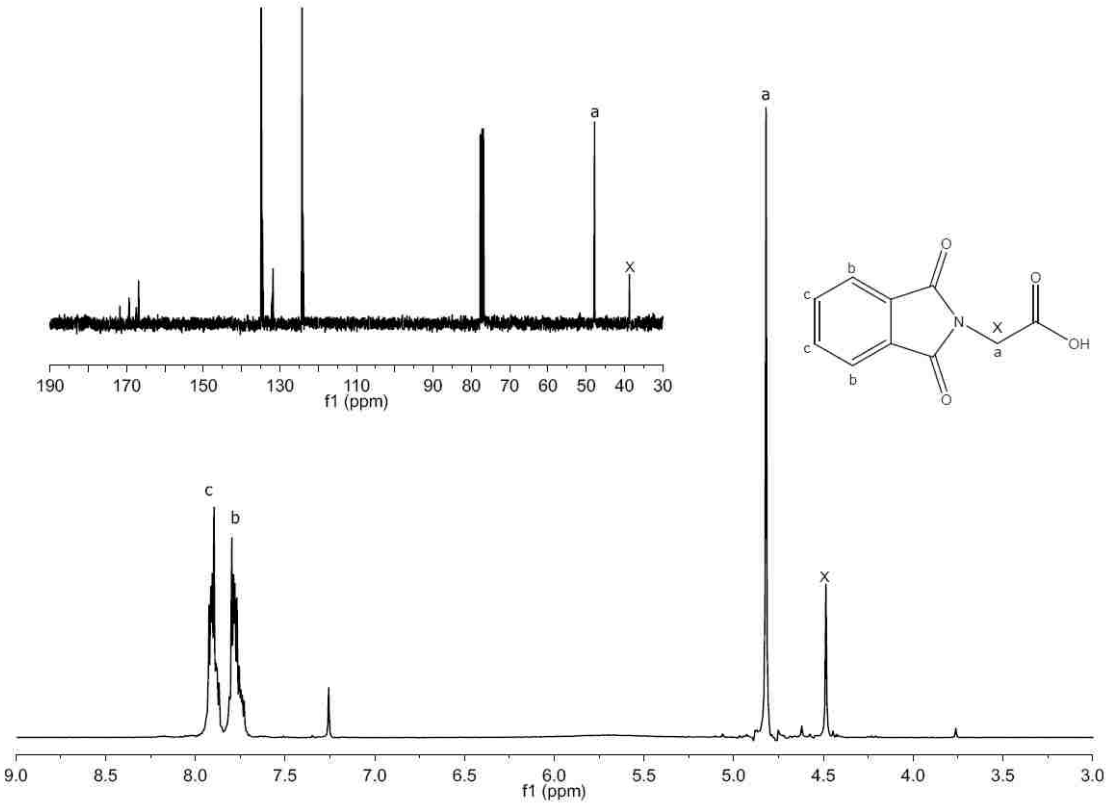

Figure 3.3.3 The ^{1}H NMR spectra of a mixture of phthalimido acetyl chloride and its acid derivative (x; ~ 25% of phthalimido acetic acid). The inset shows the extra ^{13}C signal (x) from the acid derivative

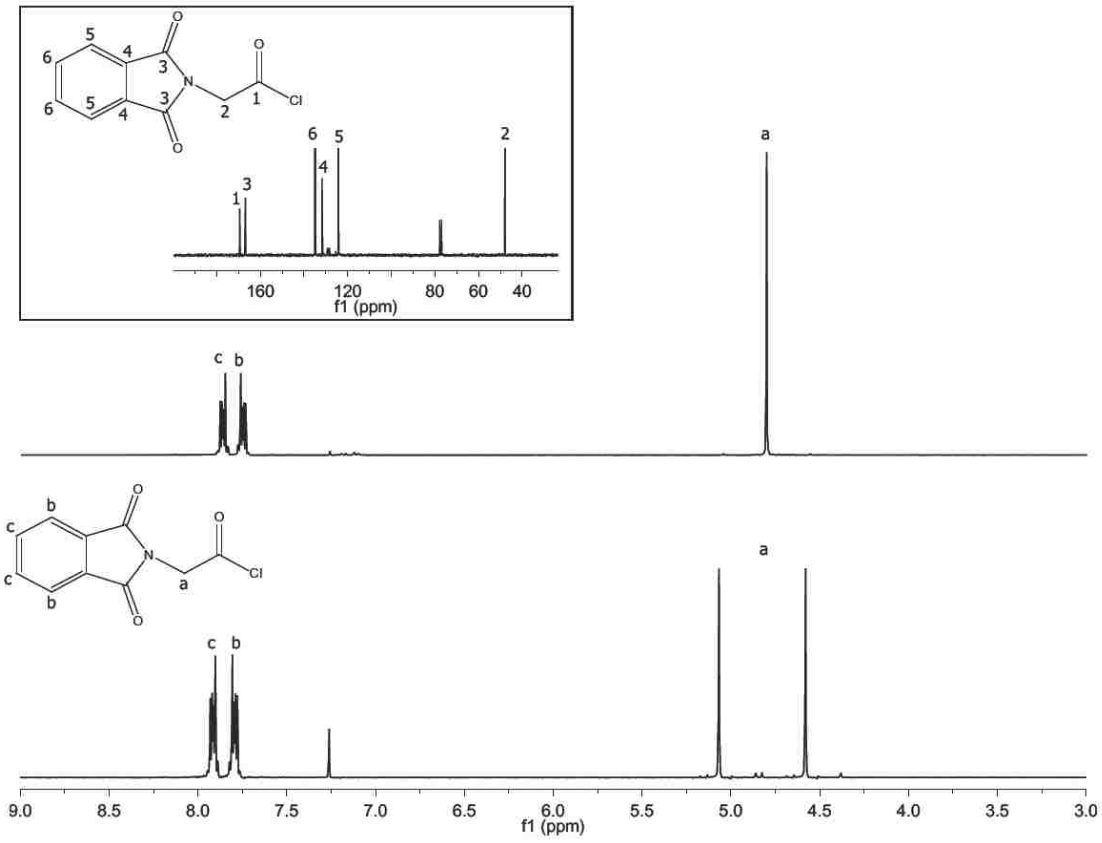

Figure 3.3.4 The ^{1}H NMR of natural abundance (top trace) and ^{13}C enriched (bottom trace) pure phthalimido acetyl chloride (in $CDCl_3$) after 3 h of refluxing phthalimido acetic acid and $SOCl_2$. Inset shows the ^{13}C NMR spectra of the natural abundance phthalimido acetyl chloride

Step 3: Ethyl phthalimido levulinate

(a) Initial attempts

^{1}H NMR of the chromatographed product of the coupling reaction of N-phthalimido acetyl chloride and 2-ethoxycarbonylethylzinc iodide exhibited chemical shifts of the desired product, ethyl phthalimido levulinate; however, very low yields were obtained. Verification of desired product in chromtographed fractions was also done by absorption spectroscopy, whereby the spectrum of the ethyl phthalimido containing fractions (judged by ^{1}H NMR and reported mp)[94] had a maximum at ~ 290 nm (Figure

3.3.5), The low yields obtained could be attributed to the partially dissolved phthalimido acetyl chloride, which as explained above is not stable and easily reverts to the acid form. The use of completely dry solvents and oxygen free atmosphere was discovered to be crucial for obtaining better product yields. Improved yields of up to 800 mg (~25%) were obtained when the coupling reaction was done in a glove box, but still employing partially dissolved phthalimido acetyl chloride. This was however still very low compared to the 92% reported by Kajiwara and Iida (2002).[94] Campbell and Johnston (1989)[95] in their synthesis of 5-amino [4-^{14}C] levulinic acid, reported this coupling reaction as the key step. They used 200 mL of ethyl acetate to dilute the reaction mixture and used only 50 mL in their washings. In the present work the lower yields obtained could possibly be due to loss during the washings therefore smaller volumes of the aqueous washes were adopted in the modified procedure briefly described below.

(b) Improved procedure

Ethyl 3-iodopropionate (~ 2.5 mL) was added to a suspension of Zn-Cu couple (1.35 g) in ~27 mL of dry toluene and ~ 2 mL of anhydrous dimethylacetamide under argon. The whole was stirred for 1 h at room temperature and at 60 °C for 4.5 h under Ar instead of 15 h. To this flask was added a suspension of 418 mg $Pd(PPh_3)_4$ in 5 mL of dry toluene under argon, followed by stirring for 5 minutes at 60 °C, after which a solution of phthalimido acetyl chloride (~ 2 g) in 5 mL of dry toluene was added and stirring continued for an additional 10 min; longer times (15 min >) have been reported to produce side products, which makes it necessary for stringent purification steps to be employed.[95] The reaction was diluted with ethyl acetate (~200 mL), washed with 1 N HCl (50 mL), saturated $NaHCO_3$ (50 mL) and brine (50 mL), dried over anhydrous

$MgSO_4$ and filtered. An orange residue (crude product) was obtained; note the difference in the color from reddish brown that was discussed earlier. Removal of solvent by rotary evaporator followed by recrystallization from absolute ethanol (5 mL) gave white crystals of pure ethyl phthalimido levulinate in 75% yield (average of 2 trials).

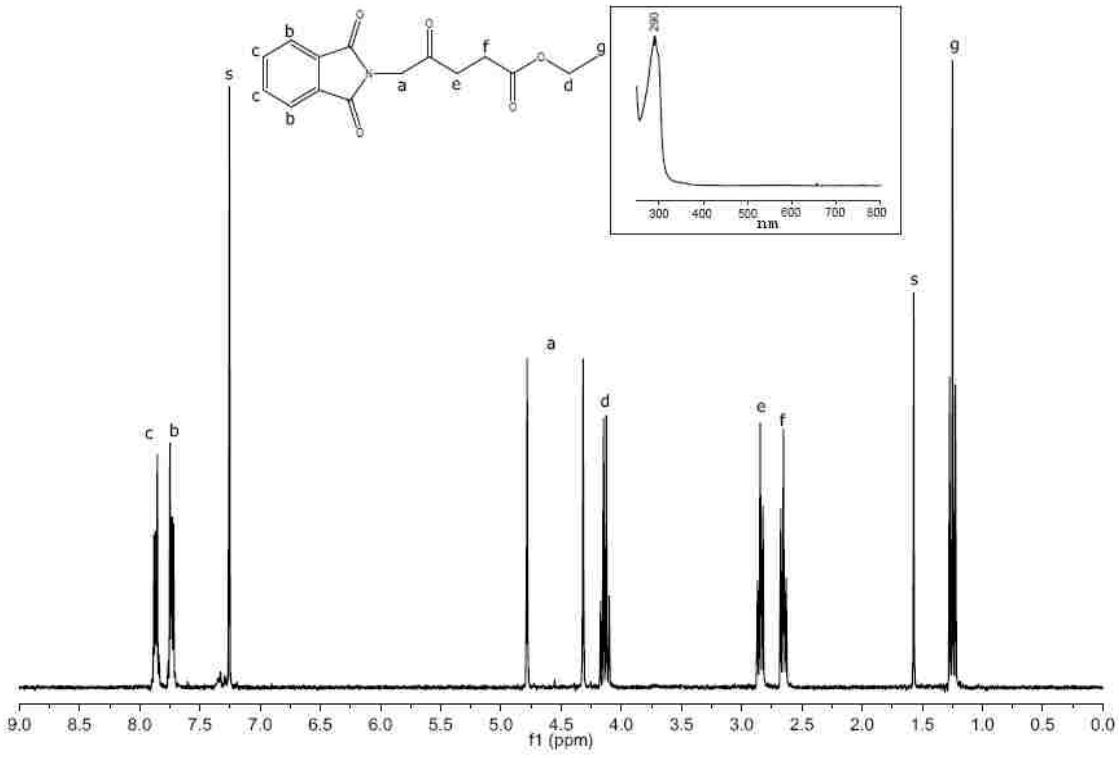

Figure 3.3.5 ^{1}H NMR of ^{13}C enriched ethyl phthalimido levulinate dissolved in $CDCl_3$ (s); Insert shows the absorption spectrum of fractions containing pure ethyl phthalimido levulinate

Step: 4 Aminolevulinic acid (ALA)

Hydrolysis of ~ 480 mg of ethyl phthalimido levulinate in 6N HCl resulted in ~ 140 mg (65 %) white crystals of pure ALA after recrystallization from ethanol-ether (Figure 3.3.6). Approximately 20 mg of the starting material, ethyl phthalimido levulinate, was recovered following evaporation of the ether layer, indicating a

reasonably high conversion rate; based on the theoretical yield calculations, ~ 60 mg of product was lost possibly during the washings (washing of the aqueous layer with diethyl ether following filtration of the hydrolysis reaction mixture) and/or the recrystallization step described section 3.2.1.

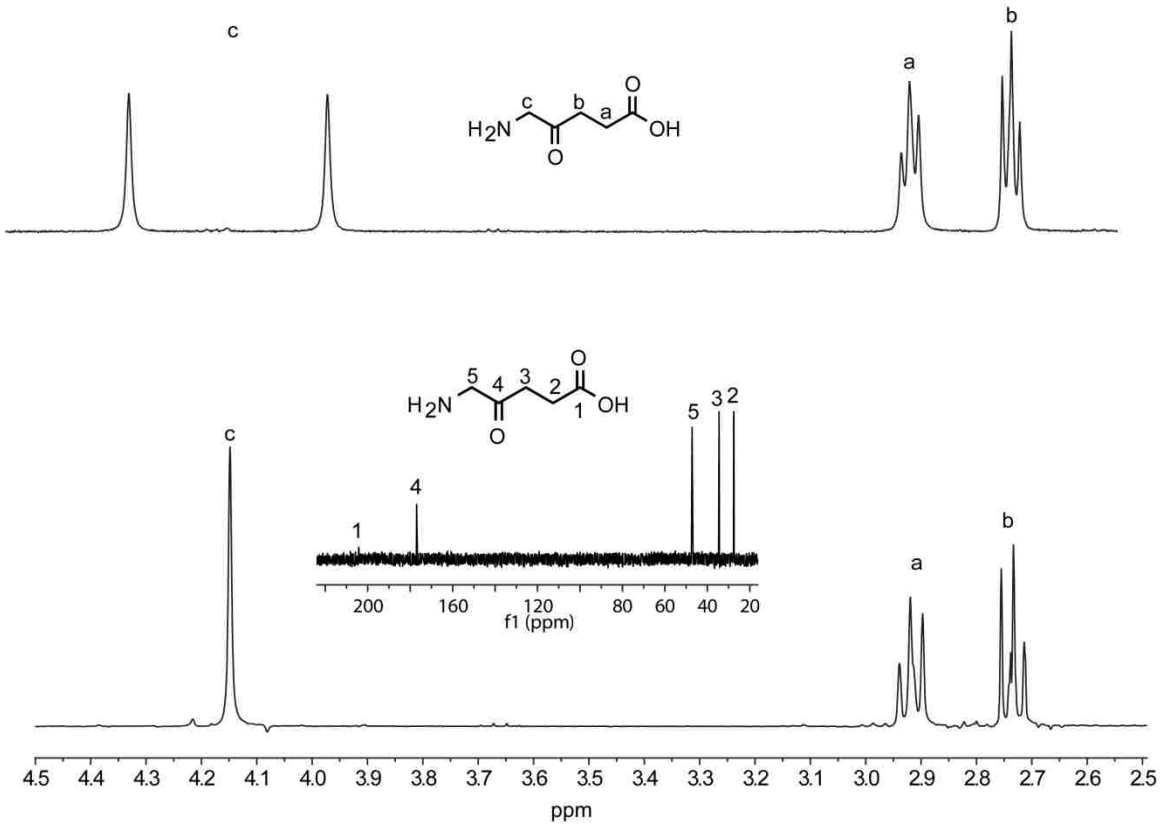

Figure 3.3.6 The ^{1}H NMR spectra of the natural abundance δ- ALA (bottom trace) and [5-^{13}C] δ-ALA (top trace) dissolved in D_2O; insert shows the 13C NMR spectrum of the natural abundance δ-ALA

3.3.2 CYP2D6 Expression

This initial trial expression of CYP2D6 from BL21 cells transformed with pUC57 bearing the truncated gene of the protein was confirmed by the CO difference spectra of the total cell lysate (Figure 3.3.7). When the cytosolic fraction was applied onto the Ni^{2+} -nitrilotriacetic acid column only a small fraction was bound and the eluted fraction exhibited spectral characteristics consistent with a hexacoordinated heme species (top trace of Figure 3.3.8).[138,139] Upon elution with the gradient described above, the initially bound fraction, however, exhibited an absorption maximum at around 415 nm (middle trace of Figure 3.3.8), which is characteristic of low spin heme protein. Expression of CYP2D6 from glycerol stocks could not be confirmed in subsequent trials; rather, an absorption spectrum characteristic of a six coordinated heme species, which was resistant to reduction, was observed (Figure 3.3.9). It is possible that the C-terminus histidine of one protein molecule coordinates to the heme iron of another CYP2D6 molecule resulting in a hexacoordinated species. Additionally, the observed optical properties of the total cell lysate could be arising from spontaneous mutations (probably deletion during storage) in the CYP2D6 gene from the frozen glycerol stocks used, considering the fact that P450 expression was successful in the first trial. On the other hand, when the expression procedure was followed by SDS electrophoresis (Figure 3.3.10), a band with a molecular weight characteristic of the truncated CYP2D6 is present in whole cells (too dilute), clarified lysate (supernatant), Ni^{2+} -bound and the flow through (FT) fraction. The pellet obtained after clarification of the cells lysate does not have the CYP2D6 band, as expected. When the expression was performed using freshly transformed BL21 cells grown in 2.5 L flasks containing a maximum of 500 mL of TB media (to allow efficient aeration), the cell lysate exhibited a Soret band around 400 nm and a shoulder at ~ 423

nm (Figure 3.3.11, trace A). The reduced CO difference spectrum shows a maximum at 443 nm, which is ~ 5 nm lower than the expected (Figure 3.3.11, trace B-A). Surprisingly, when the cell lysate was treated with 1 μL of freshly prepared 12 mg/mL $Na_2S_2O_4$, a feature at ~ 447 nm appears after 10 minutes even before adding CO (Figure 3.3.12), possibly indicating a ferrous hexacoordinated heme. Moreover this shoulder at 447 nm diminishes with bubbling of CO. It was also noted that the pCWori+ vector utilized in the subcloning of the truncated CYP2D6 was shown (sequencing performed by Gensript) to exhibit a deletion beyond the XbaI site (see Figure 3.2.2), which was initially assumed to be by design (by Ortiz de Montellano, when they constructed the P450cam expression plasmid)[140] and hence inconsequential to expression of functional protein. However the present results may be indicating the effect of the deletion on the expression, possibly resulting in an incorrectly folded protein. Obviously, it seems possible that subcloning of the truncated gene of CYP2D6 into a functional pCWori+ expression vector might result in the production of functional soluble protein. Recently, Pan, Y. *et al*[141] have designed an expression system for the full length CYP2D6 with the N-terminus modified to incorporate eight residues from bovine CYP17α. They demonstrated successful expression of CYP2D6 by immunoblotting and reduced CO difference spectral scanning, obtaining holoprotein yields of 371 pmol/mg protein. Noting that solubilization of the full length protein may require utilization of detergents; this expressed protein may be more effectively solubilized with the nanodisc technology elegantly developed by the Sligar group,[142–144] in which an encircling amphipathic membrane scaffold protein (MSP) capable of stabilizing a phospholipid bilayer functions as a belt around a hydrophobic core. The advantage of this technology is that the protein

is essentially in a native like environment, permitting better characterization by biophysical methods.

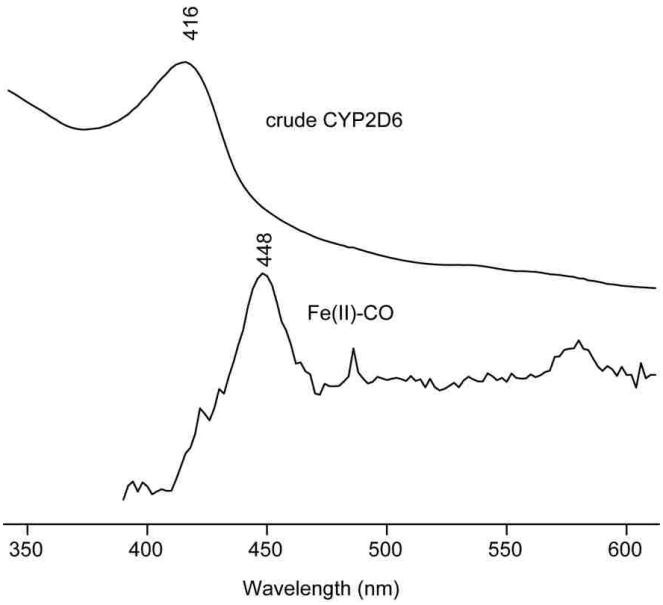

Figure 3.3.7 The absorption spectra of clarified cell lysate containing crude CYP2D6 (red trace) and the ferrous CO difference spectra of CYP2D6

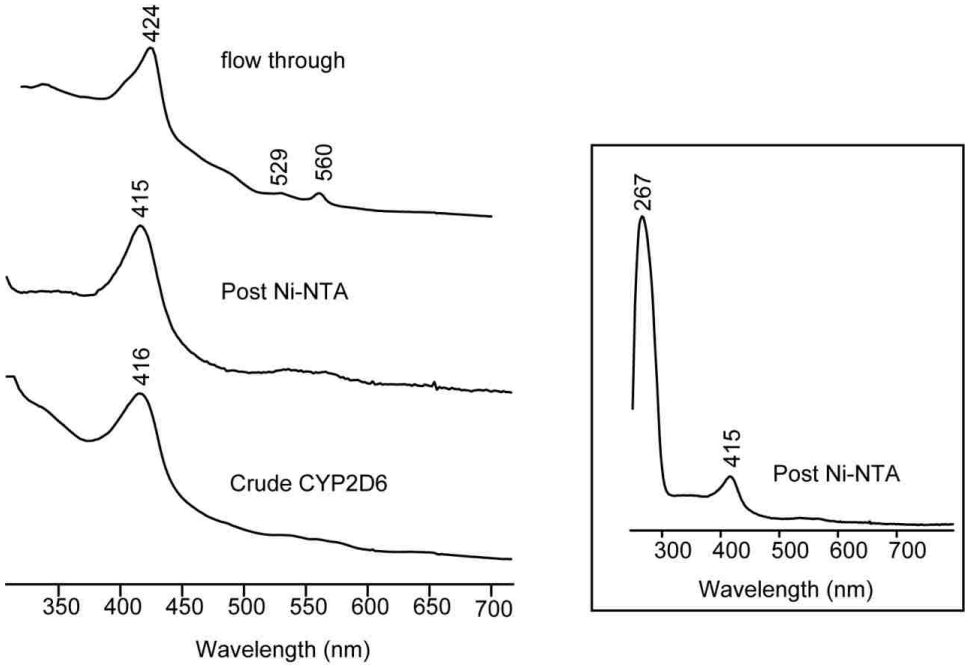

Figure 3.3.8 The absorption spectra of crude CYP2D6 (top trace), Ni^{2+} -NTA bound fraction (middle trace) and the Ni^{2+} flow through fraction (bottom trace). The insert (right) shows the full spectrum of the eluted bound fraction of CYP2D6

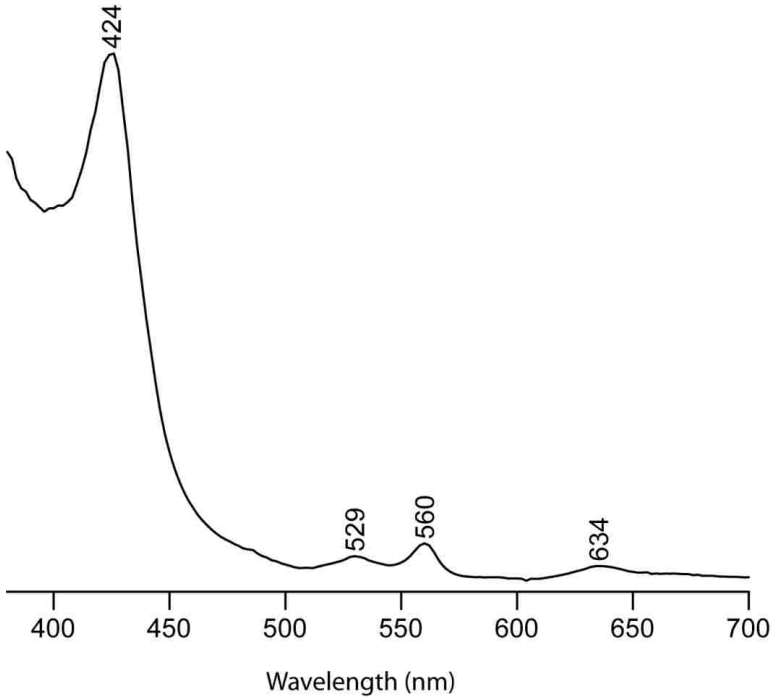

Figure 3.3.9 The absorption spectrum of the total cell lysate (from subsequent CYP2D6 expression trials) saturated with CO and incubated in excess sodium diothionite

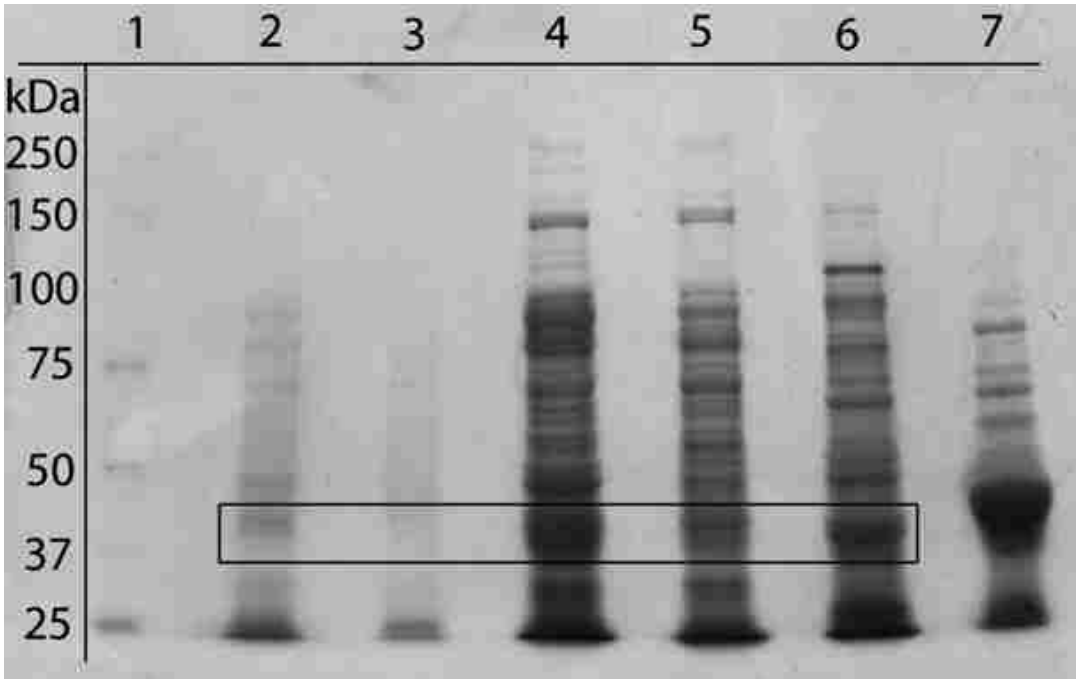

Figure 3.3.10 SDS-PAGE monitoring CYP2D6 expression and purification (bands in the black rectangular box are possibly from the truncated CYP2D6). Lane 1 (marker), 2 (whole cells), 3 (cell pellet after lysis), 4 (cytosolic fraction), 5 (Ni-NTA column flow through fraction), 6 (Ni-NTA bound fraction), 7 (CYP2D6 from Prof. Waskell).

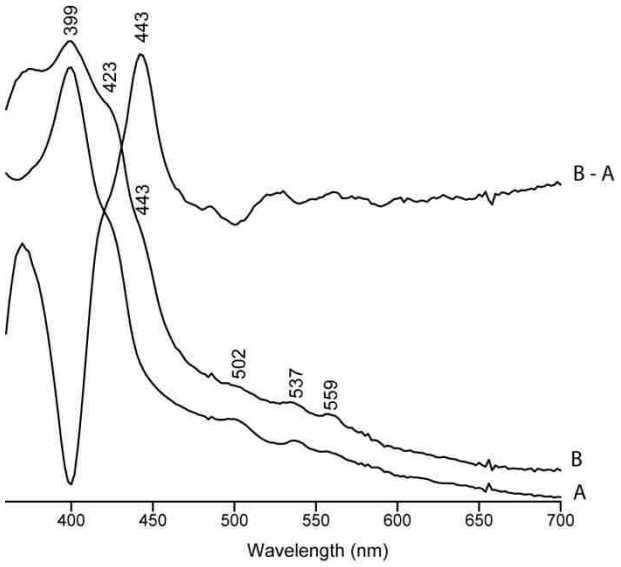

Figure 3.3.11 The UV-vis absorption spectra of CYP2D6 lysate (A), its $Na_2S_2O_4$ reduced CO form (B) and the difference spectrum of B-A

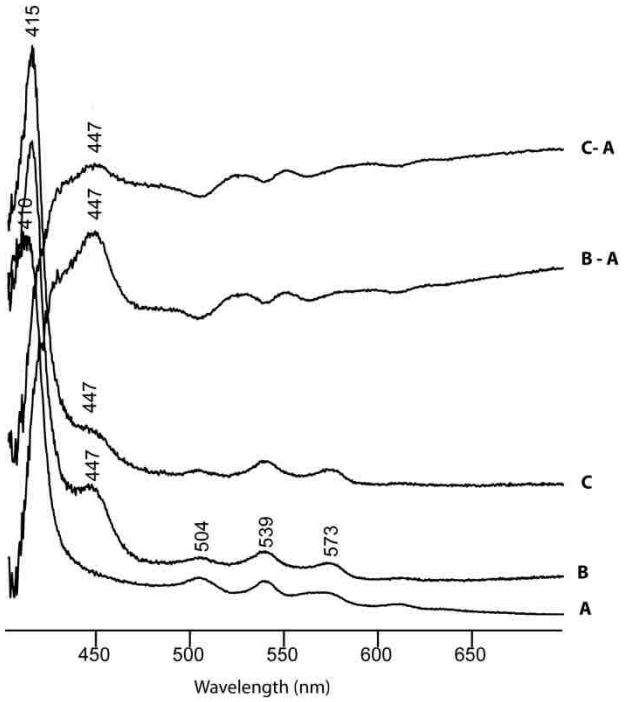

Figure 3.3.12 The absorption spectra of CYP2D6 cell lysate (**A**), Na_2SO_4 reduced forms (**B**), reduced CO forms (**C**) and the difference spectra of **B**-**A** and **C**-**A**

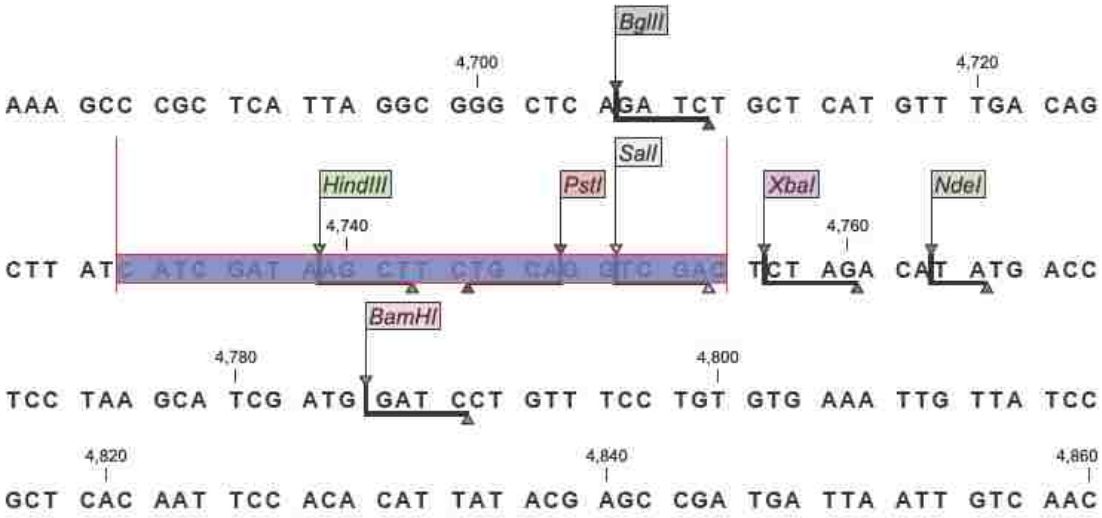

Figure 3.3.13 Part of the pCWori+ sequence in the multiple cloning site region, the highlighted part shows the deleted bases in the P450cam construct used for subcloning the CYP2D6 gene

3.3.3 Resonance Raman Spectroscopy of [5-^{13}C] δ-ALA P450cam

The high frequency resonance Raman spectra of the natural abundance and [5-^{13}C] δ-ALA SBP450cam are shown in Figure 3.3.14. The oxidation state marker band, ν_4 for the natural abundance P450cam shown in the top trace (A) occurs around 1370 cm^{-1} as expected for the ferric form of the protein, the mode is shifted by 13 cm^{-1} for the isotopically enriched analogue (trace B). This is to be expected in as much as this A_{1g} porphyrin breathing mode contains significant contributions from the C−N stretches[42–44] four of which are ^{13}C enriched (Figure 3.3.14 insert). Another mode of interest, which shifts significantly upon isotopic substitution, is the so called spin state marker band or ν_3, and has been previously shown to arise from $C_\alpha - C_m$ symmetrical stretches.[42] The other spin state marker band, ν_2 occurring at 1570 cm^{-1} for the natural abundance and contains substantial contributions from the $\nu(C_\beta - C_\beta)$ stretching mode only shifts slightly and appears as a broad band centered at 1568 cm^{-1}. Normal mode

calculations and isotopic studies of heme model compounds demonstrated mixing of the $C_\beta - C_\beta$ and $C_\alpha - C_m$ stretching modes although less significant for ν_2,[42–45] it may explain the broadening observed in the present work. Interestingly, ^{13}C isotopic substitution reveals the two vinyl stretching modes, which have been previously identified in P450cam reconstituted with protoheme-d4.[22]

The corresponding low frequency RR spectra shows further evidence of isotopic substitution particularly with the mode containing significant contributions from symmetric pyrrole deformation (ν_7) shifting down with 13 cm^{-1}.[42] Additionally, a new feature at 412 cm^{-1}, presumably arising from a vinyl bending mode, is activated in the ^{13}C enriched analogue of P450cam (Figure 3.3.15). These observations provide RR spectroscopic evidence for the successful heterologous expression of the bacterial P450cam bearing ^{13}C enriched prosthetic group at the C_α and C_m positions.

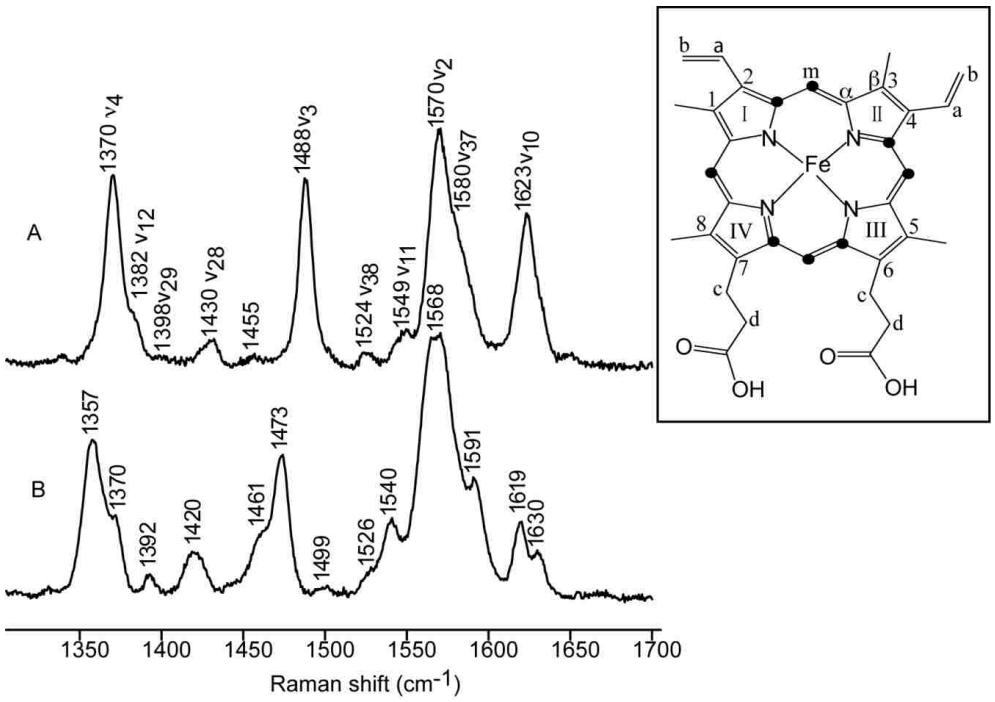

Figure 3.3.14 The high frequency RR spectra of the natural abundance (**A**) and [5-^{13}C] δ-ALA (**B)** substrate bound P450cam acquired with the 406 nm laser excitation line at room temperature. Insert: heme numbering, the ^{13}C enriched carbons are marked with black dots

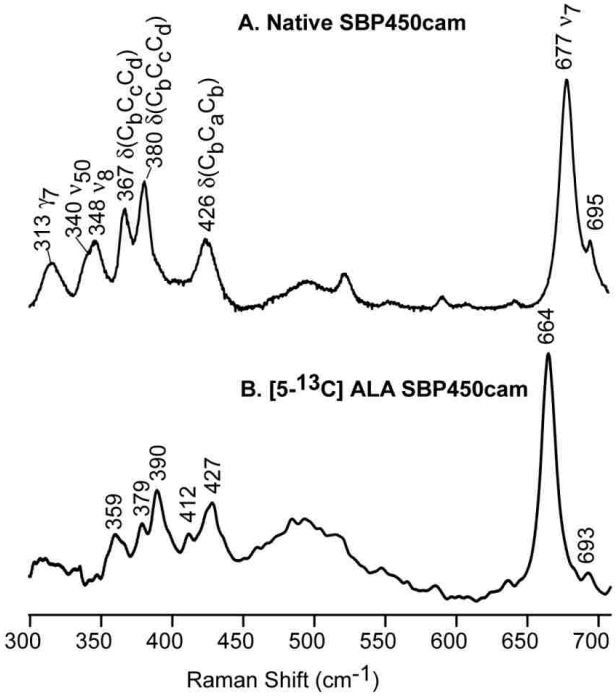

Figure 3.3.15 The low frequency RR spectra of (A) and [5-^{13}C] ALA (B) substrate bound P450cam acquired with 406 nm laser excitation

3.3.4 NMR spectroscopy of [5-^{13}C] δ-ALA P450cam

(a) Initial attempts

NMR measurements were acquired for both the high (HS) and low spin (LS) forms of natural abundance P450cam and its ^{13}C-labeled analogue. Specifically, 1D ^{13}C, ^{1}H and 2D ^{1}H-^{13}C HSQC NMR experiments were performed to identify the meso proton resonances, which are, in this case, required in NOE measurements. The inherent long electronic spin relaxation time of the heme iron causes very short relaxation times of the surrounding protons resulting in large line widths of the paramagnetically shifted resonances (Figure 3.3.16). The four hyperfine-shifted signals (A-D in Figure 3.3.16) outside of the protein envelope have been assigned to the heme peripheral methyl substituents.[72,73,145] Narrow line widths permits utilization of NMR NOE experiments in deriving distances between points of interest; therefore it is essential to obtain good quality 1D spectra, which is facilitated by using as highly concentrated protein solutions as is possible. Slightly reduced line widths are realized in the LS form of the protein, which is obtained by removal of the bound camphor, however as shown in the trace II of Figure 3.3.16, the spin state conversion from HS to LS is not 100%. This may be due to incomplete removal of the substrate (camphor) following passage of the camphor bound P450cam through Sephadex G25 column equilibrated with MOPS buffer. The optical absorption spectra however showed the characteristic 417 nm band of the camphor-free P450cam (SFP450cam). This was also observed for the 5-^{13}C-ALA SFP450cam as shown in Figure 3.3.16 (trace III); the percentage of the LS form of P450cam may be increased by passing the protein through the column (equilibrated with MOPS buffer) a couple of times before exchanging the buffer prior to collecting NMR data. In the 1D proton NMR spectra the meso protons resonances are not easily identifiable even in the low spin form.

They have been reported for P450cam to be possibly in the -20 and -40 ppm upfield region.[72] Fortunately, ^{13}C enrichment at the four methine positions permits utilization of ^{13}C-filtered NMR methods, which can facilitate the identification of the meso protons. However, the 2D NMR (HSQC) for the labeled SBP450cam (Figure 3.3.17 bottom trace), indicates no major differences from the native SBP450cam spectrum and no detectable meso resonances. The minor differences observed were later discovered to be due to the formation of the inactive form of the enzyme (Figure 3.3.18). This is possibly due to the long NMR acquisition times at room temperature, especially for the substrate free forms of the enzyme, which gave similar results.

(b) Improved methods

The utilization of a strong ligand field ligand, such as cyanide, to induce LS formation, is advantageous, noting that substrate-free LS forms, obtained by removing of the camphor substrate, are unstable and will likely convert to the P420 form during long NMR data collection. NMR studies on the cyanide complex of SBP450cam have been reported previously.[73] The low spin heme results in significantly reduced line widths, which may augment NOE sensitivity. In addition, the stability of the cyanide complex of SBP450cam permit for the acquisition of NMR data at elevated temperatures.[72] In order to improve the sensitivity of the NMR methods applied in this work, samples of the cyanide complex of both the natural abundance and ^{13}C enriched SBP450cam were employed (*vide infra*).

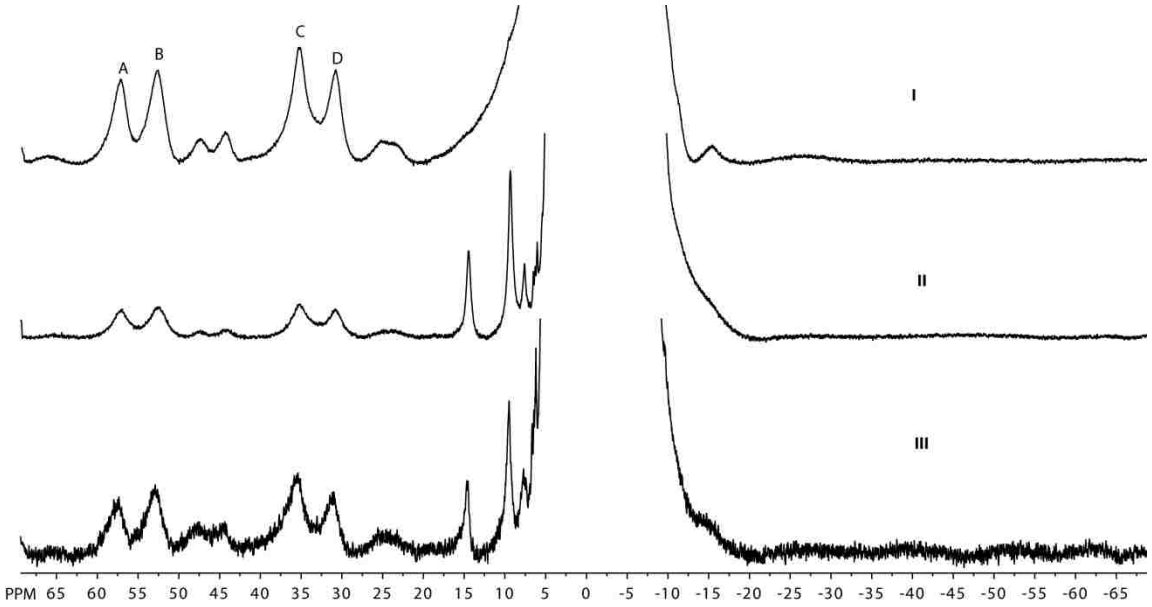

Figure 3.3.16 The 1D ^{1}H NMR of the natural abundance SBP450cam (**I**), natural abundance SFP450cam (**II**) and 5-^{13}C-ALA SFP450cam (**III**); the heme methyl resonances are denoted A-D

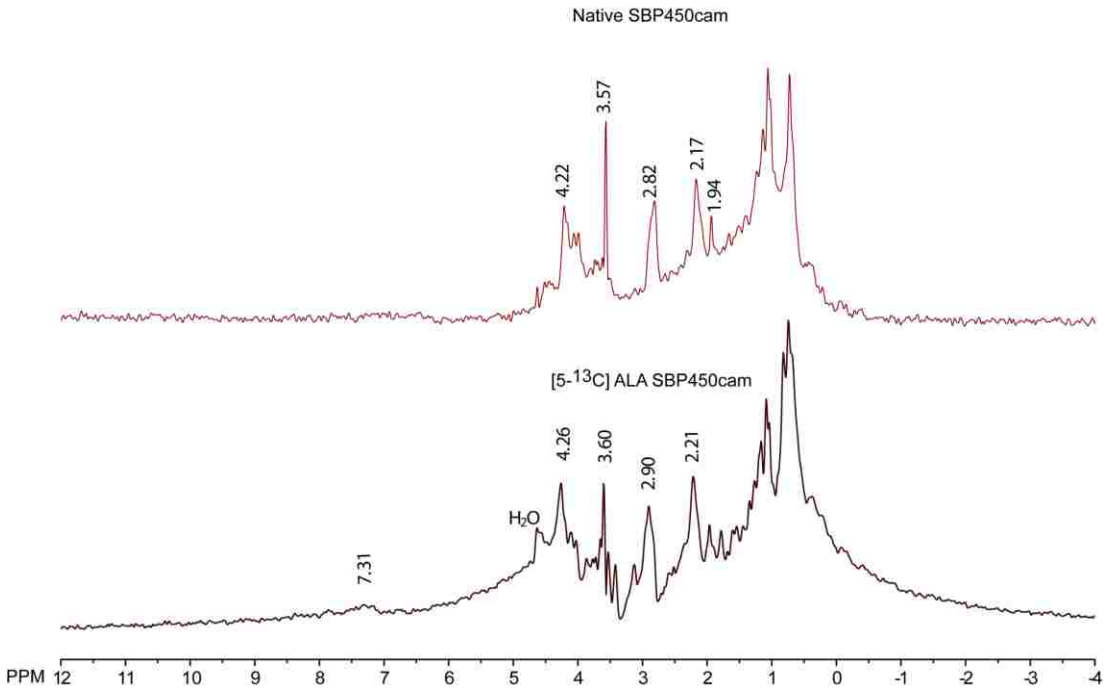

Figure 3.3.17 The 1D version of ^{1}H-^{13}C HSQC spectra of the natural abundance (top trace) and ^{13}C enriched (bottom trace) substrate-bound P450cam; sample concentration was ~0.2 mM in 30 mM deuterated phosphate buffer

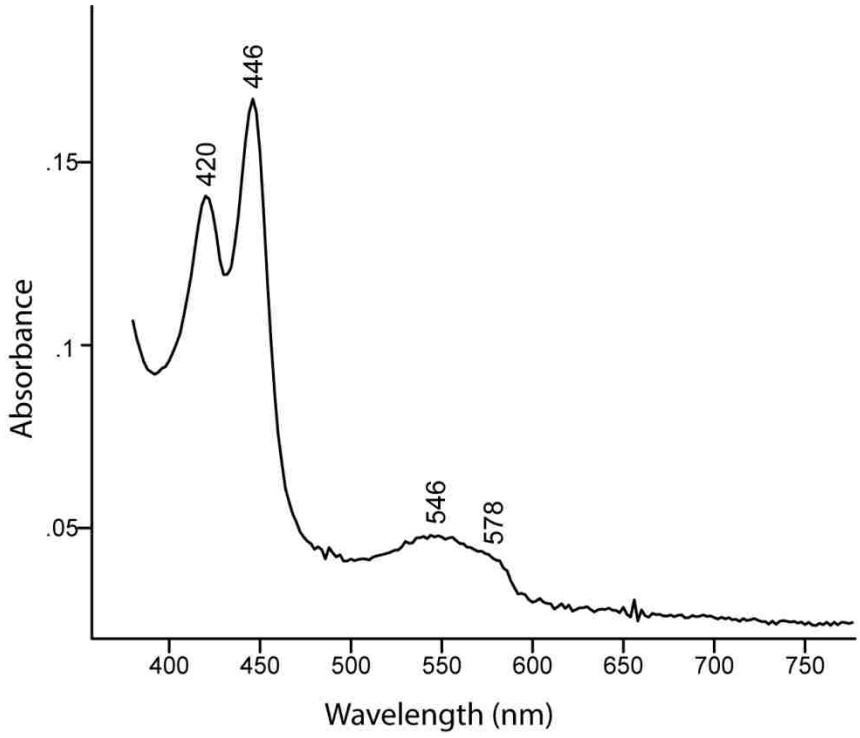

Figure 3.3.18 The absorption spectrum of [5-^{13}C] SBP450cam after collection of 1 D ^{1}H-^{13}C HSQC data

Cyanoferricytochrome P450cam NMR

The NMR samples (natural abundance and ^{13}C labeled) used in the experiments described below contained ~ 0.4-1 mM P450cam in 30 mM phosphate D_2O buffer, pH 7.4, 100 mM KCl, 10 mM KCN. The formation of the low spin substrate bound cyanoferricytochrome P450cam was verified by absorption spectroscopy (Figure 3.3.19) and is in agreement with the previously reported spectrum of the cyanide complex of microsomal P450.[146]

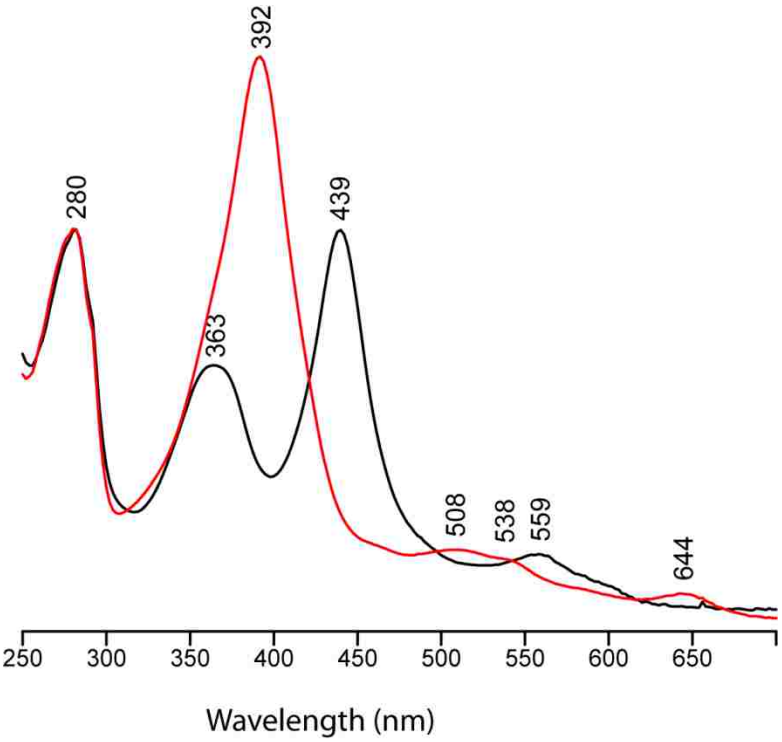

Figure 3.3.19 The absorption spectra high spin ferric substrate-bound P450cam (red trace) and its cyanide complex (black trace)

3.3.4.1 1D ^{1}H NMR

Proton NMR experiments were performed at 25 °C, for the cyanide complex of the natural abundance and ^{13}C-enriched substrate-bound P450cam, using a standard pulse sequence (Figure 3.3.20). The hyperfine shifted signals occurring at 21.8 and 11.3 ppm (black trace in Figure 3.3.20) have been assigned previously to the 8- and 3-methyl peripheral groups, respectively.[73] The 1D ^{1}H spectrum of the ^{13}C enriched cyanide complex of SBP450cam (red trace) is essentially identical to the natural abundance (black trace), as expected. However, due to the fast relaxation of protons in the paramagnetic environment, the methine proton resonances are still not detectable, even at elevated temperatures (40 °C), where only slight shifts are observed (blue trace). The 1D spectrum

was collected before and after multidimensional experiments (*vide infra*) to ensure sample integrity.

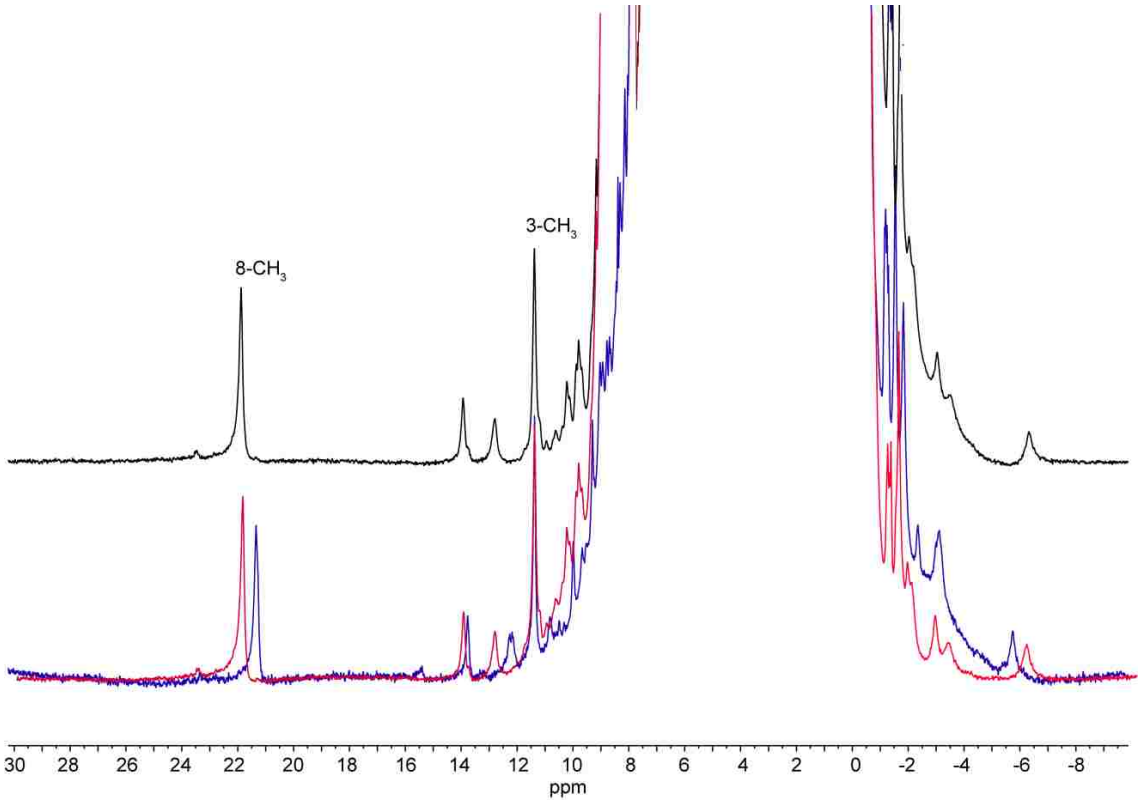

Figure 3.3.20 The 1D ^{1}H NMR spectra of the natural abundance (black) and ^{13}C enriched cyanide complex of P450cam at 20 °C (red) and 40 °C (blue)

3.3.4.2 ^{13}C NMR

In order to determine the methine proton signals using a 2 D experiment (HSQC/HMQC), a 1D ^{13}C NMR was performed at 20 °C for both the natural abundance and ^{13}C enriched cyanide complex of SBP450cam (black and red traces in Figure 3.3.21). The large line width arises from the very short relaxation time of the heme protons as mentioned above. The carbon signals **A-H** (red trace), which are clearly absent from the

natural abundance spectrum (black trace), were reasonably attributed to the ^{13}C enriched methine and C_α carbons of the heme consistent with the number of ^{13}C labeled carbons (red trace of Figure 3.3.21). Performing the experiment at 40 °C, for the ^{13}C-enriched SBP450cam, results in slight shifts to resonances A-E and attenuation of signals F, G and H and appearance of a new (N) feature around 56 ppm (blue trace). This may be due to the changes in longitudinal relaxation of the heme resonances at 40 °C.

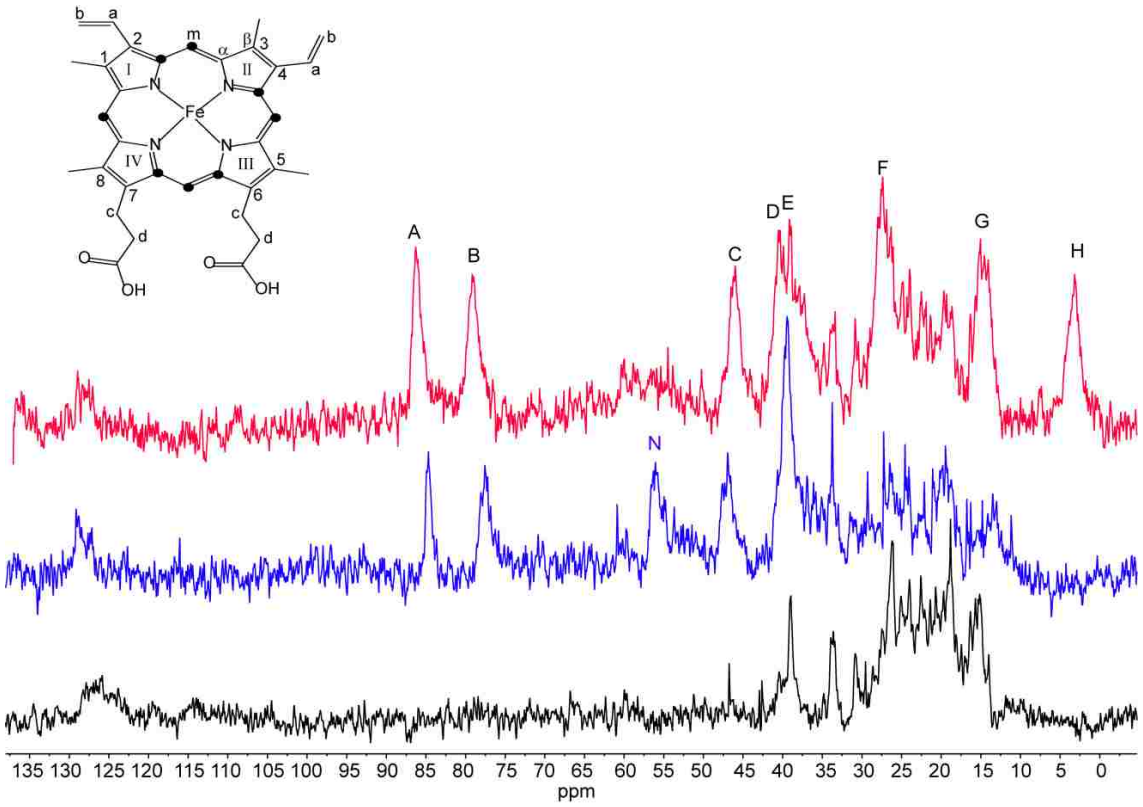

Figure 3.3.21 The ^{13}C NMR of the natural abundance (black trace) and ^{13}C enriched (top traces; red: 20 °C, blue: 40 °C) cyanide complex of P450cam. Insert shows the positions of ^{13}C enrichment (black dots)

3.3.4.3 2D HMQC

Figure 3.3.22 shows the 2D HMQC spectra of the ^{13}C enriched cyanide complex of SBP450cam collected at 25 °C (red trace) and 40 °C (blue trace) with a recycle delay of 10 ms and decoupling turned off. Protons giving rise to the signals labeled A-D are reasonably assigned to the methine positions in as much as the corresponding ^{13}C chemical shifts (A-D) are consistent with those observed in the 1D ^{13}C NMR experiment for the labeled cyanide complex of SBP450cam (Figure 3.3.21). Interestingly, the methine proton signals occur in the diamagnetic region making their identification without selective ^{13}C enrichment virtually impossible as noted in the 1D NMR experiment above. This observation has been reported earlier in a similarly ^{13}C enriched heme cofactor of *Hydrogenobacter thermophilus* cytochrome c_{552}.[80] The four cross peaks are clearly absent from the 2D HMQC spectrum of the natural abundance cyanide complex of SBP450cam (Figure 3.3.23) further confirming their assignment to the ^{13}C enriched methine positions, however specific assignments (α, β, δ and γ) is not possible at this point. In the *Hydrogenobacter thermophilus* cytochrome c_{552}, specific assignments was achieved using ^{1}H-^{1}H NOESY cross-peaks between the heme methyl and meso proton resonances.[80] Without decoupling, one will expect to observe doublets in the methine position cross peaks, however as noted above, the relatively fast relaxation, as evident from the large line widths exhibited in the ^{13}C NMR experiment, renders this spectral resolution impossible. In addition, no ^{13}C-^{13}C coupling was observed in the 1D ^{13}C spectrum due to the inherent fast relaxation of these resonances. Also, noting that one of the meso carbons (δ position) is not attached to a ^{13}C enriched pyrrole α-carbon, one would expect only ^{1}H-^{13}H coupling in contrast to the other 3 meso positions, which will exhibit coupling from both the attached proton and labeled pyrrole α-carbon. This

unique, meso δ carbon has been exploited in the assignment of the meso resonances by NOE methods in similarly[75,147] ^{13}C enriched heme oxygenases. However, probably due to fast relaxation, these couplings were not observed in the current work. The 2D HMQC spectra (obtained at 35 °C) of the cyanide complex of the heme oxygenase from *Coryne-bacterium diphtheria* (*cd*-OH) that has been reconstituted with a heme group ^{13}C-labeled at the C_α and C_m positions exhibited four correlations at {58.58, -2.58}, {33.27, 2.42}, {21.73, 7.78} and {18.75, 8.19} assigned to meso-α, γ, δ and β positions respectively.[147] In the current work a similar pattern was observed in the HMQC experiment (Figure 3.3.22) performed at 40 °C with crosspeaks appearing {84.7, 2.1}, {77.6, 4.7}, {46.9, 8.3} and {40.6, 10.8}, however, with the resonances downshifted, probably due to differences in the effect of the unpaired electron and active site structures.

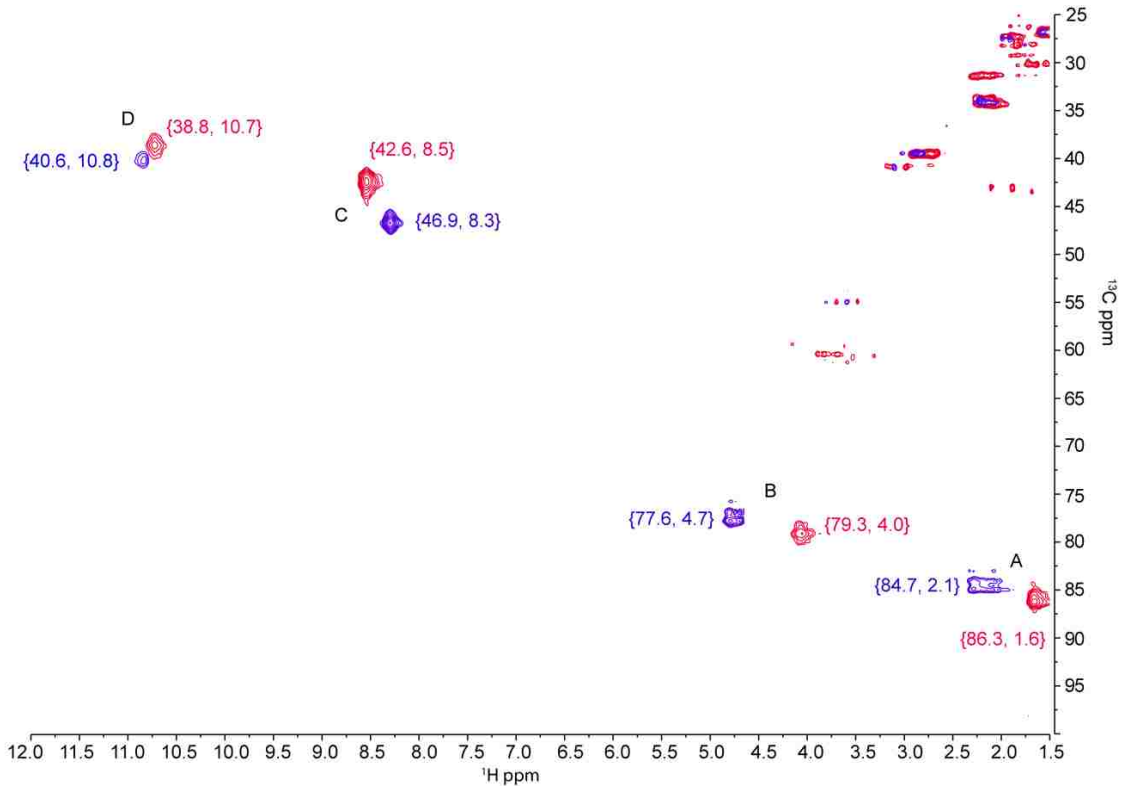

Figure 3.3.22 The 2 D HMQC spectra for the ^{13}C enriched cyanide complex of SBP450cam collected at 25 °C (red) and 40 °C (blue).

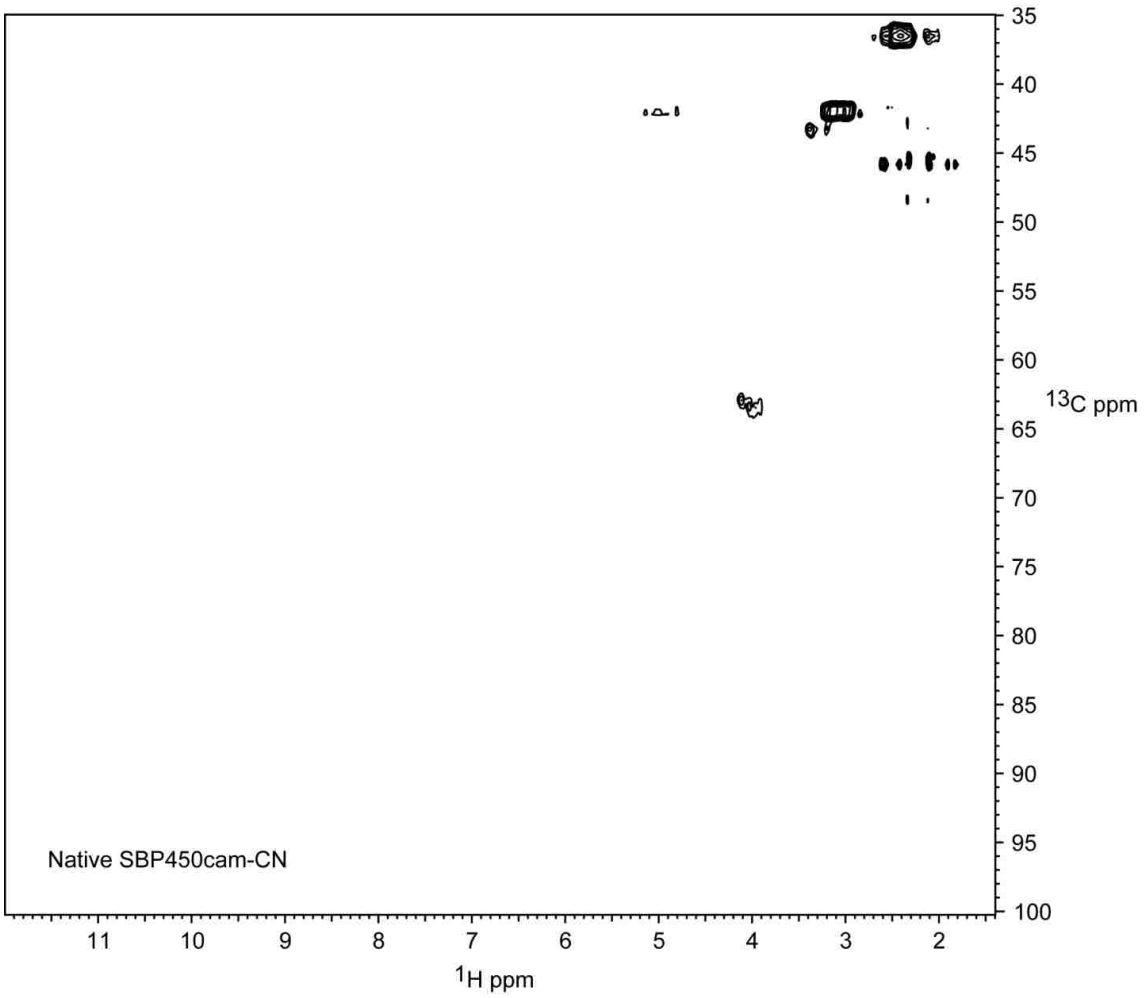

Figure 3.3.23 The 2D HMQC spectra of the natural abundance cyanide complex of SBP450cam collected overnight at 25 °C

3.3.4.4 ^{1}H-^{1}H NOESY

^{1}H-^{1}H NOESY-HMQC data was collected with 100 ms pre-saturation delay and 10 ms mixing time. However, possibly due to low sensitivity, only two of the presumably meso protons are detectable (Figure 3.3.24). The signal at 8.3 ppm exhibits 2 cross-peaks at ~ 4.01 and 1.37 ppm, which are located in the proton resonances envelope. The resonance at 4.01 ppm may be arising from the meso proton signal observed in the HMQC spectra (red cross-peak B in Figure 3.3.22), however this signal shifts to 4.7 ppm at 40 °C. Assignment of the signal at 1.37 ppm, is impossible at this point, since it may be

arising either from the protein side chain residues or the substrate camphor. However, detection of the corresponding signal at 1.37 ppm in the 1D ^{1}H spectra of the ^{13}C-enriched cyanide complex of SBP450cam is impossible due to the overwhelming protein signals. The signal might be buried in the protein envelope, making it impossible to detect, unless it was attached to a ^{13}C-enriched carbon, where detection might be possible using a double-filtered NOE. Interestingly, the ^{1}H NMR spectrum of KPi buffer containing free camphor exhibits a peak at 1.37 ppm arising from the 5 endo position of the substrate camphor (Figure 3.3.25). According to the crystal structure of the cyanide complex of P450cam, the 5 endo position is about 3.85 Å from the heme γ position; thus, the NOE at 1.37 ppm might possibly be arising from the 5 endo proton of camphor. Assignment of this resonance can be confirmed by loss of NOE upon utilization of perdueterated camphor or its substrate analogues, such as adamantanone. It is important to note that the NOE sensitivity might be improved by optimizing the mixing time and relaxation delay, this may lead to observation of additional crosspeaks, ideally from substrate protons. This will possibly lead to the derivation of distances between the heme reference points and substrate protons providing preliminary data on the disposition of the substrate in the active site pocket.

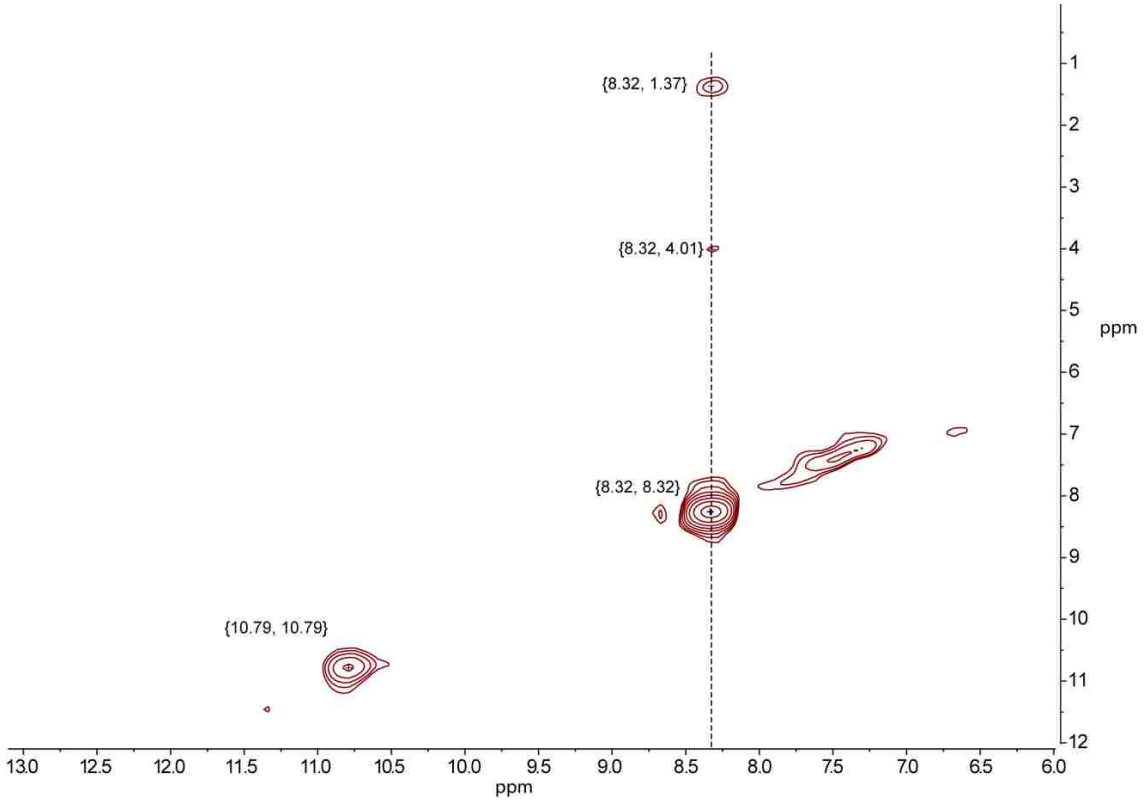

Figure 3.3.24 ^{1}H-^{1}H NOSEY-HMQC spectrum of ^{13}C-enriched cyanide complex of SBP450cam at 40 °C

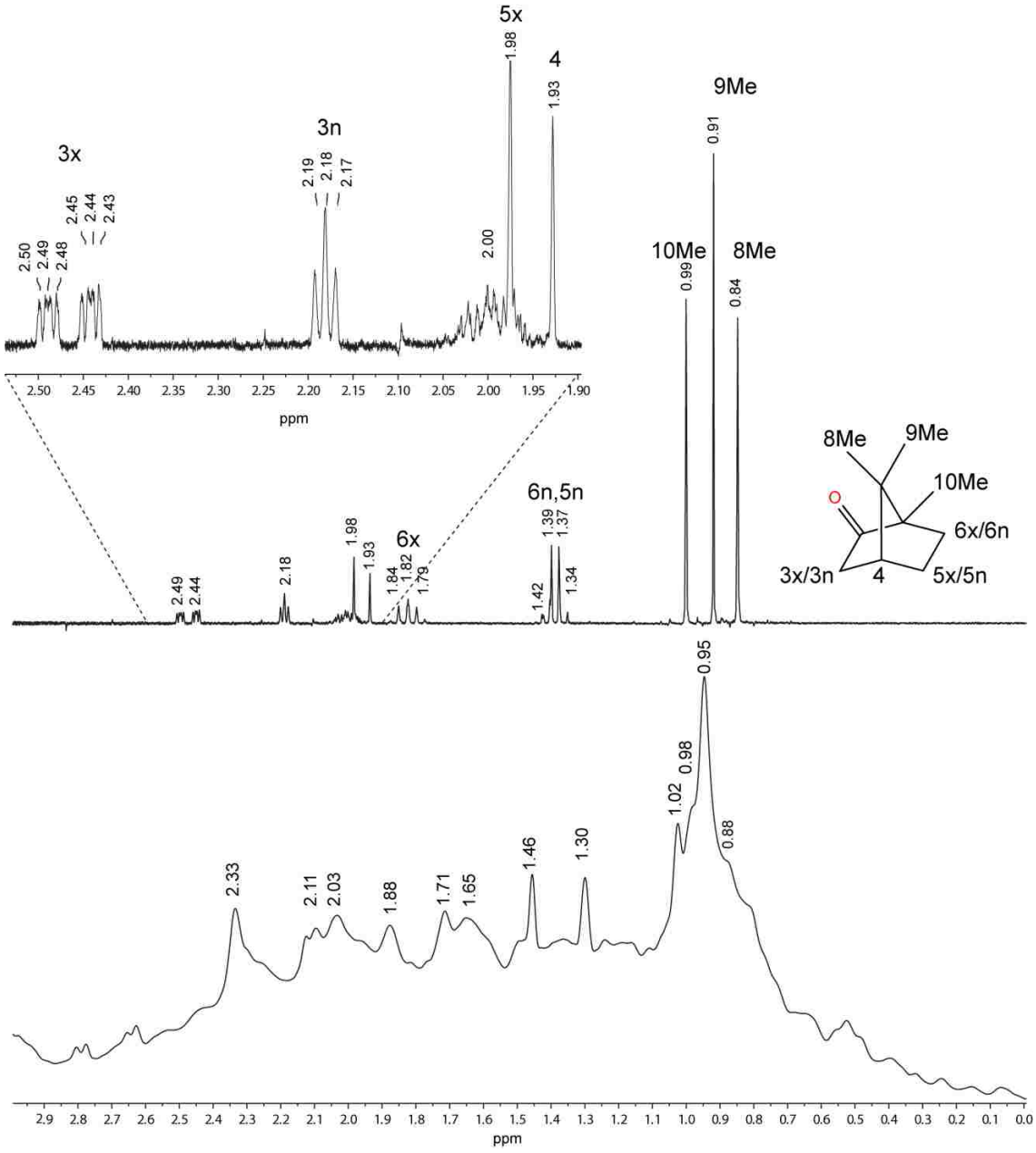

Figure 3.3.25 1D ^{1}H NMR of the ^{13}C-enriched cyanide complex of SBP450cam at 40 °C, with part of the diamagnetic region expanded (bottom trace) and KPi buffer containing 10 mM camphor (top trace)

3.4 Summary

The specific aim of this work was to exploit NMR spectroscopy in deriving experimental parameters for application in docking routines, which are commonly employed in defining relative binding affinities in drug metabolism P450s. To this end, an HU227 strain of E.coli, that lacks the δ-ALA synthase gene, was utilized in the expression of P450cam harboring a prosthetic group labeled with ^{13}C at the C_m and C_α positions by supplementing the bacterial growth media with [5-^{13}C] δ-ALA. The heme precursor was successfully synthesized in four steps from [2-^{13}C] glycine, giving yields of up to 70%. Successful incorporation of ^{13}C at the C_m and C_α positions was confirmed by RR of the ferric form of SBP450cam. Significant perturbations of the oxidation and spin state marker bands (in the high-frequency region) due to isotopic substitution were observed. In the low-frequency RR, ν_7 downshifts with about 13 cm^{-1} upon isotopic substitution. Additionally, activation of a vinyl bending mode at 412 cm^{-1} in the low-frequency RR spectra of the ^{13}C-enriched SBP450cam was observed, further confirming successful expression of isotopically labeled P450cam.

In an effort to heterologously express a ^{13}C-enriched CYP2D6, a truncated CYP2D6 gene was designed and commercially synthesized. The gene delivered in a pUC57 expression vector and transformed into *E.coli* cells, was shown to express P450 by reduced CO difference spectra of the total cell lysate. However, subcloning the gene into the pCWori expression vector, which is normally used for P450 expression, did not result in production of P450 as judged from the reduced CO difference spectra of total cell lysate. In fact, a species chacteristic of a hexacoordinated heme was observed; this was possibly due to the deletion in the pCWori sequence used for subcloning. Subcloning

of the truncated gene of CYP2D6 into a functional pCWori+ expression vector might possibly result in the production of functional soluble protein.

The ^{13}C-enriched P450cam was employed in a 'proof of principle' exercise for the strategy of defining active site structure in mammalian cytochromes P450 using NMR methods to furnish necessary experimental restrictions in docking routines. Identification of the meso protons was achieved by employing 1D ^{13}C and HMQC experiments. The HMQC spectra of cyanide complex of ^{13}C-enriched SBP450cam exhibited four cross-peaks [{46.9, 8.3}, {40.6, 10.8}, {77.6, 4.7}, {84.7, 2.1}], the proton signals lie in the diamagnetic region, making detection impossible without selective ^{13}C-enrichment. ^{1}H-^{1}H-HMQC showed that, the signal at 8.3 ppm is within NOE distance to two resonances at 1.37 and 4.01 ppm. However, assignment of these signals is impossible at this point, as they are buried in the protein envelope, although the signal at 4.01 ppm might possibly be coming from the heme meso proton, observed in the HMQC experiment performed at 25 °C. On the other hand the signal at 1.37 ppm corresponds to the 5 endo proton of camphor, which is about 3.85 Å from the heme γ position, suggesting that the observed NOE might be arising from the substrate. Utilization of perdeuterated camphor or its substrate analogues (e.g. adamantanone) and concomitant loss of NOE to the 1.37 ppm signal, will confirm its assignment to the 5 endo position. The sensitivity of the NOE experiments could be improved by utilizing highly concentrated samples and exploiting high field instruments such as the 900 MHz equipped with a cryoprobe. In addition, expression of a fully deuterated proton will aid in the identification of NOEs only between heme reference points and substrate or inhibitors. This will possibly lead to the determination of relative distances between methine protons and substrate proton resonances in the solution phase. It will be interesting to compare distances derived in the

solution phase with those calculated from the corresponding crystal structure. Inasmuch as there are still additional experiments to be done, the observation of NOEs from the heme reference points in this ‘proof of principle’ exercise project, provides an encouraging step in the direction of utilizing NMR methods in defining the active site structure.

BIBLIOGRAPHY

(1) Klingenberg, M. *Arch. Biochem. Biophys.* **1958**, *75*, 376–386.

(2) Omura, T.; Sato, R. *J. Biol. Chem* **1964**, *239*, 2370–2378.

(3) Nebert, D. W.; Nelson, D. R.; Feyereisen, R. *Xenobiotica* **1989**, *19*, 1149–1160.

(4) Nebert, D. W.; Nelson, D. R.; Adesnik, M.; Coon, M. J.; Estabrook, R. W.; Gonzalez, F. J.; Guengerich, F. P.; Gunsalus, I. C.; Johnson, E. F.; et, al. *DNA* **1989**, *8*, 1–13.

(5) Caughey, W. S. *Inorganic Biochemistry.*; Elsevier, 1973; Vol. 2, pp. 795–831.

(6) Spiro, T. G.; Li, X.-Y. *Biological Applications of Raman Spectroscopy, Vol. 3*; Spiro, T. G., Ed.; John Wiley and Sons: New York, 1988; pp. 1–37.

(7) Estabrook, R. W. *FASEB J.* **1996**, *10*, 202–204.

(8) Yu, N. -T.; Kerr, E. A. *Biological Applications of Raman Spectroscopy*; John Wiley and Sons: New York, 1988; p. 39.

(9) Poulos, T. L.; Finzel, B. C.; Gunsalus, I. C.; Wagner, G. C.; Kraut, J. *J. Biol. Chem.* **1985**, *260*, 16122–16130.

(10) Fenna, R.; Zeng, J.; Davey, C. *Arch. Biochem. Biophy.* **1995**, *316*, 653–656.

(11) Andersson, L. A.; Bylkas, S. A.; Wilson, A. E. *J. Biol. Chem.* **1996**, *271*, 3406–3412.

(12) Ortiz De Montellano, P. R. *Cytochrome P450: Structure, Mechanism, and Biochemistry*; Ortiz De Montellano, P. R., Ed.; Kluwer Academic/Plenum Publishers: New York, 2005; p. 689.

(13) Ortiz de Montellano, P. R. *Chem. Rev.* **2010**, *110*, 932–48.

(14) Kresge, N.; Simoni, R. D.; Hill, R. L. *J. Biol. Chem.* **2007**, *282*, e4–e5.

(15) Poulos, T. L. *Biochem. Biophys. Res. Commun.* **2003**, *312*, 35–39.

(16) Urlacher, V. B.; Bell, S. G.; Wong, L.-L. In *Modern Biooxidation*; Wiley-VCH Verlag GmbH & Co. KGaA, 2007; pp. 99–122.

(17) Miao, Y.; Baudry, J. *Biophys. J.* **2011**, *101*, 1493–1503.

(18) Hishiki, T.; Shimada, H.; Nagano, S.; Egawa, T.; Kanamori, Y.; Makino, R.; Park, S. Y.; Adachi, S.; Shiro, Y.; Ishimura, Y. *J. Biochemistry.* **2000**, *128*, 965–974.

(19) Poulos, T. L.; Finzel, B. C.; Howard, A. J. *Biochemistry* **1986**, *25*, 5314–5322.

(20) Denisov, I. G.; Mak, P. J.; Makris, T. M.; Sligar, S. G.; Kincaid, J. R. *J. Phys. Chem. A* **2008**, *112*, 13172–9.

(21) Sakurai, K.; Shimada, H.; Hayashi, T.; Tsukihara, T. *Acta Crystallogr. Sect. F* **2009**, *F65*, 80–83.

(22) Mak, P. J.; Kaluka, D.; Manyumwa, M. E.; Zhang, H.; Deng, T.; Kincaid, J. R. *Biopolymers.* **2008**, *89*, 1045–1053.

(23) Poulos, T. L. *Drug Metab.Dispos.* **2005**, *33*, 10–18.

(24) Sligar, S. G. *Biochemistry* **1976**, *15*, 5399–5406.

(25) Sligar, S. G.; Gunsalus, I. C. *Proc. Natl. Acad. Sci. U. S.A.* **1976**, *73*, 1078–1082.

(26) Hu, S.; Schneider, A.; Kincaid, J. *J. Am. Chem. Soc.* **1991**, *3*, 4815–4822.

(27) Mak, P. J.; Denisov, I. G.; Victoria, D.; Makris, T. M.; Deng, T.; Sligar, S. G.; Kincaid, J. R. *J. Am. Chem. Soc.* **2007**, *129*, 6382–6383.

(28) Sjodin, T.; Christian, J. F.; Macdonald, I. D. G.; Davydov, R.; Unno, M.; Sligar, S. G.; Hoffman, B. M.; Champion, P. M.; Complex, P. *Biochemistry* **2001**, *40*, 6852–6859.

(29) Macdonald, I. D. G.; Sligar, S. G.; Christian, J. F.; Unno, M.; Champion, P. M. *J. Am. Chem. Soc.* **1999**, *121*, 376–380.

(30) Davydov, R.; Makris, T. M.; Kofman, V.; Werst, D. E.; Sligar, S. G.; Hoffman, B. M. *J. Am. Chem. Soc.* **2001**, *123*, 1403–1415.

(31) Deng, T.; Macdonald, I. D. G.; Simianu, M. C.; Sykora, M.; Kincaid, J. R.; Sligar, S. G. *J. Am. Chem. Soc.* **2001**, *123*, 269–278.

(32) Simianu, M. C. Resonance Raman structural characterization of cyanide ligated cytochrome P450cam, 1995, p. 167 pp.

(33) Deng, T.; Proniewicz, L. M.; Kincaid, J. R.; Yeom, H.; Macdonald, I. D. G.; Sligar, S. G. *Biochemistry* **1999**, *38*, 13699–13706.

(34) Ferraro, J. R.; Nakamoto, K.; Brown, C. W. *Introductory Raman Spectroscopy, Second Edition.*; Academic Press, 2003; p. 434 pp.

(35) Champion, P. M.; Gunsalus, I. C.; Wagner, G. C. *J. Am. Chem. Soc.* **1978**, *100*, 3743–3751.

(36) Wells, A. V.; Li, P.; Champion, P. M.; Martinis, S. A.; Sligar, S. G. *Biochemistry* **1992**, *31*, 4384–4393.

(37) Martinis, S. A.; Blanke, S. R.; Hager, L. P.; Sligar, S. G.; Hoa, G. H.; Rux, J. J.; Dawson, J. H. *Biochemistry* **1996**, *35*, 14530–6.

(38) Kincaid, J. R. In *Porphyrin Handbook*; Academic Press, 2000; Vol. 7, pp. 225–291.

(39) Champion, P. M. *Biological Applications of Raman Spectroscopy*; John Wiley and Sons: New York, 1988; pp. 249–292.

(40) Li, X. Y.; Czernuszewicz, R. S.; Kincaid, J. R.; Spiro, T. G. *J. Am. Chem. Soc.* **1989**, *111*, 7012–7023.

(41) Hu, S.; Morris, I. K.; Singh, J. P.; Smith, K. M.; Spiro, T. G. *J. Am. Chem. Soc.* **1993**, *115*, 12446–12458.

(42) Li, X. Y.; Czernuszewicz, R. S.; Kincaid, J. R.; Su, Y. O.; Spiro, T. G. *J. Phys. Chem.* **1990**, *94*, 31–47.

(43) Kitagawa, T.; Abe, M.; Ogoshi, H. *J. Chem. Phys.* **1978**, *69*, 4516.

(44) Abe, M.; Kitagawa, T.; Kyogoku, Y. *J. Chem. Phys.* **1978**, *69*, 4526–4534.

(45) Li, X. Y.; Czernuszewicz, R. S.; Kincaid, J. R.; Stein, P.; Spiro, T. G.; Su, Y. O.; Li, X. -Y, Spiro, T. G.; Kitagawa, T.; Abe, M.; Ogoshi, H.; Kyogoku, Y. *J. Chem. Phys.* **1978**, *69*, 47–61.

(46) Choi, S.; Spiro, T. G.; Langry, K. C.; Smith, K. M. *J. Am. Chem. Soc.* **1982**, *104*, 4337–4344.

(47) Hu, S.; Smith, K. M.; Spiro, T. G. *J. Am. Chem. Soc.* **1996**, *118*, 12638–12646.

(48) Peterson, E. S.; Friedman, J. M.; Chien, E. Y. T.; Sligar, S. G. *Biochemistry* **1998**, *37*, 12301–12319.

(49) Podstawka, E.; Rajani, C.; Kincaid, J. R.; Proniewicz, L. M. *Biopolymers.* **2000**, *57*, 201–207.

(50) Mak, P. J.; Podstawka, E.; Kincaid, J. R.; Proniewicz, L. M. *Biopolymers.* **2004**, *75*, 217–228.

(51) Zbylut, S. D.; Kincaid, J. R. *J. Am. Chem. Soc.* **2002**, *124*, 6751–6758.

(52) Huang, Q.; Schweitzer-Stenner, R. *J. Raman Spectrosc.* **2005**, *36*, 363–375.

(53) Nagai, M.; Aki, M.; Li, R.; Jin, Y.; Sakai, H.; Nagatomo, S.; Kitagawa, T. *Biochemistry* **2000**, *39*, 13093–13105.

(54) Chen, Z.; Ost, T. W. B.; Schelvis, J. P. M. *Biochemistry* **2004**, *43*, 1798–1808.

(55) Cerda-Colon, J. F.; Silfa, E.; Lopez-Garriga, J. *J. Am. Chem. Soc.* **1998**, *120*, 9312–9317.

(56) Champion, P. M.; Stallard, B. R.; Wagner, G. C.; Gunsalus, I. C. *Dev. Biochem.* **1982**, *23*, 547–550.

(57) Champion, P. M.; Remba, R. D.; Chiang, R.; Fitchen, D. B.; Hager, L. P. *Biochim. Biophys. Acta* **1976**, *446*, 486–492.

(58) Champion, P. M.; Gunsalus, I. C. *J. Am. Chem. Soc.* **1977**, *99*, 2000–2002.

(59) Anzenbacher, P.; Evangelista-Kirkup, R.; Schenkman, J.; Spiro, T. G. *Inorg. Chem.* **1989**, *28*, 4491–4495.

(60) Unno, M.; Christian, J. F.; Benson, D. E.; Gerber, N. C.; Sligar, S. G.; Champion, P. M. *J. Am. Chem. Soc.* **1997**, *119*, 6614–6620.

(61) Bangcharoenpaurpong, O; Rizos, A. K.; Champion, P. M.; Jollie, D; Sligar, S. G. *J. Biol. Chem.* **1986**, *261*, 8089–8092.

(62) Hu, S.; Schneider, A. J.; Kincaid, J. R. *J. Am. Chem. Soc.* **1991**, *113*, 4815–4822.

(63) Raag, R.; Poulos, T. L. *Biochemistry* **1989**, *28*, 917–922.

(64) Kappl, R.; Hoehn-Berlage, M.; Huettermann, J.; Bartlett, N.; Symons, M. C. R. *Biochim. Biophys. Acta* **1985**, *827*, 327–343.

(65) Davydov, R.; Macdonald, I. D. G.; Makris, T. M.; Sligar, S. G.; Hoffman, B. M. *J. Am. Chem. Soc.* **1999**, *121*, 10654–10655.

(66) Garcia-Serres, R.; Davydov, R. M.; Matsui, T.; Ikeda-Saito, M.; Hoffman, B. M.; Huynh, B. H. *J. Am. Chem. Soc.* **2007**, *129*, 1402–1412.

(67) Davydov, R.; Osborne, R. L.; Kim, S. H.; Dawson, J. H.; Hoffman, B. M. *Biochemistry* **2008**, *47*, 5147–5155.

(68) Davydov, R.; Razeghifard, R.; Im, S.-C.; Waskell, L.; Hoffman, B. M. *Biochemistry* **2008**, *47*, 9661–9666.

(69) Kowalsky, A. *Polym. Prepr. (Am. Chem. Soc., Div. Polym. Chem.)* **1962**, *3*, 92*–5*.

(70) Kowalsky, A. *J. Biol. Chem.* **1962**, *237*, 1807–1819.

(71) La Gerd N., M.; Satterlee, J. D.; De Jeffrey S., R. *Nuclear magnetic resonance of hemoproteins.*; Academic Press, 2000; Vol. 5, pp. 185–298.

(72) Mouro, C.; Bondon, A.; Jung, C. De Certaines, J. D.; Simonneaux, G. *Eur. J. Biochem.* **2000**, *267*, 216–221.

(73) Wakasugi, K.; Ishimori, K.; Morishima, I. *Biochimie* **1996**, *78*, 763–770.

(74) McCullough, C. R.; Pullela, P. K.; Im, S.-C.; Waskell, L.; Sem, D. S. *J. Biomol. NM* **2009**, *43*, 171–8.

(75) Rivera, M.; Caignan, G. A. *Anal. Bioanal. Chem.* **2004**, *378*, 1464–1483.

(76) Bunce, R. A.; Schilling III, C. L.; Rivera, M. *J. Labelled Compd. Radiopharm.* **1997**, *39*, 669–675.

(77) Rivera, M.; Walker, F. A. *Anal. Biochem.* **1995**, *230*, 295–302.

(78) Bryson, D.; Lim, P.-L.; Lawson, A.; Manjunath, S.; Raner, G. M. *Biotechn. Lett.* **2011**, *33*, 2019–2026.

(79) Alontaga, A. Y.; Bunce, R. A; Wilks, A.; Rivera, M. *Inorg. Chem.* **2006**, *45*, 8876–81.

(80) Liptak, M. D.; Wen, X.; Bren, K. L. *J. Am. Chem. Soc.* **2010**, *132*, 9753–63.

(81) Jung, C. *Biochim. Biophys. Acta* **2011**, *1814*, 46–57.

(82) Su, Z.; Chen, X.; Horner, J. H.; Newcomb, M. *Chem. Eur. J.* **2012**, *18*, 2472–2476, S2472/1–S2472/14.

(83) Chen, X.; Su, Z.; Horner, J. H.; Newcomb, M. *Org. Biomol. Chem.* **2011**, *9*, 7427–7433.

(84) Sivaramakrishnan, S.; Ouellet, H.; Du, J.; McLean, K. J.; Medzihradszky, K. F.; Dawson, J. H.; Munro, A. W.; Ortiz De Montellano, P. R. *Biochemistry* **2011**, *50*, 3014–3024.

(85) Rittle, J.; Green, M. T. *Science* **2010**, *330*, 933–7.

(86) Yuan, X.; Wang, Q.; Horner, J. H.; Sheng, X.; Newcomb, M. *Biochemistry* **2009**, *48*, 9140–9146.

(87) Wang, Q.; Sheng, X.; Horner, J. H.; Newcomb, M. *J. Am. Chem. Soc.* **2009**, *131*, 10629–10636.

(88) Sheng, X.; Zhang, H.; Hollenberg, P. F.; Newcomb, M. *Biochemistry* **2009**, *48*, 1620–1627.

(89) Sheng, X.; Horner, J. H.; Newcomb, M. *J. Am. Chem. Soc.* **2008**, *130*, 13310–13320.

(90) Kellner, D. G.; Hung, S.-C.; Weiss, K. E.; Sligar, S. G. *J. Biol. Chem.* **2002**, *277*, 9641–9644.

(91) Newcomb, M.; Zhang, R.; Chandrasena, R. E. P.; Halgrimson, J. a; Horner, J. H.; Makris, T. M.; Sligar, S. G. *J. Am. Chem. Soc.* **2006**, *128*, 4580–4581.

(92) Jung, C.; de Simon, V.; Schuenemann, V. *Arch. Biochem. Biophys.* **2011**, *507*, 44–55.

(93) Luthra, A.; Denisov, I. G.; Sligar, S. G. *Arch. Biochem. Biophys.* **2011**, *507*, 26–35.

(94) Iida, K.; Kajiwara, M. *J. Labelled Compd. Radiopharm.* **2002**, *45*, 139–143.

(95) Campbell, J. B.; Johnston, J. S. *J. Labelled Compd. Radiopharm.* **1989**, *27*, 1353–1358.

(96) Kaluka, D.; Kincaid, J. R. Resonance Raman spectroscopy of cytochrome P450cam, Marquette University, 2009.

(97) Adcock, J. L.; Zhang, H. *J. Org. Chem.* **1996**, *61*, 5073–5076.

(98) McLean, M. A.; Maves, S. A.; Weiss, K. E.; Krepich, S.; Sligar, S. G. *Biochem. Biophys. Res. Commun.* **1998**, *252*, 166–72.

(99) Park, S. Y.; Yamane, K.; Adachi, S.; Shiro, Y.; Weiss, K. E.; Sligar, S. G. *Acta Crystallograph. Sect. D* **2000**, *56*, 1173–1175.

(100) Tschirret-Guth, R. A.; Koo, L. S.; Hoa, G. H.; Ortiz De Montellano, P. R. *J. Am. Chem. Soc.* **2001**, *123*, 3412–3417.

(101) Park, S.-Y.; Yamane, K.; Adachi, S.; Shiro, Y.; Weiss, K. E.; Maves, S. A.; Sligar, S. G. *J. Inorg. Biochem.* **2002**, *91*, 491–501.

(102) Puchkaev, A. V.; Koo, L. S.; Ortiz, de M. P. R. *Arch. Biochem. Biophys.* **2003**, *409*, 52–58.

(103) Puchkaev, A. V.; Koo, L. S.; Ortiz de Montellano, P. R. *Arch. Biochem. Biophys.* **2003**, *409*, 52–8.

(104) Michels, P. C.; Clark, D. S. *Appl. Environ. Microbiol.* **1997**, *63*, 3985–91.

(105) Denisov, I. G.; Hung, S. C.; Weiss, K. E.; McLean, M. A; Shiro, Y.; Park, S. Y.; Champion, P. M.; Sligar, S. G. *J. Inorg. Biochem.* **2001**, *87*, 215–226.

(106) Behan, R. K.; Hoffart, L. M.; Stone, K. L.; Krebs, C.; Green, M. T. *J.Am.Chem. Soc.* **2007**, *129*, 5855–5859.

(107) Koo, L. S.; Immoos, C. E.; Cohen, M. S.; Farmer, P. J.; Ortiz Paul R., de M. *J.Am.Chem. Soc.* **2002**, *124*, 5684–5691.

(108) Lim, Y.-R.; Eun, C.-Y.; Park, H.-G.; Han, S.; Han, J.-S.; Cho, K. S.; Chun, Y.-J.; Kim, D.; Koo, L. S.; Immoos, C. E.; Cohen, M. S.; Farmer, P. J.; Ortiz de Montellano, P. R. *Microbiol. Biotechnol.***2010**, *20*, 574–578.

(109) Barnes, H. J. *Methods Enzymol.* **1996**, *272*, 3–14.

(110) Gegner, J. A.; Dahlquist, F. W. *Proc. Natl. Acad. Sci.* **1991**, *88* , 750–754.

(111) Yun, C.-H.; Yim, S.-K.; Kim, D.-H.; Ahn, T. *Curr. Drug Metab.* **2006**, *7*, 411–429.

(112) Denisov, I. G.; Victoria, D. C.; Sligar, S. G. *Radiat. Phys. Chem.***2007**, *76*, 714–721.

(113) Shriver, D. F.; Dunn, J. B. R. *Appl. Spectrosc.* **1974**, *28*, 319–323.

(114) Wu, Q.; Balakrishnan, G.; Pevsner, A.; Spiro, T. G. *J. Phys. Chem. A* **2003**, *107*, 8047–8051.

(115) Uno, T.; Nishimura, Y.; Makino, R.; Iizuka, T.; Ishimura, Y.; Tsuboi, M. *J. Biol. Chem.* **1985**, *260*, 2023–2026.

(116) Koo, L. S.; Tschirret-Guth, R. a; Straub, W. E.; Moënne-Loccoz, P.; Loehr, T. M.; Ortiz de Montellano, P. R. *J. Biol. Chem.* **2000**, *275*, 14112–23.

(117) de, R. M.; Gambacorta, A.; Bu'lock, J. D. *Journal of general microbiology* **1975**, *86*, 156–164.

(118) Wright, R. L.; Harris, K.; Solow, B.; White, R. H.; Kennelly, P. J. *FEBS Lett.* **1996**, *384*, 235–239.

(119) Sjodin, T.; Christian, J. F.; Macdonald, I. D. G.; Davydov, R.; Unno, M.; Sligar, S. G.; Hoffman, B. M.; Champion, P. M. *Biochemistry* **2001**, *40*, 6852–6859.

(120) Jeyarajah, S.; Proniewicz, L. M.; Bronder, H.; Kincaid, J. R. *J. Biol. Chem.* **1994**, *269*, 31047–31050.

(121) Hirota, S.; Ogura, T.; Appelman, E. H.; Shinzawa-Itoh, K.; Yoshikawa, S.; Kitagawa, T. *J. Am. Chem. Soc.* **1994**, *116*, 10564–10570.

(122) Das, T. K.; Couture, M.; Ouellet, Y.; Guertin, M.; Rousseau, D. L. *Proc. Natl. Acad. Sci. U.S.A.* **2001**, *98*, 479–484.

(123) Rutter, R.; Hager, L. P.; Dhonau, H.; Hendrich, M.; Valentine, M.; Debrunner, P. *Biochemistry* **1984**, *23*, 6809–6816.

(124) Reat, V.; Finney, J. L.; Steer, A.; Roberts, M. A.; Smith, J.; Dunn, R.; Peterson, M.; Daniel, R. *J. Biochem. Biophys. Methods* **2000**, *42*, 97–103.

(125) Guengerich, F. P. *Proc. Natl. Acad. Sci. U.S.A.* **2006**, *103*, 13565–6.

(126) Ekroos, M.; Sjoegren, T. *Proc. Natl. Acad. Sci. U.S.A.* **2006**, *103*, 13682–13687.

(127) Lacy, C. F.; Armstrong, L. L.; Goldman, M. P. *Drug Information Handbook*; 15th ed.; Lexi-Comp: Hudson, OH, 2007; pp. 1899–1912.

(128) Rowland, P.; Blaney, F. E.; Smyth, M. G.; Jones, J. J.; Leydon, V. R.; Oxbrow, A. K.; Lewis, C. J.; Tennant, M. G.; Modi, S.; Eggleston, D. S.; Chenery, R. J.; Bridges, A. M. *J. Biol. Chem.* **2006**, *281*, 7614–22.

(129) Costache, A. D.; Trawick, D.; Bohl, D.; Sem, D. S. *Xenobiotica* **2007**, *37*, 221–245.

(130) Moors, S. L. C.; Vos, A. M.; Cummings, M. D.; Van Herman, V.; Ceulemans, A. *J. Med. Chem.* **2011**, *54*, 6098–6105.

(131) Stjernschantz, E.; Oostenbrink, C. *Biophys. J.* **2010**, *98*, 2682–2691.

(132) Wang, A.; Savas, U.; Hsu, M.-H.; Stout, C. D.; Johnson, E. F. *J. Biol. Chem.* **2012**, *287*, 10834–10843.

(133) Cohen, S. N.; Chang, A. C. Y.; Hsu, L. *Proc. Natl. Acad. Sci. U.S.A.* **1972**, *69*, 2110–2114.

(134) Gunsalus, I. C.; Sligar, S. G. *Adv. Enzymol. Relat. Areas Mol. Biol.***1978**, *47*, 1–44.

(135) Bauer, S.; Shiloach, J. *Biotechnol. Bioeng.* **1974**, *16*, 933–941.

(136) Gunsalus, I. C.; Wagner, G. C. *Methods enzymol.* **1978**, *52*, 166–188.

(137) Deng, S.-L.; Baglin, I.; Nour, M.; Cave, C. *Heteroat. Chem.***2008**, *19*, 55–65.

(138) Winterbourn, C. C.; Carrell, R. W. *J. Clin. Invest.* **1974**, *54*, 678–689.

(139) Uzan, J.; Dewilde, S.; Burmester, T.; Hankeln, T.; Moens, L.; Hamdane, D.; Marden, M. C.; Kiger, L. *Biophys. J.* **2004**, *87*, 1196–1204.

(140) Sibbesen, O.; De James J., V.; Ortiz Paul R., de M. *J. Biol. Chem.* **1996**, *271*, 22462–22469.

(141) Pan, Y.; Abd-Rashid, B. A.; Ismail, Z.; Ismail, R.; Mak, J. W.; Ong, C. E. *Protein J.* **2011**, *30*, 581–91.

(142) Nath, A.; Atkins, W. M.; Sligar, S. G. *Biochemistry* **2007**, *46*, 2059–2069.

(143) Sligar, S. G. *Biochem. Biophys. Res. Commun* **2003**, *312*, 115–119.

(144) Denisov, I. G.; Sligar, S. G. *Biochim. Biophys. Acta* **2011**, *1814*, 223–229.

(145) Banci, L.; Bertini, I.; Marconi, S.; Pierattelli, R.; Sligar, S. G. *J. Am. Chem. Soc.* **1994**, *116*, 4866–4873.

(146) Miyake, Y.; Mori, K.; Yamano, T. *Arch. Biochem. Biophys.* **1969**, *133*, 318–326.

(147) Caignan, G. A.; Deshmukh, R.; Wilks, A.; Zeng, Y.; Huang, H.; Moënne-Loccoz, P.; Bunce, R. A.; Eastman, M. A.; Rivera, M. *J. Am. Chem. Soc.* **2002**, *124*, 14879–14892.